Cell Search in Frequency Division Duplex WCDMA Networks

Seare Haile Rezenom

Submitted in fulfilment of the academic requirements
for the degree of Master of Science in Engineering
in the School of Electrical, Electronic and Computer Engineering
at the University of KwaZulu-Natal,
Durban, South Africa
December 2006

ABSTRACT

Wireless radio access technologies have been progressively evolving to meet the high data rate demands of consumers. The deployment and success of voice-based second generation networks were enabled through the use of the Global System for Mobile Communications (GSM) and the Interim Standard Code Division Multiple Access (IS-95 CDMA) networks. The rise of the high data rate third generation communication systems is realised by two potential wireless radio access networks, the Wideband Code Division Multiple Access (WCDMA) and the CDMA2000. These networks are based on the use of various types of codes to initiate, sustain and terminate the communication links. Moreover, different codes are used to separate the transmitting base stations.

This dissertation focuses on base station identification aspects of the Frequency Division Duplex (FDD) WCDMA networks. Notwithstanding the ease of deployment of these networks, their asynchronous nature presents serious challenges to the designer of the receiver. One of the challenges is the identification of the base station identity by the receiver, a process called Cell Search. The receiver algorithms must therefore be robust to the hostile radio channel conditions, Doppler frequency shifts and the detrimental effects of carrier frequency offsets. The dissertation begins by discussing the structure and the generation of WCDMA base station data along with an examination of the effects of the carrier frequency offset. The various cell searching algorithms proposed in the literature are then discussed and a new algorithm that exploits the correlation length structure is proposed and the simulation results are presented.

Another design challenge presented by WCDMA networks is the estimation of carrier frequency offset at the receiver. Carrier frequency offsets arise due to crystal oscillator inaccuracies at the receiver and their effect is realised when the voltage controlled oscillator at the receiver is not oscillating at the same carrier frequency as that of the transmitter. This leads to a decrease in the receiver acquisition performance. The carrier frequency offset has to be estimated and corrected before the decoding

process can commence. There are different approaches in the literature to estimate and correct these offsets. The final part of the dissertation investigates the FFT based carrier frequency estimation techniques and presents a new method that reduces the estimation error.

Dedicated in loving memory of my father

PREFACE

The research work presented in this dissertation was performed by Mr. Seare Haile Rezenom under the supervision of Professor Anthony Broadhurst at the University of KwaZulu-Natal's School of Electrical, Electronic and Computer Engineering in the Centre of Excellence in Radio Access and Rural Technologies. This work is partly sponsored by Telkom SA and Alcatel SA as part of the Centre of Excellence programme.

Parts of this dissertation have been presented at the South African Telecommunications, Networks, and Applications Conference, SATNAC 2005, held in Drakensberg, South Africa and is to be submitted for publication to the SAIEE Africa Research Journal.

The entire dissertation, unless otherwise indicated, is the author's work and has not been submitted in part, or in whole, to any other university for degree purposes.

ACKNOWLEDGEMENTS

First and foremost, I want to express my heartfelt thanks to my supervisor, Professor Tony Broadhurst, for his meticulous guidance, encouraging attitude, and endless patience. His critical insight, constant encouragement and consistently excellent advice have been very crucial to the completion of this dissertation. I have always appreciated his willingness to set aside his time to assist me in any way. His enthusiasm, professionalism and his pursuit for the highest standards of research has inspired me immensely. I am also indebted to our Head of School and Centre of Excellence, Professor Fambirai Takawira, for providing me with the excellent research facilities and support.

I am short of words to express my gratitude and appreciation for my parents. They have taught me the value of pursuing worthy goals in life with hard work and perseverance. Their love, encouragement and never-failing support throughout my life have enabled me to overcome life's challenges. My special thanks goes to all of my family, my brothers Yohannes and Samuel, and sisters Elsa and Suzie for always being there for me.

I want to acknowledge the valued financial support extended to me from Telkom SA and Alcatel SA. I would also like to thank Mrs. Bennett, Miss. Le Breton, Mrs. McGregor, Mrs. Wayne, Mrs. Truter, Mrs. Veeran and Mr. Harrison for their help in one way or another.

Last but not least, I would like to thank all my friends and post graduate colleagues for their cordial cooperation, inspiring chats, and for making the time spent together the most memorable one.

TABLE OF CONTENTS

LIST OF FIGURES

CHAPTER 1

CHAPTER 2

CHAPTER 3

CHAPTER 4

LIST OF TABLES

LIST OF ACRONYMS

1G	First Generation
2G	Second Generation
3G	Third Generation
3GPP	Third Generation Partnership Project
AM	Amplitude Modulation
AMPS	Advanced Mobile Phone System
AWGN	Additive White Gaussian Noise
BCH	Broadcast Channel
BS	Base Station
CCPCH	Common Control Physical Channel
CDMA	Code Division Multiple Access
CP	Cyclically Permutable
CPICH	Common Pilot Channel
CRLB	Cramer Rao Lower Bound
CSC	Common Short Code
DAB	Digital Audio Broadcasting
DVB	Digital Video Broadcasting
ETSI	European Telecommunications Standards Institute
FDD	Frequency Division Duplex
FFT	Fast Fourier Transform
FIR	Finite Impulse Response
FM	Frequency Modulation
GIC	Group Identity Code
GPS	Global Positioning System
GSM	Global System for Mobile Communications
IMT-2000	International Mobile Telecommunications for the 21st Century
ITU	International Telecommunications Union
LAN	Local Area Network
LEO	Low Earth Orbit
Mcps	Million chips per second
ML	Maximum Likelihood

MC	Multi Carrier
NMT	Nordic Mobile Telephony
OFDM	Orthogonal Frequency Division Multiplex
P-CCPCH	Primary Common Control Physical Channel
PDC	Personal Digital Cellular
PDF	Probability Distribution Function
PN	Pseudo Noise
PSC	Primary Synchronisation Code
P-SCH	Primary Synchronisation Channel
RS	Reed-Solomon
SC	Single Carrier
SNR	Signal to Noise Ratio
SSC	Secondary Synchronisation Code
S-SCH	Secondary Synchronisation Channel
TACS	Total Access Communications
TC	Time Code
TDD	Time Division Duplex
TDMA	Time Division Multiple Access
UMTS	Universal Mobile Telecommunications System
VHF	Very High Frequency
WCDMA	Wideband Code Division Multiple Access
WLAN	Wireless Local Area Network

CHAPTER 1

INTRODUCTION

1.1 Evolving Wireless Communication Systems

In the late 19th century, it was soon becoming clear to many researchers that transmitting information wirelessly was possible. They were investigating the possibility of transmitting radio signals using a technique commonly called the 'spark-gap transmitter' for generating radio frequency waves. In 1896, Guglielmo Marconi was awarded a patent with the British Patent Office for his work entitled 'Improvements in Transmitting Electrical Impulses and Signals and in Apparatus There-for' [1]. Although this work used various work of other scientists, the main contribution was that it could transmit signals wirelessly over a longer distance than was previously possible. Furthermore, by sending signals across the Atlantic Ocean, Marconi demonstrated successfully that radio signals can be transmitted for hundreds of kilometres. He also succeeded, through his company, to equip communication equipments in ships. Some of the human lives saved when the ship, RMS Titanic, sank in 1912 can be attributed to the radio communication devices installed onboard

that used the spark-gap wireless technology invented by Marconi. However, it should be noted that although Marconi's early demonstrations were groundbreaking at the time, his original equipments were severely limited in that the receivers were not tuned. Moreover, his technique required the entire bandwidth of the spectrum to be allocated to one transmitter.

The limitation on bandwidth was improved with the introduction of Amplitude Modulation (AM) systems by R. Fesssenden and L. de Frost in 1906, when they made the first radio audio broadcast [2]. Three years later, a broadcasting station was constructed in the United States using an improved rotary spark-gap technology. However, human voice was used to modulate the carrier frequency, and was replaced with music later on. This has paved the way for regular wireless broadcasts for entertainment. During the years 1918–1925, radio audio broadcasts were increasing in number in the United States and Europe [3].

Before the introduction of vacuum tubes in mid 1920s, the most common type of receiving terminal was the crystal set which represented an inexpensive and technologically simple method of receiving the radio frequency signal. A crystal set consists of a long wire antenna, a variable inductor and a variable capacitor that forms a tank circuit to select the desired radio frequency.

In 1933, radio technology improved significantly when Edwin Armstrong presented a paper entitled "A Method of Reducing Disturbances in Radio Signalling by a System of Frequency Modulation." In this work, Armstrong introduced the Frequency Modulation (FM) system and showed that it improved the performance of AM systems by reducing the interference generated by the electrical equipment. This led to the subsequent experimenting of FM systems for audio broadcasting and enabled in the standard analogue television transmissions in the 1940s. It was soon realised that FM radio was a much better alternative for very high frequency (VHF) radio than the AM systems.

The improvements achieved in transmitting signals wirelessly helped to design the on-board radio transmitters used in the early missions of space communications such as the Soviet Sputnik 1, which was launched in 1957. Subsequently, many satellites

were launched in the rush for space navigation systems. The amount of information collected with these satellites using radio technology proved to be of tremendous benefit to mankind as can be understood from the advantages gained from the international routing of telephone signals in the early systems.

The technological progress in radio technology during the second half of the 20th century was largely driven by the invention of the transistor. The use of transistors instead of vacuum tubes made the devices much smaller and required far less power to operate than the vacuum tube receivers. In the early 1960s, commercial transistorized radio receivers were introduced that were small enough to fit in a vest pocket, and able to be powered by a small battery. The transistor based radio receivers were durable, because there were no vacuum tubes to burn out. Over the next 20 years, transistors replaced vacuum tubes almost completely except for very high-power applications. The wide spread deployment of transistors, integrated circuits and the rise of the internet has paved the way to an exciting era of wireless communications systems which are commonly classified as the first, second and third generation networks.

The first generation of mobile telecommunication systems were developed in the 1980s and employed analogue techniques to transmit voice. The disadvantages of these systems were their limitation on capacity and mobility. It should also be mentioned that there was no international standardising bodies at this time that could have coordinated a uniform development among many countries. On the other hand, this lack of standardisation resulted in countries developing their own proprietary systems which were found be incompatible to others. Some of these standards were the Nordic Mobile Telephone (NMT), Advanced Mobile Phone Service (AMPS) and Total Access Communications (TACTS) [4].

The second generation (2G) telecommunications systems were designed to be more robust to transmit voice than the first generation systems. This is largely due the digital techniques employed that resulted in better error correction capabilities of the system. The different standards of these systems were the IS-95 Code Division Multiple Access (CDMA), Time Division Multiple Access (TDMA), Global System for Mobile communications (GSM) and the Personal Digital Cellular (PDC). Out of

these standards, GSM has proven to be the most successful system when one compares according to the number of subscribers. At the time writing of this dissertation, the GSM network has covered 29% of the world population [5]. Although the transition from the first to the second generation networks was motivated to create a digital system, the evolution towards the third generation was influenced by a rising need for higher data rates.

With the commercial success of the second generation mobile systems, many countries continued to enhance their technologies to achieve faster data rates. In Europe, the European Telecommunications Standards Institute (ETSI) formed the Universal Mobile Telecommunications System (UMTS) to standardise future activities. Similarly in Japan and Korea, the respective authorities were continuing work to standardise their own future radio communication technologies. This resulted in the International Telecommunications Union (ITU) whose objective is to create a global standard for the third generation wireless communications known as the International Mobile Telecommunication beyond 2000. The radio access technologies which were incorporated to the IMT-2000 family of specifications are the Direct Sequence (UTRA FDD), Multi- Carrier (CDMA2000), Time Division (UTRA-TDD), Single Carrier and Frequency-time (DECT) based technologies. Therefore, the International Telecommunications Union serves as umbrella of many diverse groups of technologies. Recently, there have been a growing number of countries who are upgrading to the third generation based technologies, and there will be more adoption in the future.

Many researchers and telecommunication vendor companies are stressing for a need to increase the data rates much higher than the rates of the present Third Generation systems. Hence, some authors have already started to refer to these technologies as the Fourth Generation (4G) systems, although this nomenclature has not been standardised [4]. However, this dissertation refers to these technologies as 'next generation systems'. The main objective of the next generation technologies is to increase the data throughput while at the same time increasing the robustness of the signal towards the hostile wireless channel.

The next generation networks will also enable the provision of high-data rate short-range communications as they find excellent application for wireless hot-spots. An example of this will be the high data rate Wireless Area Networks (WLAN) that is currently being considered for standardisation. A key radio access technology that is getting a strong support is the Orthogonal Frequency Multiplexing (OFDM) technique. This technique is being used in the Digital Audio Broadcasting, Digital Video Broadcasting, and has been selected to provide an evolutionary path to the 3G communications system.

1.2 Spread Spectrum Wireless Communication Systems

This section introduces briefly a communications technology used in the third generation systems to access the radio spectrum. This technology, broadly known as the spread spectrum, was originally used in military communication systems where the primary challenge was to transmit information in such a way that its interception by the enemy was made difficult, if not impossible. One of the reasons why interception of a signal was easily achieved with the previous techniques was due to the small bandwidth used for transmission, which makes it very vulnerable to pulse jamming. Therefore, to counteract this effect, the designers of the time used two techniques that form the first principles of the spread spectrum technology and can be summarised as follows.

- The bandwidth of the signal was made much greater than the message bandwidth. This was done to minimise the effects of pulse jamming.
- The bandwidth of transmission was determined by another signal which is independent of the message signal. This was intended to minimise interception by any receiver that did not know the identity of the independent signal.

Spread spectrum systems were also found to provide good resolution of the multi-path components of a transmitted signal. This characteristic has made them very attractive to be used in commercial communication systems, where the quality of reception is greatly improved by combining the multi-path components using a Rake receiver [6].

Figure 1-1 shows the basic elements of a spread spectrum communication system. It is shown that the model includes all the elements of a conventional communications system, i.e. channel encoder, modulator, demodulator and channel decoder. In addition to these elements, a spread spectrum system employs identical code generators in order to increase the bandwidth of the transmitted signal. The process of multiplying a signal with a specific code prior to transmission is termed spreading. In order to recover the transmitted signal at the receiver, a similar process is performed which is to multiply the received signal with a replica of the specific code used at the transmitter - a process termed despreading.

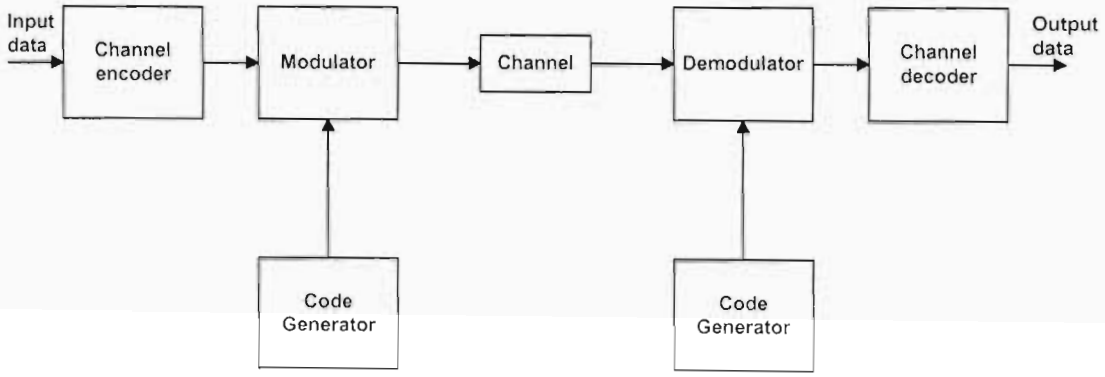

Figure 1-1: A model of a spread spectrum communications system

1.3 The Need for Synchronisation

Synchronisation procedures are generally required by various stages of a digital communications system. Synchronisation is concerned with the generation of a concurrent system of reference such that signal alignment in some particular domain is attained. Synchronisation may take place in the temporal and/or frequency domains. Synchronisation can also be viewed as an estimation problem where one or more parameters have to be determined from a given signal. Different levels of synchronisation may be defined such as carrier, code, bit, symbol, frame and network synchronisation.

In Section 1.2, the basic building blocks of a spread communication system has been described. It has also been mentioned that identical code generators need to be used in order to properly decode the transmitted information data. One of the main challenges for the designer of a spread spectrum communications receiver is to align the codes used at the transmitter with a locally generated code at the receiver. This problem is commonly referred to as code acquisition and its importance as an essential function of a spread spectrum system has always been recognised. A widely used technique for code synchronisation is to search through all potential code phases until synchronisation is achieved. Each code phase is evaluated by attempting to despread the received signal. If the code phase is correct, despreading will occur and the signal can be decoded. If the code phase is wrong, the signal will not be decoded and the communications process will fail.

This dissertation considers a synchronisation problem in a frequency division duplex (FDD) Wideband Code Division Multiple Access (WCDMA) system. This system uses many codes to separate the transmitters and the receivers require a design in such a way that the correct transmitted code has to be detected efficiently. This problem is exacerbated by equipment limitations, such as the carrier frequency offset. Therefore, this dissertation also investigates the damaging effect of the carrier frequency offset on the synchronisation process and presents some mitigation techniques.

1.4 Dissertation Outline

Chapter 2 starts by introducing code acquisition systems in CDMA2000 and WCDMA networks. In order to appreciate the current specifications in the 3GPP Standard, the pioneering research efforts in code acquisition in a WCDMA system are presented. This is followed by describing the several synchronisation codes which are used to assist in the code acquisition procedure. Moreover, some of the downlink channels that represent the WCDMA base station data are presented. A model for the base station is then developed. This model is used to generate the transmitted base station data. Finally, the effect of the carrier frequency offset on the transmitted base station data is illustrated.

In Chapter 3, an overview of the research efforts in the literature directed at improving the performance of the cell searching system is presented. The effects of the carrier frequency offset are then examined and some mitigation techniques are explored. This is followed by an investigation of the wireless channel considered in this dissertation which uses filtering two white Gaussian variates to generate a Rayleigh process. A new method of exploiting the symbol structure of a WCDMA frame is presented and its performance is compared with the conventional system by considering the Stage 3 of the cell searching system. It is shown that this method provides an improvement when compared to the conventional system. It is also shown that the choice of the correlation length used in cell searching systems need not be restricted to limited values.

In Chapter 4, the estimation of a carrier frequency offset in a WCDMA system is emphasised. A mathematical model for carrier frequency estimation is formulated. A literature review of the estimation techniques for the carrier frequency offset is then presented. This chapter examines the fast Fourier transform (FFT) based carrier frequency estimation technique. A new algorithm that builds on the conventional FFT based algorithm is then presented. The performance of the new method is examined in an additive white Gaussian noise and flat fading channels. This chapter provides performance results of the proposed method which show significant improvements when compared to the conventional method. This chapter also presents an analytical treatment of the subject. Finally, a technique is examined to enhance further the performance of carrier frequency offsets.

In Chapter 5, conclusions are drawn and some topics for future work are described.

1.5 Original Contributions in this Dissertation

The original contributions in this dissertation include:

1. A technique that exploits the correlation interval of the symbols in a WCDMA frame using variable chip correlation lengths

2. A technique that estimates the carrier frequency offset in a WCDMA receiving terminal which is based on the fast Fourier transform

Parts of the work in this dissertation have been presented, or submitted by the author to the following conferences and journals:

1. S. Rezenom and A. Broadhurst, "Stage 3 performance of W-CDMA cell search for various chip correlation lengths", *South African Telecommunication, Networks and Applications Conference (SATNAC)*, September 2005, Drakensberg, South Africa.

2. S. Rezenom and A. Broadhurst, "Window function effects on the performance of an FFT-based W-CDMA frequency offset estimator", to be submitted to the *SAIEE Africa Research Journal.*

CHAPTER 2

FUNDAMENTALS OF WCDMA CODE ACQUISITION

2.1 Introduction

The third generation radio access technologies, CDMA2000 and WCDMA, employ different techniques to communicate between the receiving terminal and the transmitting base station. This is accomplished when the receiving terminal acquires the correct code that spread the transmitted signal at the base station. Although the emphasis of this dissertation is on a WCDMA system, code acquisition in a CDMA2000 system is briefly described in Section 2.2. In Section 2.3, an overview of code acquisition in a WCDMA system is described citing some differences with the CDMA2000 system. Section 2.4 discusses selected research efforts on code acquisition in WCDMA systems which were finally incorporated into the 3GPP Standard. In Section 2.5, the procedures of code acquisition as outlined by the 3GPP Standard are presented. Several synchronisation codes are used to assist in WCDMA code acquisition and their construction is described in Section 2.6. In order to simplify the process of code synchronisation at a receiving terminal, the WCDMA base station transmits several types of downlink channels which are presented in Section 2.7. Section 2.8 presents a model for a transmitting base station. Finally, in Section 2.9, the effect of carrier frequency offset on the transmitted data is illustrated.

2.2 Code Acquisition in a CDMA2000 System

Code acquisition in a CDMA2000 system is based on a synchronous system. All the base stations are synchronised to a universal time source, such as the Global Positioning System (GPS). The base station transmits a common pilot channel which contains a short pseudo noise (PN) code. The different phases of this PN code are used to differentiate the base stations deployed in the system.

In a CDMA2000 system, the base station transmits the same PN code with different phase offsets [7]. The number of available phase shifts determines the maximum number of available base stations to be used in the system. Hence, each base station uses a unique PN phase offset used for its identification. CDMA200 systems use 512 phase offsets of a unique PN code to differentiate between transmitters. Therefore, to correctly identify the transmitting base station, the receiving terminal has to acquire the exact starting point of the short PN code of the base station. In effect, this means the terminal has to search for this short code by correlating the received signal with each shift of the unique PN code. The peak correlation value will thus identify the transmitting base station.

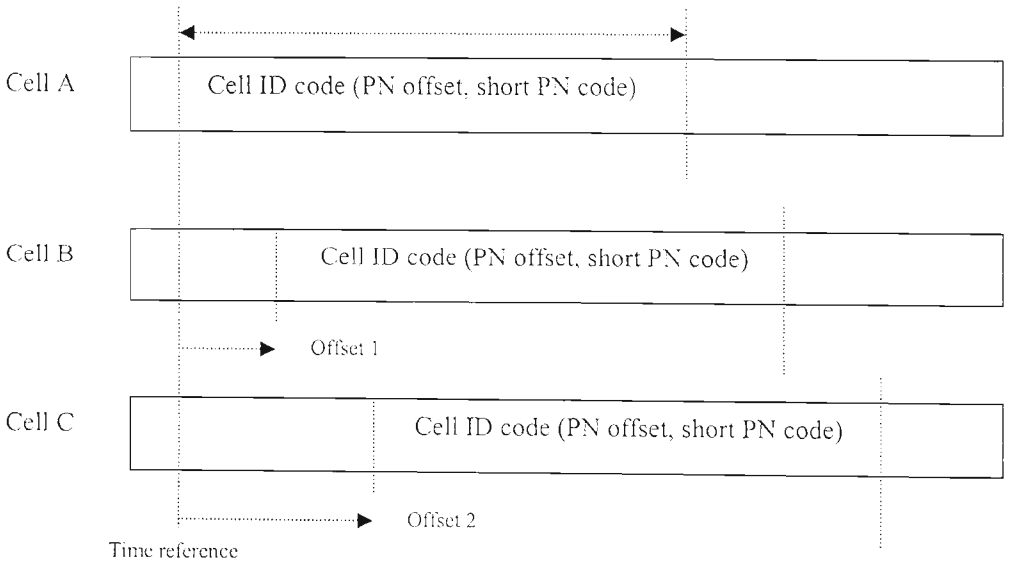

Figure 2-1: Synchronisation in a CDMA2000 system.

Figure 2-1 shows PN code allocation in a CDMA2000 system. In this illustration, three base stations are using the same PN code but with different offsets. The timing reference used is also shown. Each base station transmits according to the required PN offset. Here, Cell B and Cell C transmit according to the specific shifts 'offset 1' and 'offset 2'. It is the task of the mobile station to accurately determine this unique PN offset. Assuming the GPS gives accurate timing reference, cell search proceeds by correlating the received sequence with the specific shifts of the PN codes. The point of maximum correlation is used to determine the offset and a possible candidate of the serving base station.

2.3 Code Acquisition in a WCDMA System

Unlike CDMA2000, the WCDMA system uses asynchronous transmission. The transmitting base stations are not synchronised to any external time source. Therefore, the concept of using different code shifts of the same scrambling code, as used in the CDMA2000 system, cannot be employed here as there is no known timing reference. Moreover, there is no known code and frequency reference. The 3GPP standard [8] has 512 scrambling codes to differentiate the base stations from one another. This allows for each base station to be identified by these scrambling codes. Each base station uses one and only one of these 512 scrambling codes to scramble its data before transmission. These scrambling codes are also known as base station identities.

The receiving terminal needs to have a mechanism that searches through the 512 scrambling codes in order to identify the correct transmitting base station. Figure 2-2 shows three WCDMA base stations, each using a 10 ms scrambling code to transmit its data. It should be noted that these codes are different from each other. In order to communicate to the base station, a receiving terminal has to identify one of these three scrambling codes. A detailed treatment of the scrambling code generation is given in Section 2.6.

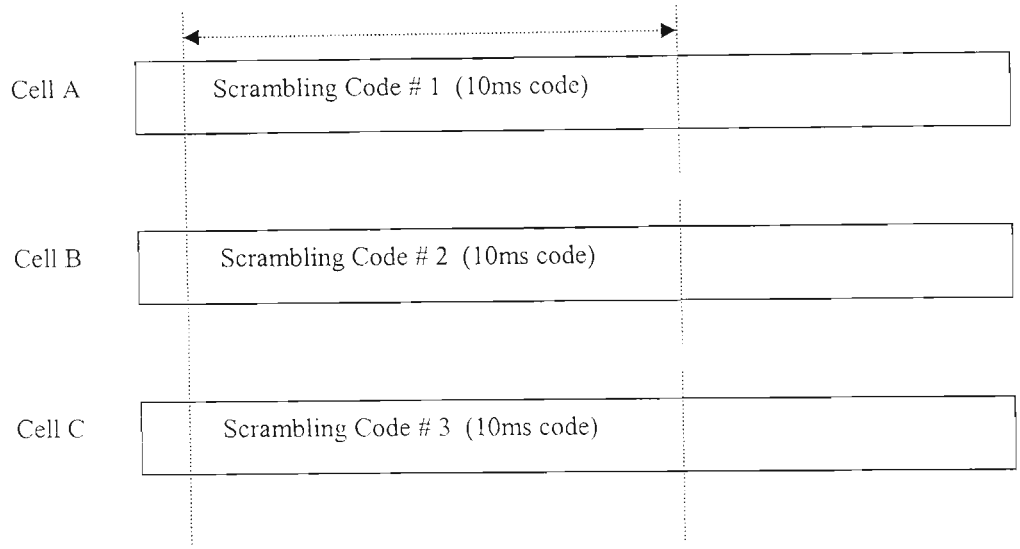

Figure 2-2: Code allocation in a WCDMA System

Network planning in a WCDMA system requires allocation of scrambling codes to the base stations. Code acquisition in an asynchronous system thus involves the process of searching for a particular scrambling code used by a transmitting base station.

During transmission, the transmitted signals encounter propagation uncertainties such as multipath fading, Doppler shift and due to equipment limitations frequency offset, clock drift, etc. It is important to mention at this point that cell search does not only deal with time and code acquisition. The process of frequency acquisition is also included in the process. Since the receiving terminal is operating in such hostile radio channel conditions, the receiver is presented with a daunting task of identifying this long scrambling code out of a potential set of 512 candidate codes.

2.4 Background on Cell Search

A receiving terminal must search through all scrambling codes to synchronise and communicate with the transmitting base station. A simple conceptual approach requires a sequential search through all the scrambling codes, as used in [9], to determine the scrambling code that would give peak correlation. An assumption made

in this approach, which is very hypothetical, is the existence of a perfect match in frame timing between the received signal and the unknown scrambling codes. This makes the acquisition time and implementation complexity of the receiver to be very large.

Another approach would be to assemble parallel correlators, each matched to the 512 scrambling codes. The complexity of such a system would be enormously large. Neither of the previous two approaches can be realistically implemented. The challenge of cell searching systems is designing techniques that decode the transmitted scrambling code with good reliability and implementation complexity.

In this section, some of the important research efforts that consolidated the cell searching algorithms are overviewed. The first documented study to decrease the complexity of cell search was reported in 1996 when Adachi *et al.* proposed a two-stage procedure that reduced the acquisition time and implementation complexity. One year later, this was improved further when Higuchi *et al.* proposed a three-stage procedure and showed it performed better when compared to Adachi *et al.* This proposal formed part of Japan's submission to the WCDMA standardising body. The cell searching procedures were further refined when Nystrom *et al.* and Sriram *et al.* proposed techniques that contributed significantly to decrease the level of complexity. An overview of the contributions made by these authors is presented below.

2.4.1 Adachi *et al.*

In order to improve on the concept of sequential searching of the scrambling code from the received signal, Adachi *et al.* in [10] proposed a technique whereby each base station transmits a short code at the start of its frame. This short code (which the authors called the Common Short Code) identifies the start of the frame. At the receiving end, the terminal searches for the common short code and once a good correlation candidate with the common short code is found, it searches through the 512 scrambling codes to identify the transmitting base station.

Figure 2-3 shows three base stations transmitting the same common short code with different signal strengths. The receiving terminal correlates the received signal with the common short code. The signal from Base Station 2 (BS 2) is shown to have the highest correlation value. This indicates the frame timing of the received signal. The mobile terminal would then proceed to correlate each of the scrambling codes used by the system with the received signal. The scrambling code with the highest correlation value will be selected as a successful candidate to identify the base station. It should be noted that this method is a two step procedure.

Step 1: Identify the timing information

Step 2: Identify the scrambling code

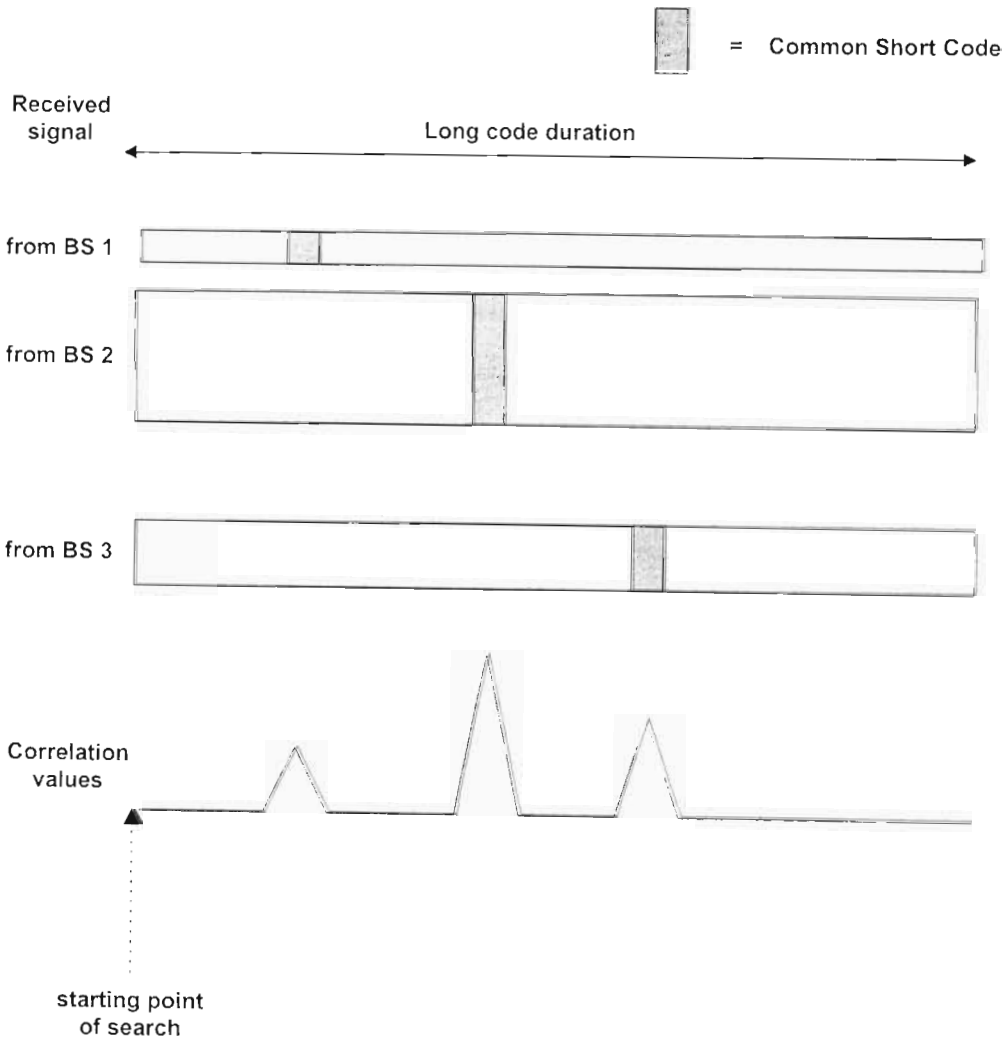

Figure 2-3: Adachi *et al.*'s two step cell searching procedure

For the common short code, the authors used 64 chip sequences selected from a set of orthogonal Gold sequences and a matched filter with the same sequence was used at the receiver. The authors reported acquisition using this technique takes less than 900 ms in 90 % of the terminals within the base station coverage area when simulated in a Rayleigh fading channel.

2.4.2 Higuchi *et al.*

Although the technique proposed by Adachi *et al.* was unique in its contribution to identify the timing information, its disadvantage lies in using one common short code for every frame. This approach delays the identification of the scrambling code as the receiver waits for one frame or more to start the second step. For example, if the terminal fails to identify a strong timing candidate within one frame due to channel fluctuations, it will have to extend the search to the next frame. Moreover, it still has to correlate the received signal with each of the 512 scrambling codes bringing more delays. Therefore, further enhancements are required to counteract this effect and Higuchi *et al.* in [11] proposed a technique to achieve that.

These authors investigated the effect of grouping the scrambling codes and transmitting information about the grouped codes. They used the term 'Group Identification Codes' (GIC) to represent information about the code groups. Each GIC would then represent several scrambling codes. The base station transmits the group code of its scrambling code along with the traffic data.

Figure 2-4 shows a transmission schematic of the base station proposed by the authors. The frame is divided into M parts called slots and the common short code is transmitted in each slot. This is an improvement to [10] which uses one short code per frame. The GIC is transmitted together with the common short codes in each slot. However, to reduce interference, the long scrambling code is masked at the positions where the GIC and common short codes are transmitted. This helps to increase the reliability of timing detection at the receiver.

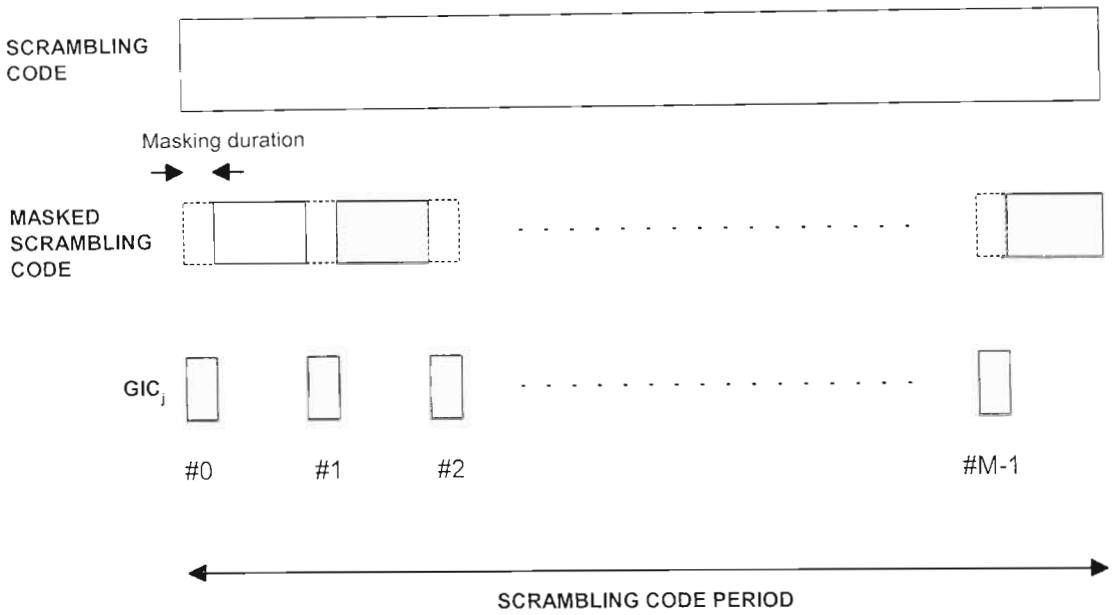

Figure 2-4: Schematics of Higuchi *et al.*'s algorithm

At the receiving end, the terminal uses a filter matched to the common short code to determine the timing information. However, unlike Adachi *et al.*'s method, this procedure will only give the start of timing of a particular slot. Once the terminal acquires the timing information, it continues the search by correlating the received signal with each of the available code groups. The success of this step gives the group identity of the transmitted scrambling code. The search continues to find the transmitted scrambling code by correlating the received signal with all the scrambling codes represented by the group codes. The best candidate in this stage will then give the transmitted scrambling code and the timing of the frame. Contrary to [10], this method identifies the frame timing once it determined the transmitted scrambling code. Therefore, their algorithm is summarised as,

Step 1. Identify the slot timing

Step 2. Identify the code groups

Step 3. Identify the scrambling code and the frame timing

2.4.3 Nystrom *et al.*

A subsequent study by Nystrom *et al.* [12] showed further improvement to the complexity by combining the detection of the group identity code and frame boundary in one stage. To accomplish this goal, the authors introduced a specially designed orthogonal modulation sequence when selecting codes for GIC [12]. The essential improvement in this algorithm is the advantage gained in identifying the frame timing before the start of brute force de-scrambling. This can be illustrated further as follows. Consider a GIC code of length n chips, chosen from a list of L scrambling code groups as was used by Higuchi *et al.* This GIC can be written as

$$C_j = \left(c_{j,0},\ c_{j,1},\ c_{j,2},\ \ldots\ c_{j,n-1}\right) \qquad j = 0,\ 1,\ \ldots\ L-1 \tag{2.1}$$

and is selected from a list of scrambling code group C

$$\widetilde{C} = \left(C_0,\ C_1,\ C_2,\ \ldots\ C_{L-1}\right) \tag{2.2}$$

Their contribution is in modulating the above sequence with a specially designed sequence H

$$H = \left(h_0,\ h_1,\ h_2,\ \ldots\ h_{N_s-1}\right) \tag{2.3}$$

where N_s represents the total number of slots in the frame . The sequence in (2.2) is now modified to

$$\widetilde{C} = \left(h_0 C_j,\ h_1 C_j,\ h_2 C_j,\ \ldots\ h_{N_s-1} C_j\right) \qquad j = 0,\ 1,\ 2,\ \ldots\ L \tag{2.4}$$

It is seen in (2.4) that each slot in the frame contains a different code when compared to (2.1) which uses the same code. In this technique, to represent the group identity, the base station transmits (2.4) instead of (2.1) as was used in Higuchi *et al.* The remaining transmitted codes remain unchanged.

In order to explain the decoding of (2.4) at the receiving terminal, consider the received sequences at each of the masked positions in the frame can be written as

$$r = (r_0, r_1, \ldots r_{N_S-1}) \tag{2.5}$$

The terminal computes the metric A,

$$A = \begin{pmatrix} r_0 C_0^H & r_1 C_0^H \ldots & r_{N_S-1} C_0^H \\ \vdots & \ddots & \vdots \\ r_0 C_{L-1}^H & r_1 C_{L-1}^H \cdots & r_{N_S-1} C_{L-1}^H \end{pmatrix} \tag{2.6}$$

where C_L^H represents the Hermitan of the group identity matrix in (2.4). Let $\widetilde{H}$ denote a matrix that contains all the cyclic shifts of (2.3) and can be written as

$$\widetilde{H} = \begin{pmatrix} h_0 & h_1 \ldots & h_{N_S-1} \\ \vdots & \ddots & \vdots \\ h_{N_S-1} & h_{N_S-2} \cdots & h_0 \end{pmatrix} \tag{2.7}$$

The terminal then computes the decision metric

$$D = A\widetilde{H}^H \tag{2.8}$$

where $\widetilde{H}^H$ is the Hermitan of $\widetilde{H}$. The row and column that maximise the decision metric D gives the group code identity number and the start of frame boundary, respectively.

This method improves the detection performance as it allows for the simultaneous detection of the code group and the frame timing. The authors reported a decrease in complexity as compared to Higuchi *et al.* However, they mentioned a slight increase in processing delay. The procedures in the algorithm can be summarised as

Step 1. Timing synchronisation

Step 2. Code group and frame identification

Step 3. Scrambling code identification

2.4.4 Sriram *et al.*

One disadvantage of Nystrom *et al.* is that, if the modulation sequence in (2.3) is not cyclically distinct, many of the rows in (2.7) would not be different. The terminal would then find it difficult to distinguish between shifts in the received code words leading to a false detection of frame boundary.

To counteract this problem, Sriram *et al.* in [13][14] employed a different code selection scheme to represent the code group identity. The authors used a class of error correcting codes called cyclically permutable (CP) codes [15] to transmit information about the scrambling codes. These codes have been employed in pulse position modulation systems and as hopping sequences for frequency-hopped spread spectrum systems.

By definition, a CP code of length n is a set of code words such that no code word is a cyclic shift of another, and each code word has n distinct cyclic shifts [14]. For example, consider the following sequence

$$\widehat{C} = \left(\widehat{C}_0, \widehat{C}_1, \widehat{C}_2, \ldots \widehat{C}_{N_g-1}\right) \tag{2.9}$$

This sequence is a CP code and is transmitted by the base station in each slot position of the frame to represent information about the code groups. As each cyclic shift of the (2.9) is a different codeword, the terminal can use this to establish the timing of the frame boundary.

In addition to using the CP codes, the authors extended the concept further by choosing the cyclically permutable code to be a subset of an error correcting cyclic block code. For this purpose, they selected the Reed Solomon (RS) codes because they have a maximum possible distance between code words for a given block length

[14]. For example, for a frame consisting of 16 slots, an RS (16,3) over GF(17) is used which can encode $17^2 = 289$ code groups. Alternatively, for a frame consisting of 15 slots, and RS (15,3) over GF(16) is used and can encode $16^2 = 256$ code groups using the CP codes.

At the receiving end, the procedures are similar to [12] and are summarised as

Step 1: Identify the timing
Step 2: Identify the code groups and the frame boundary timing
Step 3: Identify the scrambling code

The main contribution of this method is detection of the frame boundary timing with a high reliability than [12]. The authors reported a significant improvement in synchronization can be obtained using this code selection. As a result, their scheme is presently used to transmit grouping information about the scrambling code in the 3GPP standard [8].

2.5 The 3GPP Standard

The research efforts described in the previous section were submitted for consideration to the WCDMA standardising body. In due process, some enhancements were made and it was finally incorporated into the Standard. It should be noted that the 3GPP standard introduced new notations to the synchronisation codes previously proposed by some authors. The common short codes that were used by Adachi *et al.* and Higuchi *et al.* became the Primary Synchronisation Codes (PSC). The synchronisation codes that were derived from the cyclically permutable codes, as proposed by Sriram *et al*, were termed the Secondary Synchronisation Codes (SSC). The length of these codes is changed to 256 chips instead of the 64 chips, as was first employed in [10][11]. It should also be noted that the design of the synchronisation codes can be extended to cater for either 64 or 256 chips. Moreover, the Standard specified the use of 15 slots in one WCDMA frame. Previously, some authors used 16 slots in their studies [12][13] while others used 15 slots [16][17].

In [18], the 3GPP Standard specified three steps to be used for cell search in the WCDMA system. The following paragraphs describe the three steps as they appear in [18].

Step 1: Slot synchronisation

Step 2: Frame synchronisation and code-group identification

Step 3: Scrambling-code identification

During the first step of the cell search procedure, the receiving terminal uses the primary synchronisation code to acquire slot synchronisation to a cell. This is typically done with a single matched filter (or any similar device) matched to the primary synchronisation code which is common to all cells. The slot timing of the cell can be obtained by detecting peaks in the matched filter output.

During the second step of the cell search procedure, the receiver uses the secondary synchronisation code to find frame synchronisation and identify the code group of the cell found in the first step. This is done by correlating the received signal with all possible secondary synchronisation code sequences, and identifying the maximum correlation value. Since the cyclic shifts of the sequences are unique the code group as well as the frame synchronisation is determined.

During the third and last step of the cell search procedure, the terminal determines the exact primary scrambling code used by the found cell. The primary scrambling code is typically identified through symbol-by-symbol correlation over the CPICH with all codes within the code group identified in the second step. After the primary scrambling code has been identified, the Primary CCPCH can be detected and the system and cell specific BCH information can be read.

The structure and function of the WCDMA channels used in the Standard, such as the CPICH, CCPCH and BCH are presented in Section 2.7.

2.6 Synchronisation Code Design

Research into the construction of the synchronisation codes started with the use of the common short codes proposed in [10][11], where the authors used a 64 chip short Walsh orthogonal codes. Similarly, the codes presented in [11] used similar codes to separate the group identities. In [19], the authors employed a modulation sequence to achieve further separation between the group identity codes. In [13], the authors used CP codes for the group identity codes.

The above approaches were finally incorporated to the Standard in [8] with some modifications. This section presents the current design techniques for the synchronisation codes used in the WCDMA system.

2.6.1 Primary Synchronisation Code

In Section 2.4, it was discussed that Higuchi *et al.* proposed a common short code to recover the timing information. In [20], a submission by Siemens to the 3GPP, the authors proposed a hierarchical sequence with good correlation properties in the presence of a frequency error. In a similar submission, Texas Instruments in [21][22] proposed synchronisation codes based on the Golay sequences [23] and their results showed a reduction in complexity and good autocorrelation properties. In a subsequent effort, [24] combined the merits of the previous techniques and proposed a generalised hierarchical Golay sequences. They found out that these sequences have a lower complexity than either of the previous submissions while preserving the good autocorrelation properties even under high frequency errors.

In [8], the 3GPP standard incorporated the generalised hierarchical Golay sequences [24] to construct the PSC codes. Let the vectors u and v be defined as

$$u = (x_1, x_2, \ldots, x_{16}) = (1, 1, 1, 1, 1, 1, -1, -1, 1, -1, 1, -1, 1, -1, -1, 1) \quad (2.10)$$

$$v = (1, 1, 1, -1, -1, 1, -1, -1, 1, 1, 1, -1, 1, -1, 1, 1) \quad (2.11)$$

The PSC code C_{psc} is then constructed as

$$C_{psc} = (1+j)(u \otimes v) \tag{2.12}$$

where j is the complex notation and $\otimes$ is the Kroneker product [25]. The sequence (2.12) represents a 256 chip-long sequence transmitted in the first 256 chips of every slot of a WCDMA frame and is the same throughout the system.

2.6.2 Secondary Synchronisation Code

There are a total of 16 secondary synchronisation codes that are generated by the base station. The 16 secondary synchronisation codes $\{C_{ssc}^1, C_{ssc}^2, ..., C_{ssc}^{16}\}$ are complex-valued with identical in-phase and quadrature components. These are constructed according to the 3GPP Standard [8] from position-wise multiplication of a Hadamard sequence and a sequence z, defined as:

$$z = (b, b, b, -b, b, b, -b, -b, b, -b, b, -b, -b, -b, -b, -b) \tag{2.13}$$

where

$$b = (x_1, x_2, x_3, x_4, x_5, x_6, x_7, x_8, -x_9, -x_{10}, -x_{11}, -x_{12}, -x_{13}, -x_{14}, -x_{15}, -x_{16}) \tag{2.14}$$

and $(x_1, x_2, ..., x_{16})$ is described in (2.10).

The rows of the Hadamard matrix H_8 are used to construct the sequence recursively as follows

$$\mathrm{H}_0 = (1)$$
$$\mathrm{H}_k = \begin{pmatrix} \mathrm{H}_{k-1} & \mathrm{H}_{k-1} \\ \mathrm{H}_{k-1} & -\mathrm{H}_{k-1} \end{pmatrix} \tag{2.15}$$

where $k \geq 1$. Let $h_k(i)$ represent the i^{th} symbol of the sequence H_k in (2.15) and $z(i)$ denote the i^{th} symbol of the sequence in (2.13) where $i = 0,1,2,\ldots,255$. The m^{th} SSC sequence C_{ssc}^m with $m = 1,2,\ldots,16$, is constructed as

$$C_{ssc}^m = (1+j)\left(h_k(0)\times z(0),\ h_k(1)\times z(1),\ \ldots,\ h_k(255)\times z(255) \right) \tag{2.16}$$

where $k = 16\times(m-1)$. The sequence (2.16) thus represents the 256 chip long SSC code sequence used in the first 256 chips of every slot in a WCDMA frame.

2.6.3 Scrambling Code

The scrambling code is employed as a means of base station separation. It spreads the base band signal into a wideband signal. Given the sensitivity of a CDMA system, the scrambling codes must maintain very good auto-correlation properties. This requirement calls for the timing between the receiving terminal and the base station must be maintained within a range of one chip period. A timing offset of more than one chip between the data sequences of the receiver and the base station destroys the good autocorrelation and results in the failure of the receiver communications process. Therefore, the 3GPP standard proposed the use of Gold codes as a downlink scrambling codes to identify base stations. This dissertation uses the generator algorithm proposed by the 3GPP standard [8].

Gold codes have very good correlation properties. There are a total of $2^{18}-1 = 262143$ Gold code sequences. Of these only 512 are employed to identify base station identities. There is a special method of selecting these 512 codes from the possible set of $2^{18}-1$ codes. The codes are numbered as $0,1,2,\ldots,262142$. Let $n = 16\times BS_{ID}$ where $BS_{ID} = 0,1,2,\ldots,511$ is the primary scrambling code set and n is

the scrambling code number. The primary scrambling code set BS_{ID} is used to represent the cell identification. It is divided into 64 code groups. Each code group consists of 8 scrambling codes. When there is a need to identify a base station with BS_{ID}, it scrambles its data using the scrambling code number $n = 16 \times BS_{ID}$.

The base station also uses another scrambling code called the secondary scrambling code. It is used to scramble other data that are not associated with base station identification. These are numbered as $n = 16 \times BS_{ID} + k$, where BS_{ID} is the primary scrambling code set and $k = 1,2,...,16$ is the secondary scrambling code set within the primary code set. For every primary scrambling code set, there are 15 secondary scrambling codes. However, only the primary scrambling code set is used for cell identification purposes.

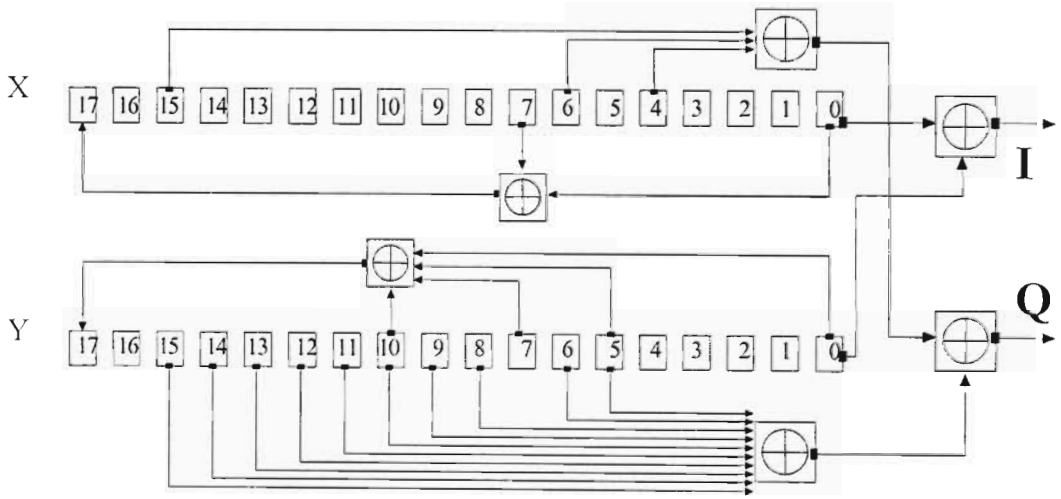

Figure 2-5: Scrambling code generator [TS 25.213]

The generator of the scrambling codes uses two shift registers X and Y. This is shown in Figure 2-5. Each register uses 18 clocked shift registers with feedback of the data using modulo-2 adders ⊕ with the exclusive-OR operation. This generates the I and Q channel scrambling codes.

To illustrate the scrambling code generation process, consider a case where it is desired to represent a base station with an identification number BS_{ID}. Therefore, the corresponding scrambling code number $n = 16 \times BS_{ID}$ has to be generated. The following procedure is performed by the generator.

Step 1: Register X initialised as $X_0 = 1, X_1 = X_2 = \ldots X_{17} = 0$

Step 2: Register X is shifted n times.

Step 3: Register Y initialised as $Y_0 = Y_1 = \ldots X_{17} = 1$

Step 4: Clock Registers X and Y and collect I and Q outputs to fill up a frame (38400 chips)

Step 5: Go to Step 1 for the next frame.

2.7 WCDMA Downlink Channels

Culminating from the various studies mentioned, the 3GPP standard uses different types of channels to facilitate the synchronisation process. These are the Primary Synchronization Channel (P-SCH), the Secondary Synchronization Channel (S-SCH), the Common Pilot Channel (CPICH) and the Primary Common Control Physical Channel. However, the frame structure in a WCDMA system is presented here first.

2.7.1 Frame Structure of a WCDMA System

For purposes of providing an easier evolutionary path from the GSM system, the WCDMA system is designed to be compatible with it. The frame length of the WCDMA system is thus maintained at 10 ms [8]. The frame structure of a WCDMA system [8] is shown in Figure 2-6.

Each frame is of 10 ms duration and contains 38400 chips. There are 15 slots in each frame containing 10 symbols of 256 chips. Different spreading factors may be used which may lead to different data rates. Nonetheless, the chip rate is fixed at 3.84 Mcps.

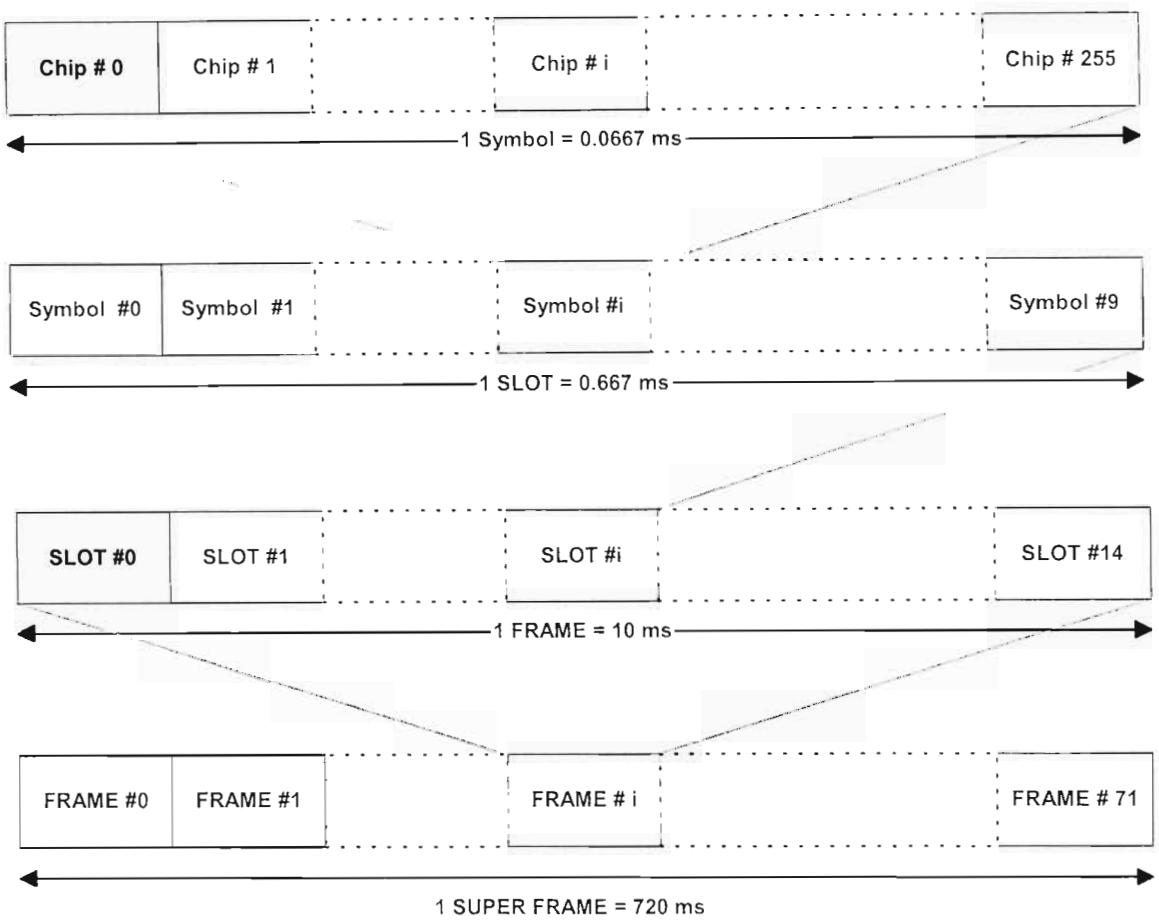

Figure 2-6: Frame structure of a WCDMA system

2.7.2 Primary Synchronisation Channel

The Primary Synchronisation Channel (P-SCH) is made up of the primary synchronisation code which is transmitted as the first 256 chips of each slot and occupies one-tenth of the time slot as shown in Figure 2-7.

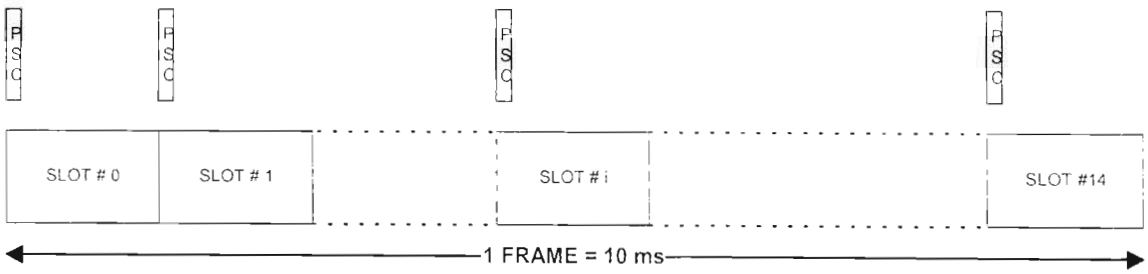

Figure 2-7: Primary synchronisation channel allocation in a WCDMA system

In one frame therefore, 15 PSC codes are transmitted. This constitutes the P-SCH. The PSC is the same for all cells as it is the same from slot to slot. The main use of the PSC sequence is to acquire a timing reference with the base station. The mobile station has to search for this particular code to acquire a timing reference. The detection of the PSC at the receiver signals the start of the slot of the base station data.

2.7.3 Secondary Synchronisation Channel

The secondary synchronisation channel represents a scrambling code transmitted by the base station. In the current standard, there are 16 secondary synchronisation codes available. Let C_{ssc}^{m} where $m = 1,2....,16$ denote the available SSC codes. However, since there are 15 slots in a frame, only 15 SSC can be used to make the S-SCH. In the 3GPP standard [8], such an arrangement of the S-SCH in a frame represents one scrambling code group. Since there are eight long scrambling codes with a code group, this S-SCH sequence thus represents eight scrambling codes. This gives 64 possibilities of S-SCH allocations in a frame to completely represent the 512 scrambling codes that are available codes to identify base stations.

To further illustrate the S-SCH allocation in a frame, one needs to look at the code group table used by the Standard as shown in the Appendix. This table lists the values of m used to construct the appropriate secondary synchronisation code C_{ssc}^{m}. The order of the codes given in the table must be used to fill a secondary synchronisation channel according to the scrambling code desired to be transmitted. For example, if it is desired to identify a base station with $BS_{ID} = 5$, a scrambling code $n = 16 \times BS_{ID} = 90$ needs to be generated as explained in Section 2.6 to scramble the data. The base station needs to transmit the group code of this scrambling code. It should be noted that the first eight base station identities, $BS_{ID} = 0,1,2,...,7$, belong to the first scrambling code group in order to represent all the 512 codes in 64 code groups. It follows that $BS_{ID} = 5$ belongs to the first code group. To determine the order of the SSC, and subsequently the S-SCH to be used, the base station transmitter needs to look at the Appendix. It can be seen that the SSC sequence

$\{1, 1, 2, 8, 9, 10, 15, 8, 10, 16, 2, 7, 15, 7, 16\}$ would have to be transmitted at each of the slots in the frame. This order of the SSC must be maintained through all frames transmitted by the base station. This situation is depicted in Figure 2-8 which illustrates the P-SCH and S-SCH transmission structure in a WCDMA frame for a base station with $BS_{ID} = 5$.

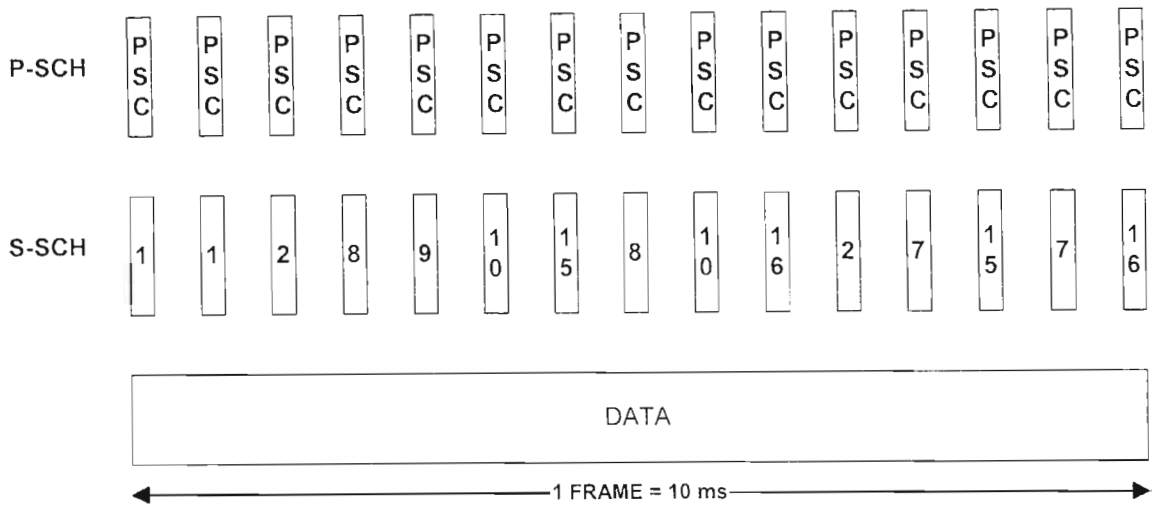

Figure 2-8: Allocation of synchronisation channels in a WCDMA frame

2.7.4 Common Pilot Channel

The Common Pilot Channel (CPICH) is an un-modulated fixed power channel scrambled with the cell specific scrambling code. It is made up of a pre-defined symbol sequence. As it has a spreading factor of 256 chips, there are 10 symbols (20 bits) in each slot. This gives a symbol rate of 15 kbps. Owing to its fixed power, it can be used as phase reference, channel estimation, and hand over measurements. Figure 2-9 shows the arrangement of the CPICH in a WCDMA frame and super frame.

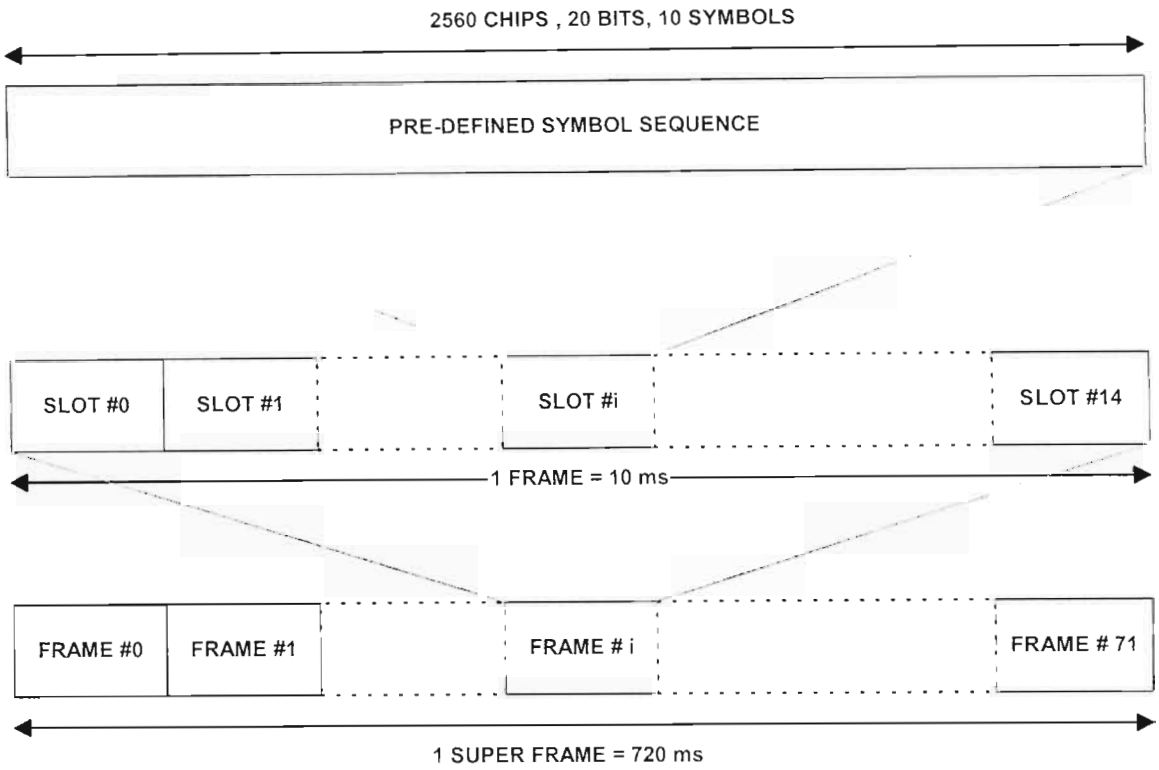

Figure 2-9: CPICH channel arrangement

2.7.5 Primary Common Control Physical Channel

The Primary Common Control Physical Channel (P-CCPCH) contains the broadcast information of the base station. This broadcast information is transmitted in the Broadcast Channel (BCH). It contains random access codes, code channels of other common channels and other base station information absolutely necessary for system proper system functions. It is a pure data channel. It has a fixed data rate of 30 kbps. Its transmission scheme is depicted in Figure 2-10. It can be observed that the P-CCPCH is not transmitted at the first 256 chips of each slot. Instead the synchronisation codes are transmitted in this time period. The P-CCPCH needs to be demodulated by all mobile stations in the system. Therefore high transmission power is needed to enable this effect.

The P-CCPCH has a great importance in cell search. Since it contains the necessary base station information, the success of cell search depends on the successful decoding of the data in this channel. Moreover, in a process of hand over, where a

mobile station needs to change its location to another cell, there is no need to search through all the scrambling codes to synchronise to this new station. However, this can be achieved with less effort by reading the scrambling codes of the nearby station contained in the broadcast channel.

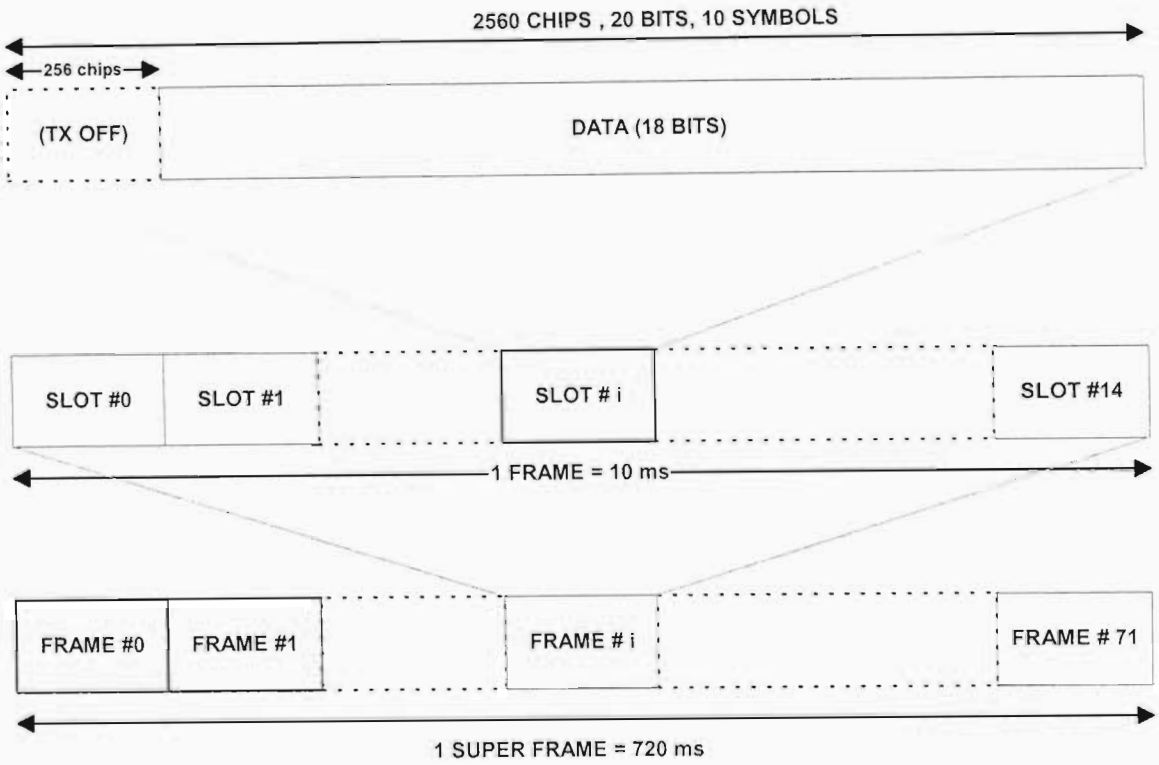

Figure 2-10: P-CCPCH channel arrangement

2.8 Base Station System Model

A WCDMA base station needs to send the correct order of the synchronisation codes. It also needs to scramble the data with the assigned scrambling code. The base station system model used in this thesis is shown in Figure 2-11. The synchronisation channels, P-SCH and S-SCH, are combined together to form the synchronisation channel. The CPICH represents a predefined sequence that is scrambled by the cell specific scrambling code. A string of 1's is assumed to model this predefined sequence which is then scrambled by the scrambling code. All other data sequences from the base station are modelled as intracellular interference.

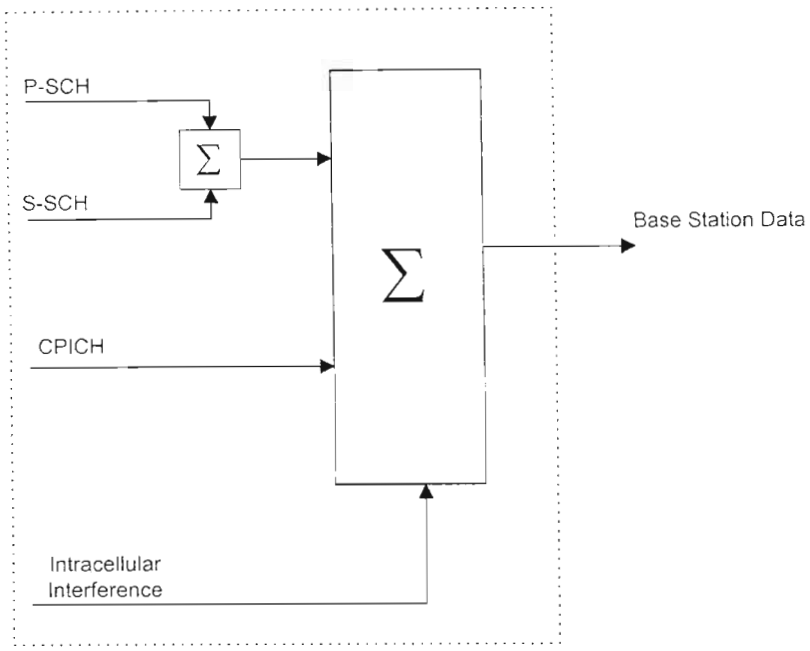

Figure 2-11: Base Station System Model for Cell Search in a WCDMA System

Figure 2-12(a)-(c) shows a WCDMA base station data with PSC, SSC and CPICH data spread with a cell-specific scrambling code. There is no noise added. The power of the CPICH signal shown in Figure 2-12 is limited to 10 % of the total base station power as required by the Standard. In Figure 2-12(a), the in-phase component of the WCDMA signal is shown. A similar signal can be generated for the quadrature component. It can be seen that the synchronisation codes are shown as peaks. This is due to the selection of the power levels of the PSC and SSC codes in relation to the CPICH codes. If the power of the CPICH signal is made larger, the distinct appearance may not be obtained. Moreover, the appearance can also change if the signal encounters a noisy channel. A closer look of the first 256 chips of the I and Q parts is shown in Figure 2-12(b) and Figure 2-12(c) respectively.

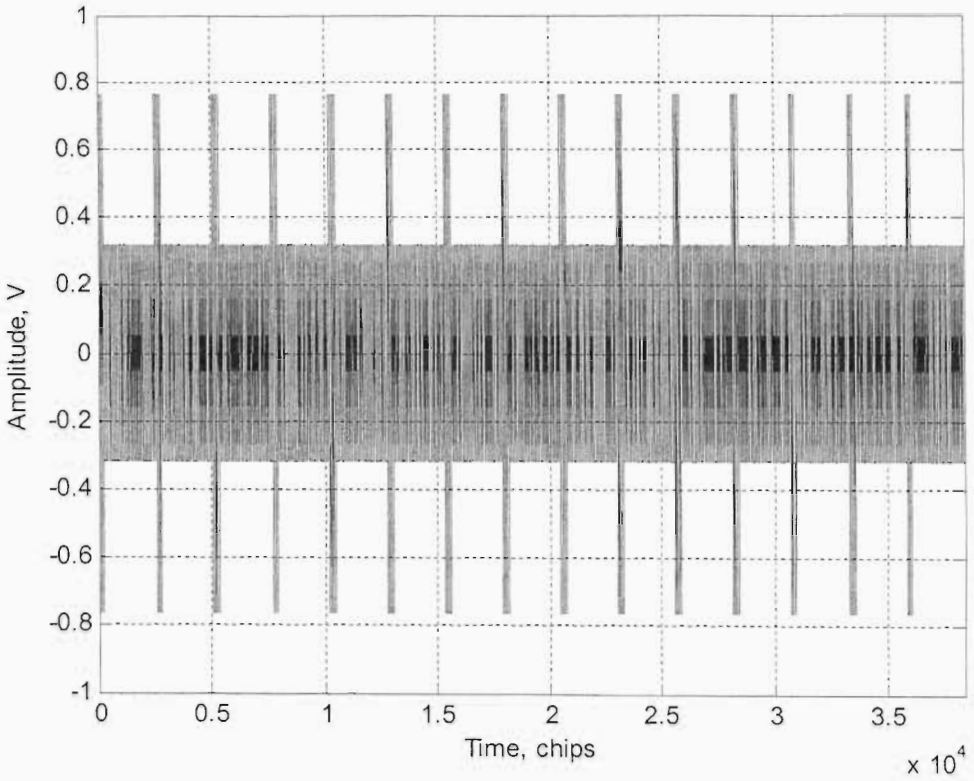

Figure 2-12(a): WCDMA base station data - I channel (10 ms frame)

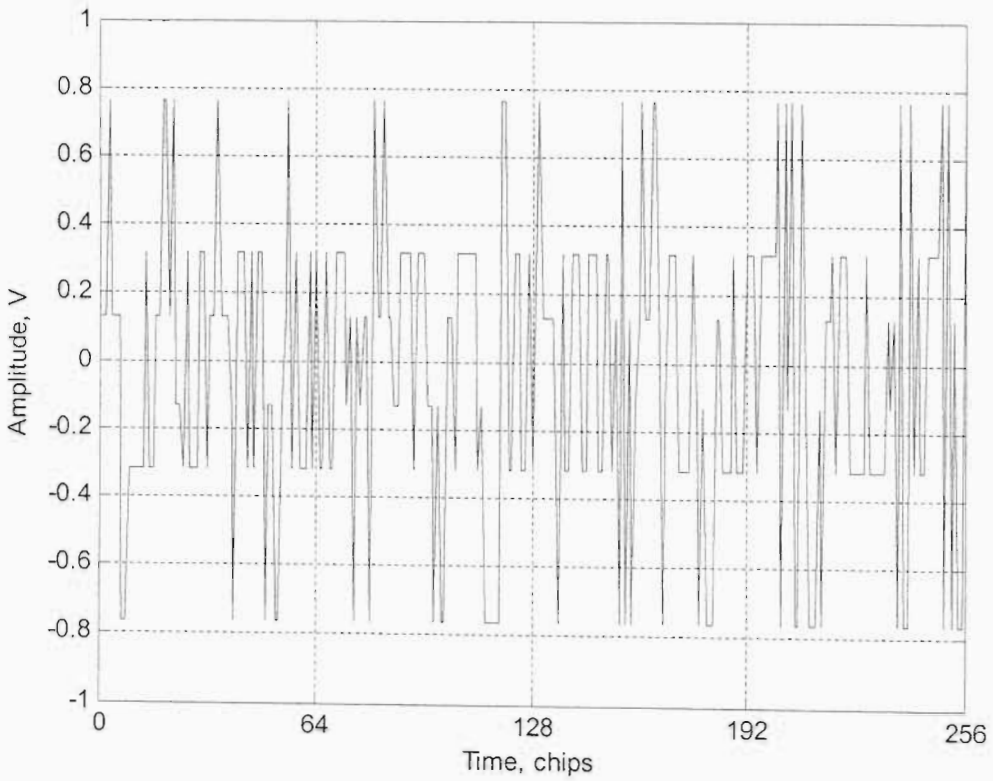

Figure 2-12(b): WCDMA base station data - I channel

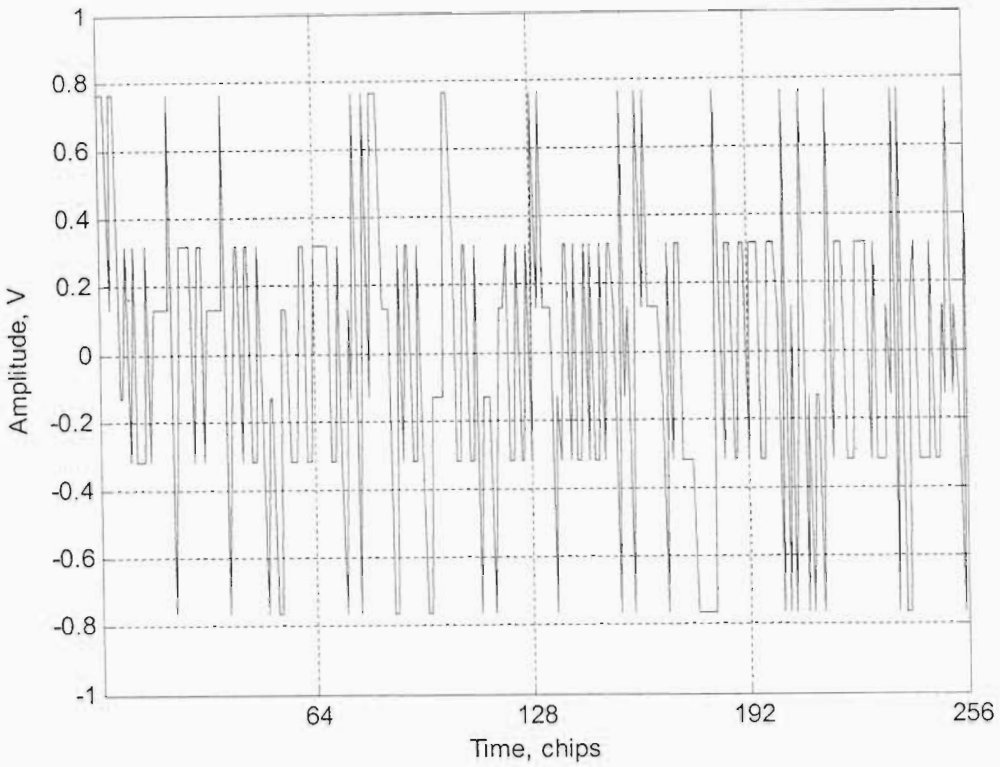

Figure 2-12(c): WCDMA base station data - Q channel

2.9 Factors that affect Cell Search Procedure

As with most RF signal processing, there are serious impairments imposed on transmitted base station data that affect the cell search process. These are mostly RF related impairments to the received signal that originate due to the use of non-ideal components at the receiver. These are the effects of frequency offset, phase noise, dc offset, I/Q imbalances, etc. This section highlights the effect of frequency offset on the WCDMA base station data.

In a WCDMA environment, the most detrimental RF impairment is caused by the presence of frequency offset at the receiver. Carrier frequency offsets arise due to crystal oscillator inaccuracies at the receiver and their effect is realised when the voltage controlled oscillator at the receiver is not oscillating at the same frequency as that of the transmitter. This is seen as a frequency offset to the receiver. It affects most of the communications functions. Most crystal oscillators used in WCDMA receivers

have an inaccuracy between 3 – 13 ppm [16]. In a 2 GHz operating environment of CDMA systems, this translates to a frequency offset range of 6 – 26 kHz.

To illustrate the effects of this offset, the base station data is simulated and corrupted with the frequency offset. The following figures show the impairments to the base station data when the frequency offset is increased from 0 – 20 kHz. Figure 2-13(a) shows the first 3 slots of a WCDMA data containing the primary synchronisation code, secondary synchronisation code, common pilot channel and most importantly it is scrambled by a Gold code as discussed in Section 2.6. There is no frequency offset in this base station signal. Hence, it shows only the base station data with the synchronisation channels seen as bursts.

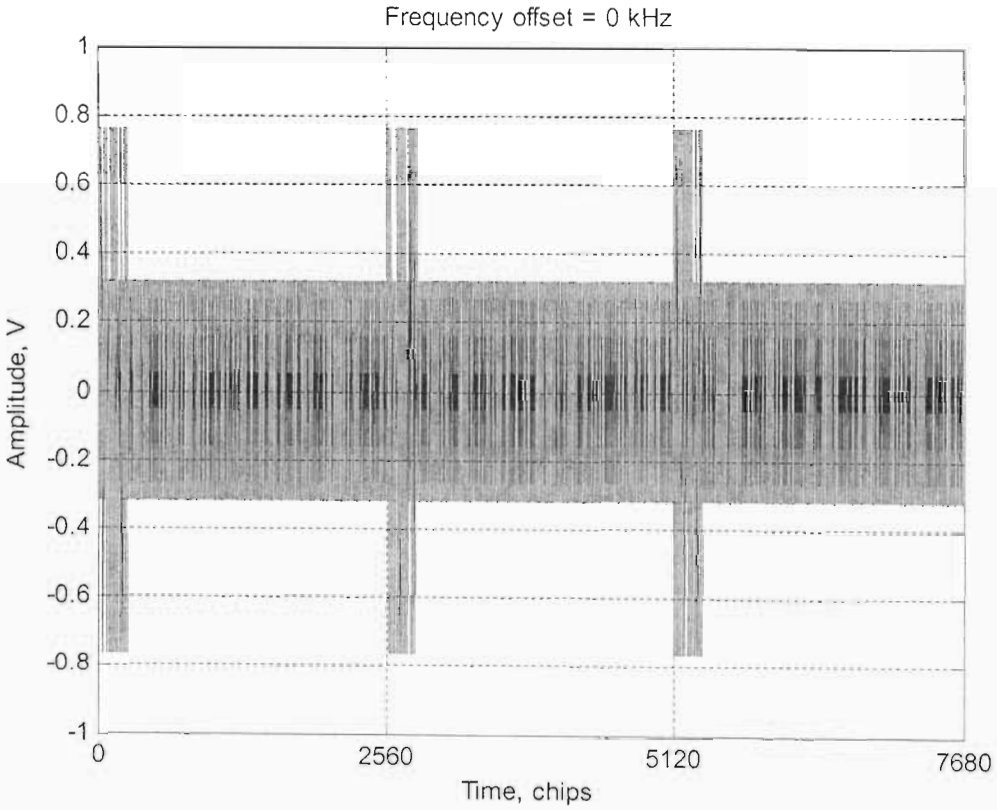

Figure 2-13(a): WCDMA signal with 0 Hz frequency offset

The base station data degrades very slowly when a frequency offset of 1 kHz is introduced as shown in Figure 2-13(b). It can be seen that some portion of the original data is being chopped off by the presence of the frequency offset. This effect is more pronounced in the second occurrence of the synchronisation codes, which are greatly diminished, compared to their original value. Moreover, there is a phase reversal that is justified by a change in polarity of the signal.

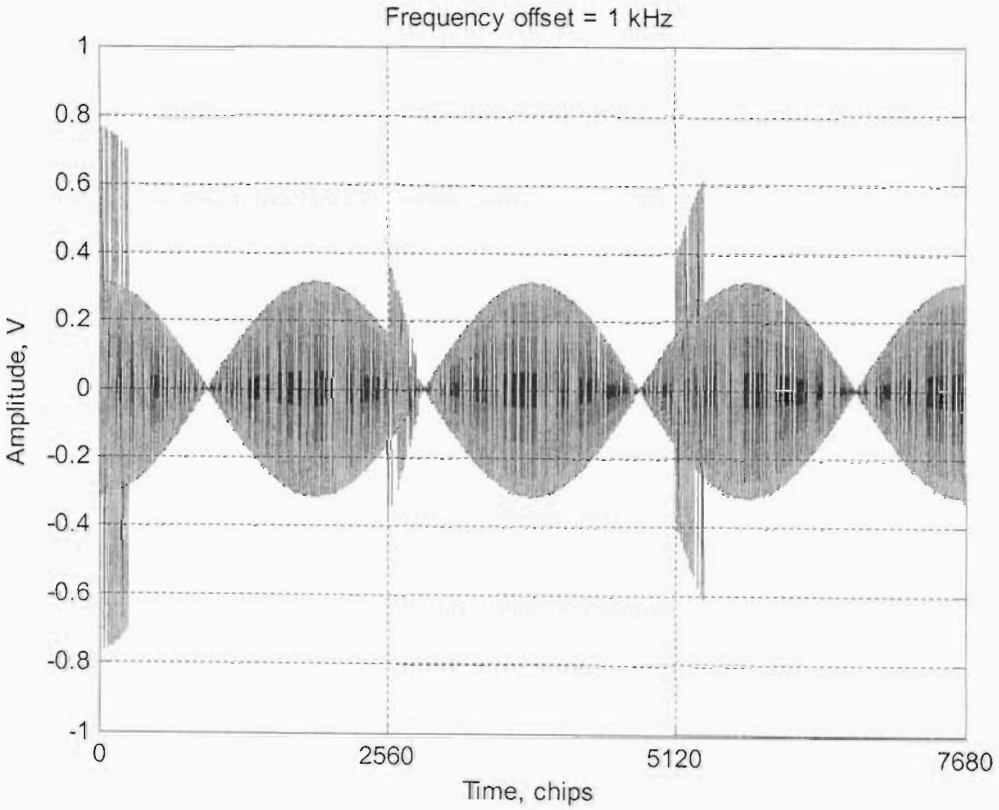

Figure 2-13(b): WCDMA signal with 1 kHz frequency offset

Figure 2.13(c) and Figure 2.13(d) show a WCDMA signal corrupted by frequency offset values of 10 kHz and 20 kHz respectively. The degradation is serious in these cases and reliable signal recovery is difficult unless complex algorithms are used [16].

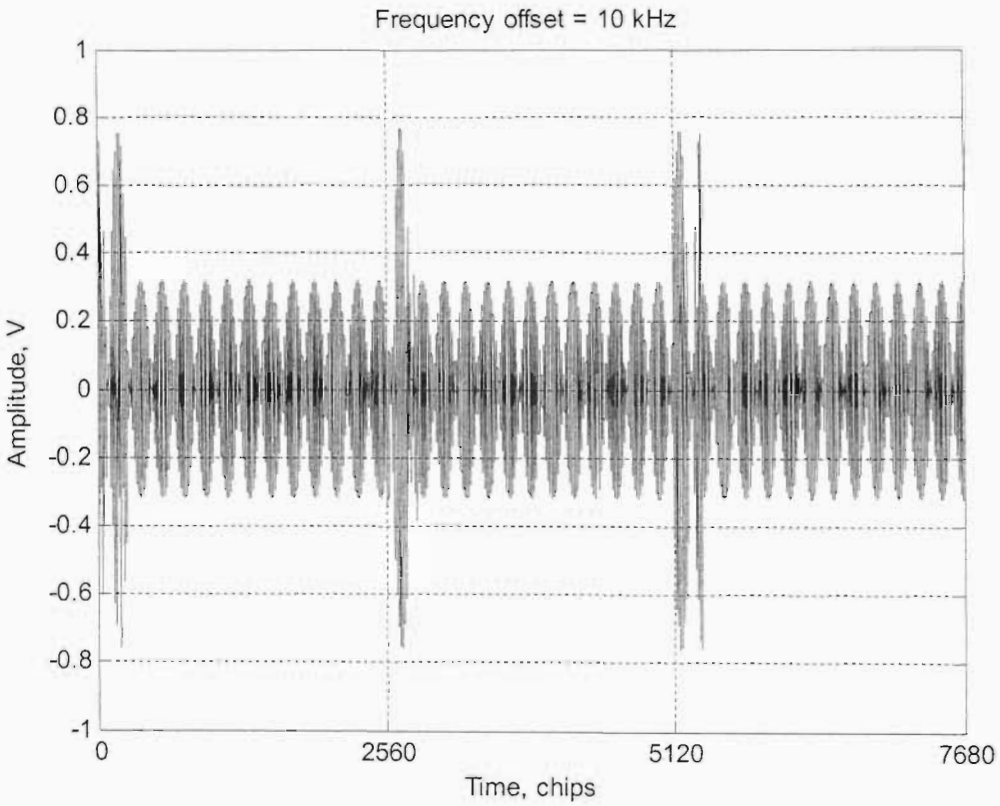

Figure 2-13(c): WCDMA signal with 10 kHz frequency offset

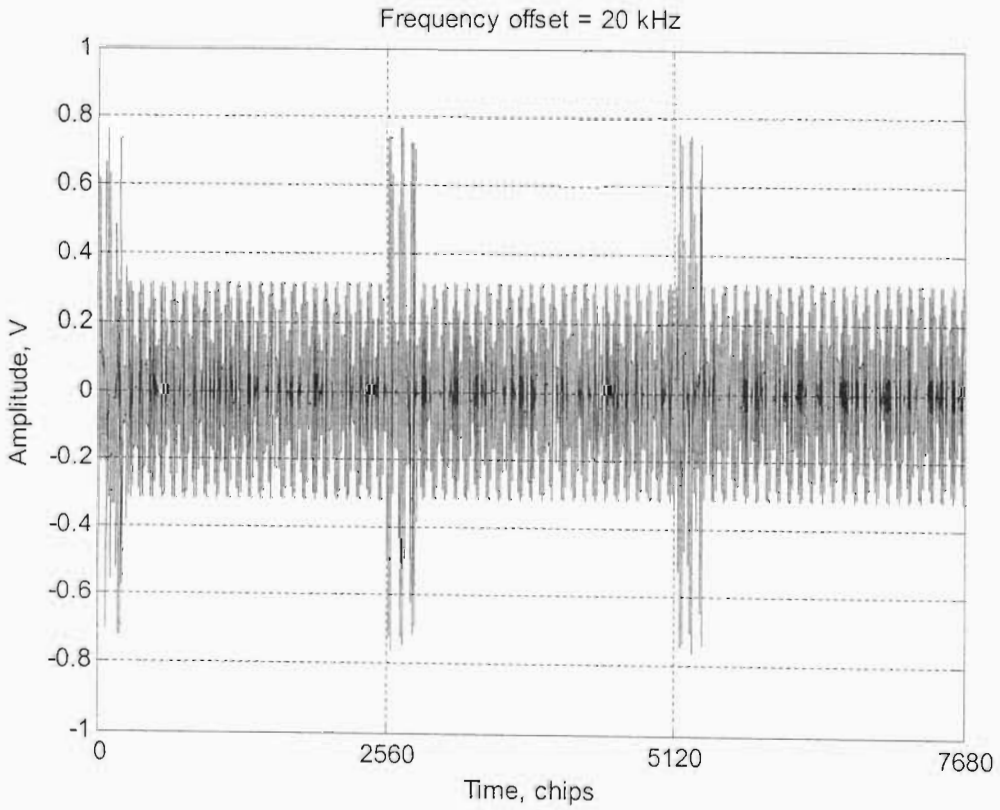

Figure 2-13(d): WCDMA signal with 20 kHz frequency offset

2.10 Summary

This chapter has introduced the basic principles of code synchronisation in CDMA2000 and WCDMA systems. In order to understand the origins of the frame structure and the cell search procedure used in the current 3GPP Standard, selected research efforts from the literature were discussed. The code construction procedures for the various codes used in the synchronisation process were then presented. The channel structure of a WCDMA system and the most important channels used in code synchronisation were also discussed. In order to understand the nature of the signal transmitted by the base station, simulations were used to construct a WCDMA signal that includes the synchronisation codes and the cell-specific scrambling code. Finally, the effect of carrier frequency offset on the transmitted signal was illustrated.

CHAPTER 3

PERFORMANCE ENHANCING STUDIES

3.1 Introduction

In Chapter 2 of this dissertation, an overview of the pioneering research efforts for the cell searching systems has been presented. These efforts led to the standardisation of the cell searching algorithms. It has also been mentioned that cell search in a WCDMA system is a three step process. However, the performance of these systems and the techniques used to improve their performance was not discussed in Chapter 2. Section 3.2 of this chapter begins by presenting an overview of the research efforts in the literature directed at improving the performance of the cell searching system. In Section 3.3, the three stage cell searching algorithm is presented. In Section 3.4, the effects of the carrier frequency offset are discussed and mitigation techniques are explored. The modelling of the wireless channel is presented in Section 3.5 by considering the filtering of two white Gaussian noise samples to generate the coefficients of a flat fading channel. In Section 3.6, a method that exploits the symbol structure of a WCDMA frame is proposed and its differences with the conventional symbol structure are highlighted. In order to investigate the performance of this method, the third stage of the cell searching process is selected and the simulation model used is presented in Section 3.7. The simulation results of the proposed algorithm are presented in Section 3.8. Finally, in Section 3.9, a summary of this chapter is presented.

3.2 Performance Enhancing Studies

Ever since Adachi *et al.* [10] proposed the first cell searching system, several researchers continued investigating techniques to improve its performance. Furthermore, the first release of the cell searching procedures by the 3GPP Standard encouraged further research to improve the performance. Although the 3GPP Standard outlined the procedures for cell search, it did not specify a particular technique of identifying the transmitted scrambling code. Therefore, several authors and device manufacturers use their own proprietary systems to search for the scrambling code. It should be noted that any proposal intended to improve the searching system must adhere to the 3GPP standard. This section presents several efforts in the literature directed to improve the performance of cell searching systems.

3.2.1 Generalised Overview

In [26], the authors pointed out that previous work had been based on the assumption that there is only one carrier frequency and that it is known to the receiving terminal. They studied a practical system whereby the receiving terminal does not have *a priori* knowledge of the carrier frequency. Therefore, the terminal will have to search through a list of all the WCDMA carrier frequency candidates. As the WCDMA frequency band is 60 MHz and the nominal carrier spacing is 5 MHz, the receiving terminal will have to search the raster positions of the entire WCDMA frequency band to determine the correct transmitting carrier frequency and subsequently process the cell searching algorithms. This scenario was investigated in [26].

In [16][17], Wang *et al.* showed that some key parameters of the cell searching system such as the loading factors of the synchronisation channels, can be optimised to reduce the overall searching time. Furthermore, they showed the effects of large frequency offsets can be reduced by partial symbol de-spreading followed by non-coherent combining. They also investigated techniques of using a coherent combining scheme for Stage 2 of the searching system and reported that such a system reduces the search time. Moreover, a majority vote based detection for Stage 3 of the

searching algorithm was proposed. They also proposed techniques to reduce the initial carrier frequency offset.

The authors in [27] investigated the impact of the cell searcher on the system performance in a WCDMA network. In this regard, they investigated the impact of the power allocation ratio of the synchronisation and control channels on the performance of the cell searching algorithms using system level simulation. They reported that optimal performance can be obtained when less that 11.4% of the base station power is allocated to the synchronisation and the control channels. They indicated that although ratios higher than the value specified are good for handover, they are found to degrade the service quality.

A similar conclusion was made when the authors in [16][17] reported that there is not much performance improvement by increasing the power of the pilot channel CPICH to more than 10% of the base station power. Moreover, they noted that when power of the pilot channel falls lower than 5% of the base station power, there is a significant penalty in detecting the transmitted scrambling code. They also investigated the power allocation ratio between the synchronisation channels and the overall base station. Their results show that when this power ratio falls below 10% of the base station power, there is a severe degradation of performance. Considering these investigations, it can be noticed that these power allocation ratios need to be selected very carefully to optimise the performance of cell searching systems in a practical WCDMA network. In another study, the effect of the synchronisation channel on bearer performance was studied in [28] wherein the authors proposed an adaptive synchronisation method for cell search in WCDMA systems by incorporating a power method and controller units to the conventional method to improve performance. Their algorithm depends on estimating the channel conditions using the power meter and they concluded this method decreases the average implementation complexity while increasing the acquisition time.

In [29], the authors investigated the performance analysis of the transfer power allocation of the synchronisation codes PSC and SSC of a WCDMA system in an additive white Gaussian noise channel. They reported good performance can be achieved when the power of the PSC and the SSC is allocated in the ratio of 3 to 1.

However, other research efforts [17][30] showed that good performance is obtained when the total power allocated to the synchronisation channel is divided equally between the primary and secondary synchronisation channels when simulated in a Rayleigh fading channel. They also showed that multi-slot and multi-frame non-coherent accumulation improves the synchronisation performance for low signal-to-noise ratios.

In [31], the authors outlined some assumptions used in the previous efforts on the WCDMA searching system, i.e. the sampling at the output of the chip matched filter is perfect and the chip clock of the transmitter is known precisely to the receiving terminal. Hence, they investigated techniques to counteract the clock drift and the effects of non-ideal sampling. In a similar approach, the authors in [32] studied the effect of clock drift and proposed a time tracker to alleviate the clock drift. In a related study, [33] proposed enhancements to the WCDMA searcher by investigating the effects of over sampling, non-ideal sampling, and multiple code-time hypotheses for each of the three stages. They reported considerable improvements when taking four code-time hypotheses with an over-sampling factor of 4 or more in low signal-to-noise ratio environments.

In [34], the authors proposed an initial cell searching scheme robust to carrier frequency offset by using partial symbol de-spreading similar to [16][17]. In [35], the authors investigated the effect of the carrier frequency offset on slot detection in WCDMA cell searchers. They showed that the carrier frequency offset degrades the slot detection performance and proposed a coherent method to mitigate the problem. They reported that a partial correlation length of 64 chips gives the best slot detection performance for carrier frequency offsets of up to 20 kHz. Similarly, [36] proposed a cell searching scheme robust to carrier frequency offset in WCDMA systems. They employed an inner slot differential combining scheme for accumulating PSC correlation using partial chip correlation lengths of 64 chips.

In [37], the authors claimed that the computational complexity of the conventional systems is large and proposed techniques of reducing the complexity of the Stage 2 of the searching process by 70 % using a partial fast Hadamard transform. In a related study of reducing the complexity of cell searching systems, the authors in [38]

exploited the structural characteristics of the PSC sequences made up of the generalised hierarchical Golay sequences and proposed a decoding scheme that reduces the complexity further. In [39], a cell searcher architecture is presented that utilises a memory digital matched filter optimised for acquisition speed and low power consumption. They reported this method reduces the power consumption and chip area when compared to the register based direct implementation.

There are some efforts in the literature that endeavour to search for the transmitted base station identity using an approach different from the standardised algorithms. One of these research efforts is the work done in [40] wherein the authors proposed modulating the primary synchronisation codes already used in the Standard with a specific polarisation code. They found out that such an approach does not change the structure of the WCDMA channels. They reported that their algorithm can reduce the base station transmission power and the complexity of the receiver when compared to the conventional one. Other searching approaches include the I/Q multiplexing based scheme [41][42][43], cluster pilot based scheme [44], code hopping based searching scheme [45]. However, research using these algorithms is not pursued further although in some cases they are reported to achieve similar performance compared to the standardised algorithms.

3.2.2 Types of Cell Search

There are two types of cell search presented in the literature. These are the serial cell search system and the parallel cell search system. The serial cell search system was used in the early searching algorithms in [10][11]. Parallel cell searching systems are investigated in [16][17] as an alternative option to improve performance. Analytical investigation of these two techniques in a Rayleigh fading channel was studied in [46][47][30]. In [47], the authors analysed a serial cell searching system over a Rayleigh fading channel as was done earlier in [46], but with a more detailed state diagram. Their analysis can be used to determine the effect of threshold setting and power allocation of the synchronisation channels. In [30], the authors analysed the performance of serial and parallel cell searching systems in a Rayleigh fading channel. They extended the efforts of [47] to include the parallel cell searching system.

In [48], a hybrid cell searching system was reported. The authors investigated an optimal operating point for a receiving terminal using a hybrid system whereby the first two stages are running in parallel while the third stage is running in series with the previous two stages. However, most authors use the serial and parallel systems. The following two sections briefly present the serial and parallel searching systems.

3.2.2.1 Serial Cell Search

In a serial cell search, the three stages are executed in a serial arrangement. Figure 3-1 shows the schematics of a serial cell searching system in which Stage 1, Stage 2 and Stage 3 are arranged serially. N_1, N_2 and N_3 represent the number of slots needed to complete Stage 1, Stage 2 and Stage 3, respectively. The slot timing candidate obtained from Stage 1 is used to trigger Stage 2, which in turn gives its frame timing and code group identity candidates to start Stage 3. Stage 3 gives the scrambling code candidate.

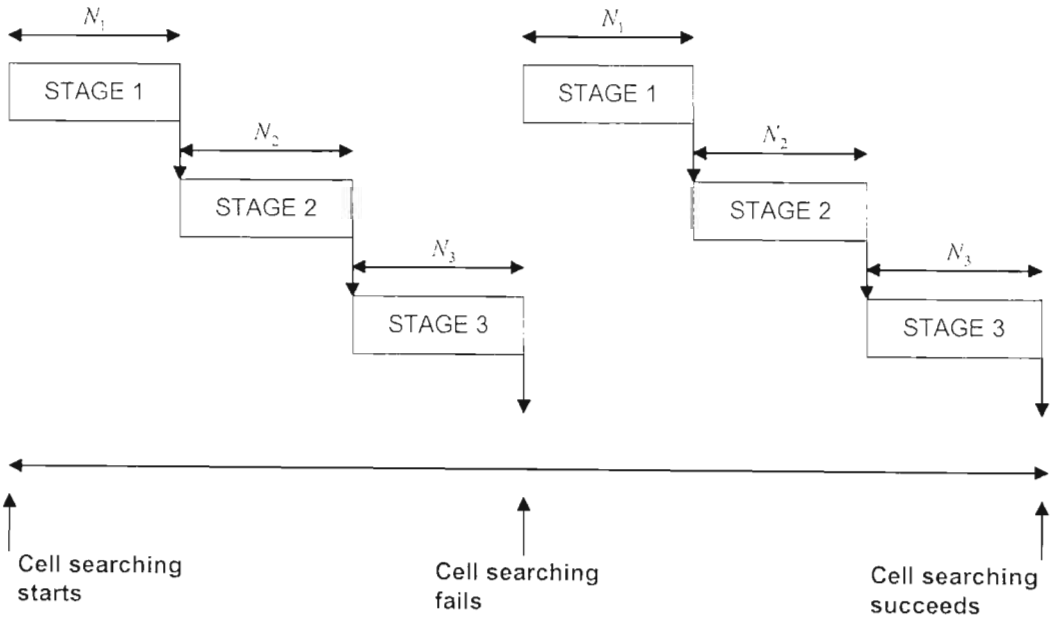

Figure 3-1: Schematics of a serial cell searching system

If the scrambling code detected in Stage 3 is different from the one which is transmitted by the base station, the process fails and a new one starts by executing the steps serially. This process continues until the correct transmitted scrambling code is

detected in Stage 3. Serial cell search was studied by several authors and a good analytical discourse can be found in [30].

3.2.2.2 Parallel Cell Search

In a parallel cell search, the three stages are executed in parallel. Figure 3-2 shows a parallel cell searching scheme. N_1, N_2 and N_3 represent the number of slots needed to complete Stage 1, Stage 2 and Stage 3, respectively, and the parallel operation necessitates the use of an equal number of slots $N_1 = N_2 = N_3$ for each of the three stages [30]. When the search starts at point A, Stage 1 computes the timing candidate and triggers Stage 2. Unlike in the serial cell search, however, Stage 1 continues to search for another timing candidate. At point B, once the timing information is received, Stage 2 searches for the code group and frame boundary information and hands over its candidates to Stage 3 at point C, whilst continuing to search for new candidates.

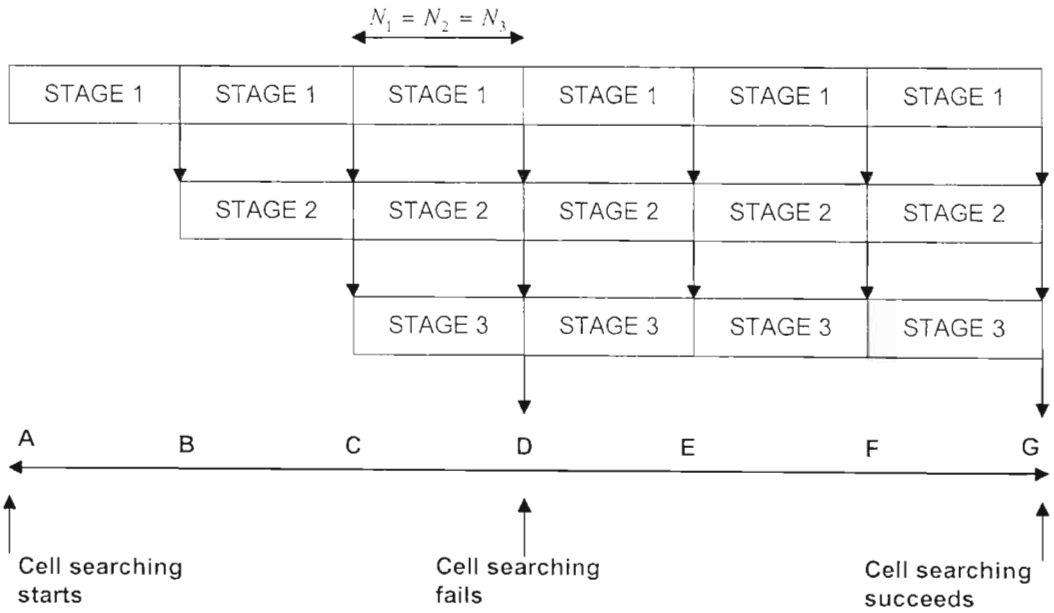

Figure 3-2: Schematics of a parallel cell searching system

Once Stage 3 receives the required candidates from Stage 2, it searches for the transmitted scrambling code and gives its candidate outputs at point D. The candidate scrambling code is compared with a pre-defined threshold and if it fails, Stage 3

continues to find another candidate using new candidates from Stage 1 and Stage 2, which by now are running in parallel. This process continues until the candidate scrambling code exceeds the pre-defined threshold in Stage 3, at which point, the search will be completed. This is shown in point G. Although the parallel cell searching scheme has greater implementation complexity than the serial one, it has a better acquisition performance as was reported by several authors [16][17][30].

3.2.3 Combining Schemes

In order to enhance the performance of code acquisition in CDMA systems, correlators outputs are combined [49] to form a decision variable. Several combining schemes are reported in the literature. In WCDMA systems, the outputs of a correlator or a matched filter are combined to increase the likelihood of code acquisition [34][49]. This section discusses the three types of combining schemes used for cell searching algorithms. These are the non-coherent, coherent and differentially coherent combining schemes.

3.2.3.1 Non-coherent Combining Scheme

In this combining scheme, the outputs of the correlators or matched filters are combined non-coherently. Figure 3-3 shows a non-coherent combining scheme applied used to correlate the coefficients of the matched filter (MF) with the received symbols. Each output of the matched filter is squared before combining with similar outputs from other correlations of the received signal. This increases the likelihood of code acquisition as a decision is made after accumulating the correlator outputs over many symbols.

This method can be used when the phase of the received signal is unpredictable due to channel effects or carrier frequency offset errors [34]. Non-coherent combining of correlator outputs is ideal to use for fast fading channels [49][50].

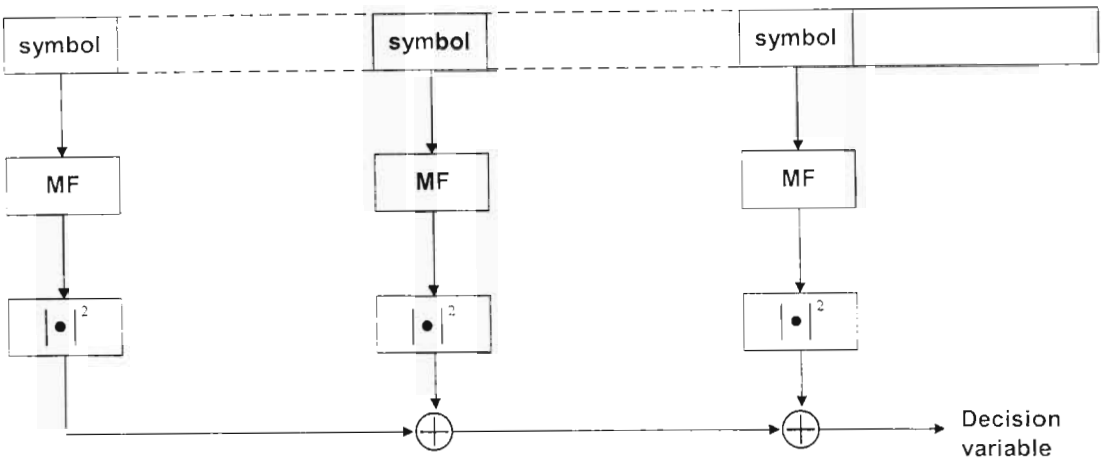

Figure 3-3: Non-coherent combining scheme

3.2.3.2 Coherent Combining Scheme

In this method, the outputs of a correlator or a matched filter are simply combined with similar outputs which are accumulated to form a decision variable. Figure 3-4 shows the schematics of a coherent combining scheme wherein the received symbols are correlated with the coefficients of the matched filter before combining into a decision variable. Coherent combining has an advantage over the non-coherent combining because it averages the noise components included in the matched filter outputs [34]. However, this scheme gives good performances only if the phase of the received signal is known [34]. The possibility of this using method into the second stage of the cell search was investigated in [17] where the information from the first stage is used to provide some phase reference for the second stage.

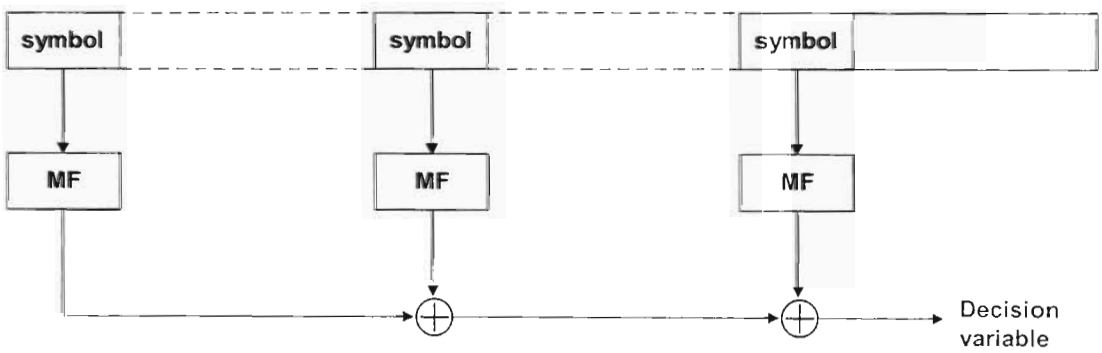

Figure 3-4: Coherent combining scheme

3.2.3.3 Differentially Coherent Combining Scheme

The differential combining scheme exploits the advantages of the coherent and non-coherent combining schemes. Differential combining schemes has been studied in [49] and is shown to outperform the other two combining schemes by reducing the effects of phase rotations due to carrier frequency offset and fading, and allows differential processing outputs to be combined coherently without severe degradation. However, it comes at a cost of hardware complexity. Figure 3-5 shows a differentially coherent combining scheme. It can be seen that the matched filter outputs are processed first before combining.

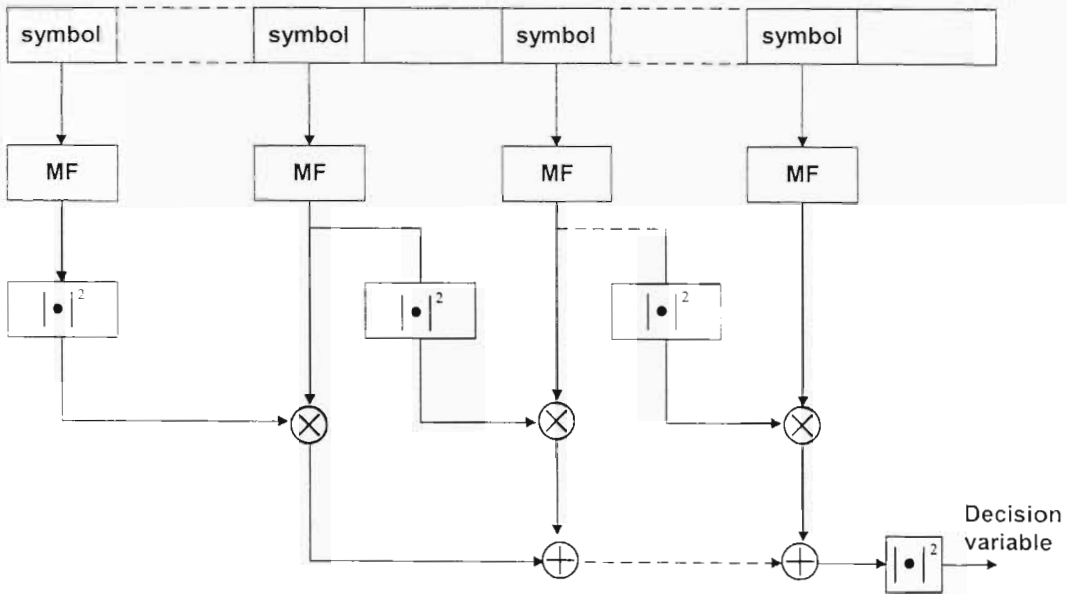

Figure 3-5: Differentially coherent combining scheme

3.3 Cell Searching Algorithms

In Chapter 2, the procedure for cell search as outlined in the 3GPP Standard [18] was briefly presented. In order to understand this process, the three step cell searching algorithms are explained in greater depth in this section.

3.3.1 Stage 1 – Timing Identification

In Stage 1, the WCDMA mobile terminal searches for the start of slot timing of the received sequences. To accomplish this, it correlates the primary synchronisation code with the received signal. Since the PSC is 256 chips long, the terminal correlates this code, accumulates the correlation values and decides on the maximum value to select a candidate for the slot timing. Let $C_{psc}(n)$ represent the n^{th} chip of the PSC code and $R(i)$ denote the i^{th} sample of the received sequence. Hence, the mobile terminal computes the correlation metric over one slot duration T (T = 2560 chips) as

$$w(i) = \left| \sum_{n=0}^{255} C_{psc}(n)\, R(i+n) \right|, \qquad i = 0,1,2,...,T-1 \tag{3.1}$$

The candidate slot timing is selected from the total T possible hypotheses as

$$\hat{i} = \arg\max_{i} \{w(i)\} \tag{3.2}$$

The maximum correlation value of (3.1) is sometimes compared with some threshold before it is declared as a potential slot timing candidate. Some authors consider the threshold to be 3 dB lower than the autocorrelation of the PSC sequences [10][11] while others simply use the maximum correlation value without comparing it with any threshold [16].

The correlation values over a number of slots are usually combined to give a reliable slot timing candidate [16], reduce the effect of noise and exploit post-detection diversity combining [14]. The accumulation of the correlation values over N_S slots can be expressed as

$$\tilde{w}(i) = \sum_{j=0}^{N_S-1} w(i+jT) \tag{3.3}$$

where i and T are as defined above. Hence, (3.2) can be applied on (3.3) to give a candidate based on combining multiple slots.

It should be noted that the 3GPP Standard does not specify a particular implementation technique to perform the correlations. Thus, either a bank of correlators or a matched filter can be used for detecting the slot timing. Most research papers state the use of a matched filter for this stage.

3.3.2 Stage 2 - Frame and Code Group Identification

In Stage 2, the mobile terminal identifies the start of the frame and determines the identity of the code group used at the transmitting base station. It determines which of the 16 secondary synchronisation codes $\left\{C_{ssc}^{1}, C_{ssc}^{2}, ..., C_{ssc}^{16}\right\}$ is sent by the transmitter on its synchronisation channel. As soon as the candidates for the timing information are detected from Stage 1, the received sequences are correlated with each of the 16 SSC sequence using either a matched filter or a bank of correlators as

$$S_m(k) = \left| \sum_{j=0}^{255} C_{ssc}^{m}(j)\, R^{k}(j) \right|, \qquad m = 1,2,...,16, \quad k = 0,1,2,..., N_s - 1 \tag{3.4}$$

where $C_{ssc}^{m}(j)$ is the j^{th} sample of the SSC sequence C_{ssc}^{m} and $R^{k}(j)$ is the j^{th} sample of the k^{th} slot of the received sequence. The terminal then accumulates the SSC values in different frames as

$$\tilde{S}_m(k) = \sum_{\substack{j=0 \\ (j \bmod 15)=k}}^{N_s-1} S_m(j), \qquad m = 1,2,...,16, \quad k = 0,1,2,..., N_s - 1 \tag{3.5}$$

The terminal would then use the brute force method to compute the correlation values of combinations based on the RS codes as well as shifts listed in the Appendix. This can be written as

$$X(i,j)=\sum_{k=0}^{14}\tilde{S}_{\Omega_i(k+j \bmod 15)}(k)\,, \qquad i=1,2,...,64, \quad k=0,1,2,...,14 \tag{3.6}$$

where $\Omega(i,j)$ represents the i^{th} code group and the j^{th} value of the list in Appendix A. Therefore, the metric in (3.6) represents the detected reference weight for the scrambling code group which is assumed to be the i^{th} code group and the j^{th} slot. Hence, the estimated value of the scrambling code group is found by maximising (3.6) for the i^{th} code group as

$$\hat{i}=\arg\max_{i}\{X(i,j)\} \tag{3.7}$$

and the estimated frame boundary can be found similarly by maximising (3.6) for the j^{th} value as

$$\hat{j}=\arg\max_{j}\{X(i,j)\} \tag{3.8}$$

Hence, $(\hat{i},\hat{j})$ gives the estimate for the scrambling code group and the frame boundary. Figure 3-6 summarises the decoding scheme undertaken by a mobile terminal to determine the order of the frame and the code group identification.

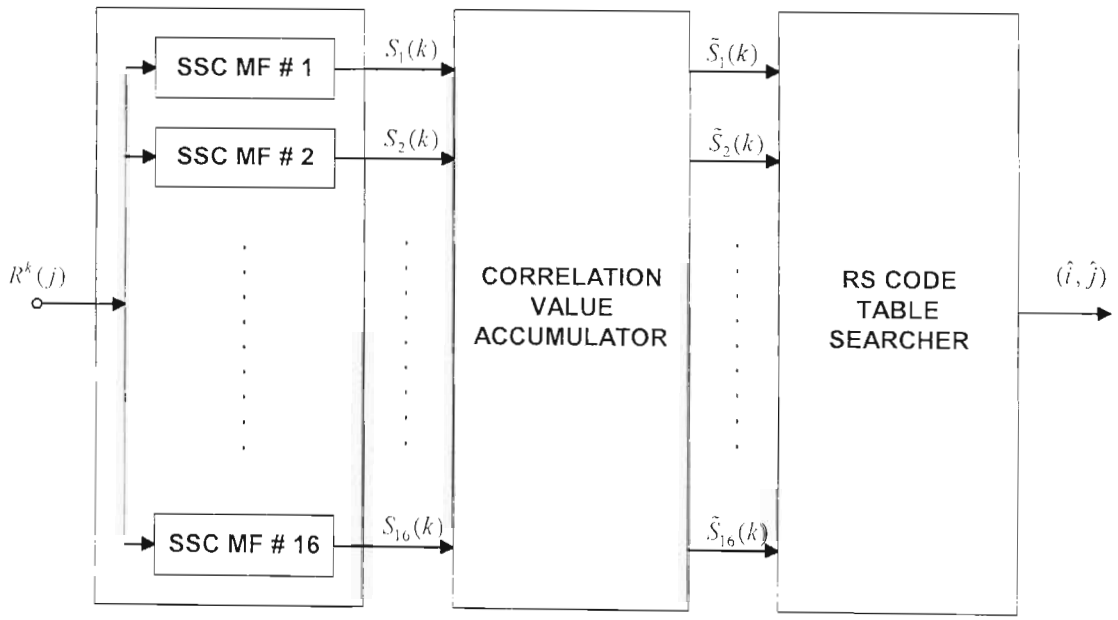

Figure 3-6: Decoding schematics of the Stage 2 algorithm

3.3.3 Stage 3 – Scrambling Code Identification

In Stage 3, the mobile terminal determines the identity of the cell-specific scrambling code. It is to be noted that once the terminal receives candidates from the first two stages, it knows the start of frame and the code group identity. In [18], the Standard uses eight scrambling codes per code group. Therefore, in this stage, the mobile terminal correlates the received signal with each of the eight scrambling codes to determine the successful candidate. For each CPICH symbol in the received frame, the terminal chooses the scrambling code with the largest correlation value. Similar correlation operations are extended to all symbols in the received frame and the largest values of the scrambling codes chosen. In the end, the terminal collects votes based on majority hits for the scrambling codes tested. The scrambling code with the largest majority votes is accepted only after comparing it with a pre-determined threshold.

This stage is very crucial to the success of the code identification and subsequently to the process of frequency recovery. Hence, in order to minimise unnecessary activities of the mobile terminal, a very tight probability of false detection is desirable to select the threshold T_h thereby reducing false alarms [16][17].

For a desired probability of false detection P_{FA}, the threshold T_h can be set using union bounds as [17]

$$P_{FA} = N_{SC} \sum_{j=T_h-1}^{J} \binom{J}{j} \left(\frac{1}{N_{SC}}\right)^{j} \left(\frac{N_{SC}-1}{N_{SC}}\right)^{J-j} \tag{3.9}$$

where N_{SC} is the number of scrambling codes per scrambling code group and J is the number of symbols over which the terminal accumulates the majority votes. To achieve a $P_{FA} = 10^{-4}$ using eight scrambling codes per code group with $J = 150$ symbols used for majority voting, the threshold is found to be 38 [17]. This means, the majority votes for any of the eight scrambling codes recorded by the terminal must be larger than 38 before declaring the candidate successful. Similarly, for a

$P_{FA} = 10^{-3}$, the threshold is 35 [17]. In this dissertation, $P_{FA} = 10^{-4}$ is considered with $J = 150$. Nonetheless, (3.9) can be used to determine the threshold for other parameters desired.

Hence, the correlations of the received signal with each of the k scrambling codes can be represented as

$$D(q,k) = \sum_{j=0}^{S-1} \left| R(j+Sq) C^{(k)}(j+Sq) \right|^2 \tag{3.10}$$

where $D(q,k)$ is the correlation value of the received signal with each of the q^{th} symbol of the k locally generated scrambling codes $C^{(k)}(\bullet)$, where $k = 0,1,2,...,7$ and $q = 0,1,2,...,149$ (denotes the number of symbols in one frame). The symbol duration in chips is S ($S = 256$).

The most likely transmitted scrambling code is identified as follows. Let $\Lambda(k)$, k as defined above, represent a counter at the terminal that collects votes associated with each symbol of the eight scrambling codes. For example, $\Lambda(3)$ will represent the number of times (of possible 150 symbols) the scrambling code number $k = 3$ has achieved a high correlation value in (3.10). The total sum of votes in the counters is equal to the number of symbols in the frames considered (i.e. 150 symbols for one frame). This can be written as

$$\sum_{k=1}^{8} \Lambda(k) = 150 \times (number\ of\ frames) \tag{3.11}$$

After accumulating votes for all the symbols, majority voting is done to choose the most likely transmitted code. This is verified by comparing the chosen vote with the threshold T_h.

3.4 Mitigating the Effects of Carrier Frequency Offset

This section presents an overview of the effects of carrier frequency offset on the received signal sequence and then presents mitigation techniques used to counteract them. In Chapter 2, the effect of carrier frequency offset on the transmitted data has been illustrated. It has been shown that the carrier frequency offset removes some parts of the transmitted signal. It has also been shown that the carrier frequency offset causes signal phase rotations that vary in proportion to the carrier frequency offset and has been shown to cause serious degradation to the received signal [17][35].

A closer look at the signal rotation in the received signal sequence reveals the time duration during which the signal rotation remains constant. This can be investigated by studying the cosine function for different values of carrier frequency offset. Let $\cos(2\pi \Delta f\, t)$ represent the cosine function that models the carrier frequency offset. Assuming perfect sampling at $t = i T_c$, where $i = 1, 2, \ldots$ the zero crossing of the cosine function can be found by solving $\cos(2\pi \Delta f\, z T_c) = 0$ and can be written as

$$z = \frac{1}{4 \Delta f\, T_c} \tag{3.12}$$

where T_c is the chip duration and Δf is the carrier frequency offset. Therefore, it can be noticed that the signal rotation in the received signal sequence remains constant over z chips. Table 3-1 presents the number of chips over which signal rotation is prevented.

Table 3-1: Duration of signal rotation for different carrier frequency offsets

Frequency Offset (kHz)	Signal rotation interval (chips)
0	No rotation
5	192
10	96
15	64
20	48

It can be seen that the time duration of the signal rotation decreases as the carrier frequency offset increases. For a carrier frequency offset of 20 kHz, the signal phase remains constant for 48 chips only. Therefore, it can be concluded that to preserve the integrity of the transmitted signal at the receiver in the presence of carrier frequency offset, the length of the correlator output has to be adjusted accordingly.

Chulajata *et al.* investigated the effect of carrier frequency offset on the outputs of a matched filter to detect the slot timing and showed that the degradation factor imparted on the received signal can be written as [35]

$$D(\Delta f) = \left[\frac{\sin(\pi M \Delta f T_c)}{\pi M \Delta f T_c} \right]^2 \tag{3.13}$$

where M is the matched filter correlation interval, T_c is the chip duration, and Δf is the carrier frequency offset. Table 3-2 presents the degradation factors for different values of the carrier frequency offset. It is shown that the degradation factor assumes values between 0 and 1. A degradation factor close to 1 means the received signal encounters lower degradation as compared to a value closer to 0 where the received signal encounters severe degradation.

Table 3-2: Degradation factor due to carrier frequency offset

	Carrier frequency offsets			
M	5 kHz	10 kHz	15 kHz	20 kHz
16	0.9986	0.9943	0.9872	0.9774
32	0.9943	0.9774	0.9496	0.9119
64	0.9774	0.9119	0.8106	0.6839
128	0.9119	0.6839	0.4053	0.1710
256	0.6839	0.1710	0.0000	0.0427

It can be noticed that the higher the carrier frequency offset in the received signal, the more severe the degradation due to the effects of signal rotation. An exception can be found when a carrier frequency offset of 15 kHz encounters the received signal. For a correlation interval of 256 chips, it is observed that the degradation is more severe

than when a carrier frequency offset of 20 kHz encounters the received signal. This can be explained by the time duration that causes signal rotation for the carrier frequency offset of 15 kHz. This can be read from Table 3-1 to be 64 chips. Hence, in this case, the degradation is severe due to the complete rotation of all received signal sequences within the 256 chip duration.

Hence, to counteract the severe degradation caused by high values of carrier frequency offset, most authors use partial symbol de-spreading techniques with some form of combining. For example, Wang *et al.* in [17] proposed the use of 64 chips combined non-coherently to search for the synchronisation codes with a frequency offset of 20 kHz. A similar approach was considered in [34]. In [35], Chulajata *et al.* proposed a coherent slot detection scheme using partial symbol despreading.

3.5 Modelling the Wireless Channel

The wireless channel is defined as the link between the transmitter and the receiver. This section presents the technique used to model the wireless channel considered in this dissertation.

The simulation of many communication systems necessitates for the received signal amplitudes to have a Rayleigh distribution. The probability distribution function of the received signal amplitude r conditional on the mean power p_o is given by the Rayleigh distribution function [51]

$$f_{r/p_o} = \begin{cases} \dfrac{r}{p_o} e^{\left(\frac{-r^2}{2p_o}\right)} & 0 \le r < \infty \\ 0 & r < 0 \end{cases} \tag{3.14}$$

In [52], the authors note that the discrete time samples of a realistic Rayleigh fading process must necessarily be correlated, and that the correlation depends on the relative motion of the receiving terminal to the transmitter, number of propagation paths,

antennae characteristics, etc. There are many ways to generate correlated Rayleigh random variates that model the effects of fading. Some of these are the inverse discrete Fourier transform [52][53], the filtered white Gaussian noise process [54][55][56] and the superposition of sinusoids [57]. A quantitative comparison of the three methods of generating the random variates can be found in [52].

This dissertation uses the filtered white Gaussian noise process of generating the correlated Rayleigh variates to model the flat fading channel. It involves filtering two independently distributed zero-mean half-variance white Gaussian processes which are then combined to form a Rayleigh distribution. This is shown in Figure 3-7.

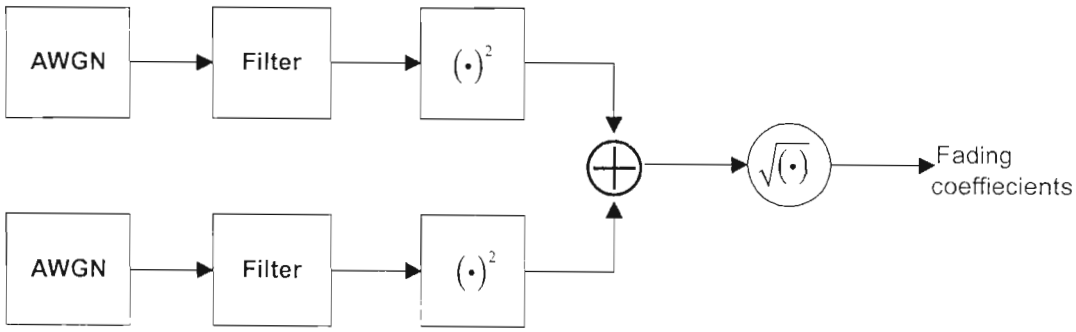

Figure 3-7: A filtered white Gaussian noise model

The choice of the type of filter used depends on how closely it realises the continuous autocorrelation of the scattered received signal which is given by [57]

$$R(\tau) = J_0(2\pi f_m \tau) \tag{3.15}$$

where f_m represents the Doppler frequency normalised to the sampling frequency and τ represents the delay and $J_0(\cdot)$ is the zero-order Bessel function of the first kind [58]. Although some authors showed a third order Butterworth filter can be used [54], this dissertation uses the filter specifications presented in [56] which the authors showed to relate well to the autocorrelation function given by (3.15). The coefficients of this finite impulse response (FIR) filter considered are given by [52]

$$h[n] = \begin{cases} \left(\frac{f_m}{\pi}\right)^{1/2} \frac{\Gamma\left(\frac{3}{4}\right)}{\Gamma\left(\frac{5}{4}\right)}, & n = \frac{L_f - 1}{2} \\ \left(\frac{f_m}{\pi}\right)^{1/4} \Gamma\left(\frac{3}{4}\right)\left[n - \frac{L_f - 1}{2}\right]^{-1/4} J_{1/4}\left(2\pi f_m\left[n - \frac{L_f - 1}{2}\right]\right), & 0 \le n \le L_f - 1,\ n \ne \frac{L_f - 1}{2} \end{cases} \tag{3.16}$$

where f_m represents Doppler frequency normalised to the sampling frequency, $\Gamma(\bullet)$ is the Gamma function [58], L_f is an odd-numbered filter length and $J_{1/4}(\bullet)$ represents a non-integer Bessel function of the first kind defined as [58]

$$J_v(z) = \left(\frac{z}{2}\right)^v \sum_{k=0}^{\infty} \frac{\left(-\frac{z^2}{4}\right)^k}{k!\,\Gamma(v+k+1)} \tag{3.17}$$

where $v = 1/4$ and $\Gamma(\bullet)$ is as defined above.

In order to investigate the validity of the fading simulator considered, the probability density function of the fading coefficients is compared with the theoretical Rayleigh distribution function described in (3.14). The fading coefficients are generated by passing random Gaussian samples through the FIR with the filter coefficients described in (3.16). In order to achieve this, two independent zero-mean and unity-variance Gaussian variates are used. A Doppler frequency corresponding to a mobile velocity of 5 km/hr is considered. The coefficients are assumed constant for one frame giving a sampling frequency of 100 Hz. A filter length of $L_f = 127$ taps is used and a total of 10^5 samples are considered. Figure 3-8 shows a comparison of the probability density functions of the coefficients generated using the fading coefficients modelled as shown in Figure 3-7 with the corresponding theoretical Rayleigh function calculated using (3.14). It can be seen that the PDF of the fading simulator closely relates to the analytical Rayleigh function.

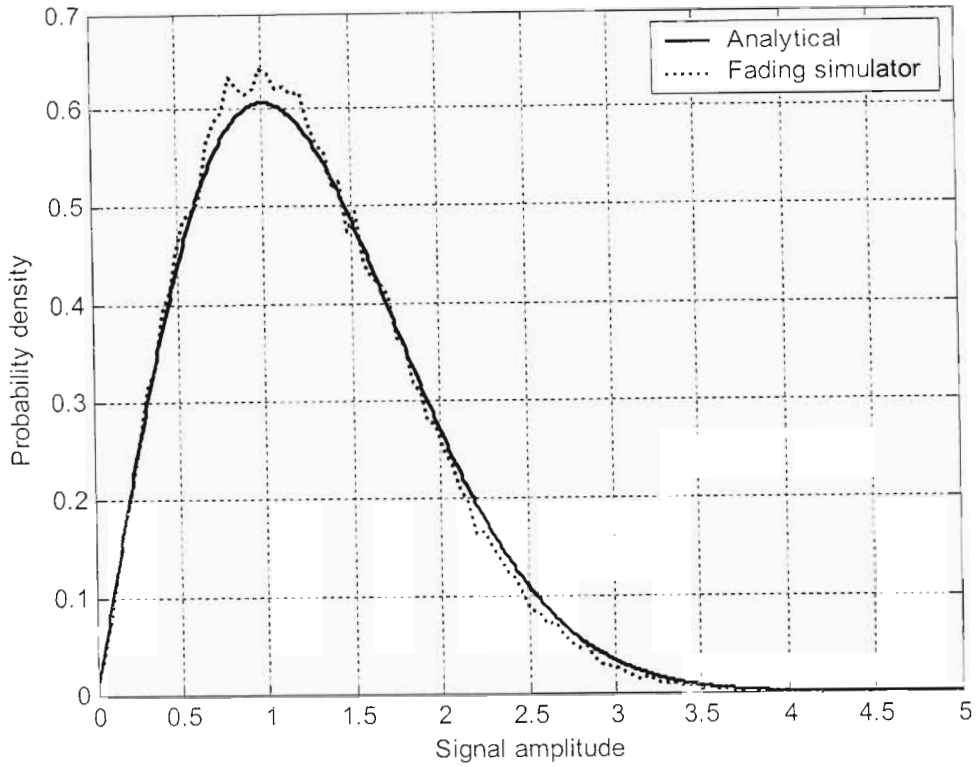

Figure 3-8: PDF of the fading simulator

3.6 Proposed Enhancement

This section presents the proposed system enhancement that exploits the symbol arrangement when performing the correlations in a WCDMA frame. The symbol exploitation techniques of the conventional and proposed algorithms are presented below.

3.6.1 Conventional Symbol Arrangement

The process described in Section 3.3 follows a conventional way of exploiting the correlation length for large carrier frequency offsets. In this scheme, each correlation symbol of 256 chips is divided equally according to the correlation length used. Figure 3-9 shows the symbol arrangement of the conventional algorithm for correlation lengths of 128 and 64 chips. Similarly, the 256 chip symbol can be arranged to accommodate the correlation lengths of 16 and 32 chips. For example, for

a carrier frequency offset of 20 kHz, the 256 chip symbol is divided into four 64 chip divisions as shown in Figure 3-9(b). The outputs of these correlations are then non-coherently combined.

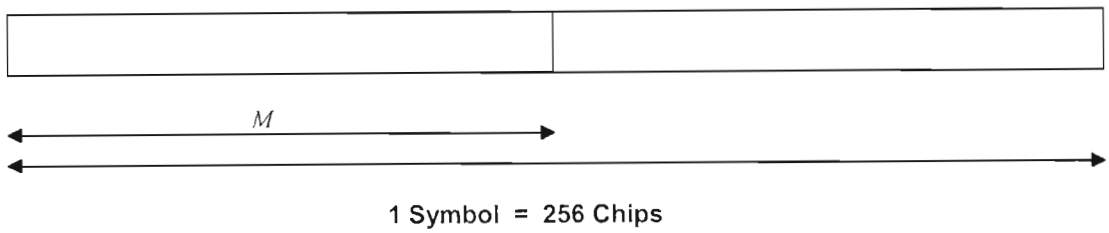

(a)

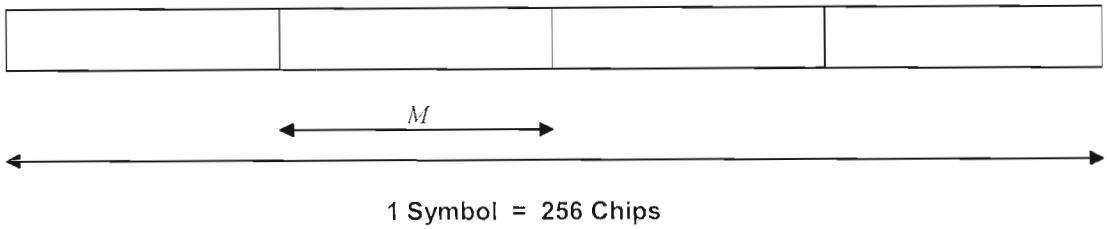

(b)

Figure 3-9: Symbol arrangement in a conventional algorithm

The short coming of the above method lies in its inability to determine the performance when a correlation length different from M = 16, 32, 64, 128, 256 chips is used. Most authors limit the correlation length to these values when investigating the effects of carrier frequency offsets [16][17][34]. However, this raises a question whether there is a possibility of using an arbitrary correlation length.

3.6.2 Proposed Symbol Arrangement

The algorithm proposed by the author in [59] improves on the above problem by investigating the possibility of using correlation lengths that lie in between the values specified above. To do this, the 256 chip correlation interval is exploited in a different way. Two parallel correlators are employed as shown in Figure 3-10 where the 256 chip symbol is shown divided into two and four partial correlation intervals of length M (M does not have to be a factor of 256). This results in an overlap which is shown shaded. This overlap region is exploited in such a way that the correlations normally

neglected using the conventional algorithm are considered by the proposed algorithm, especially when a large carrier frequency offset degrades the received signal.

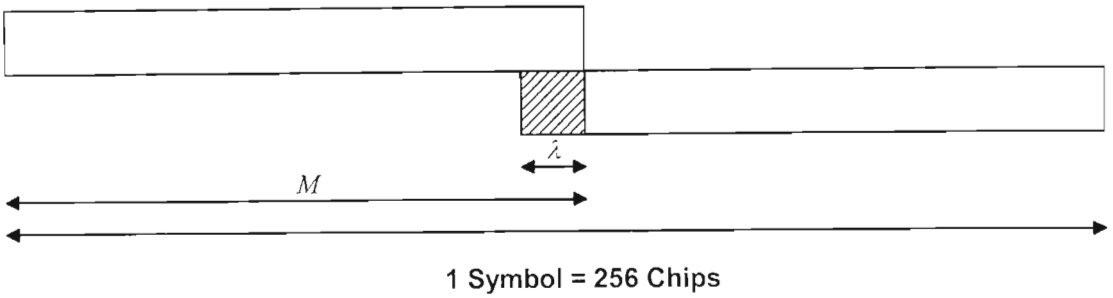

(a)

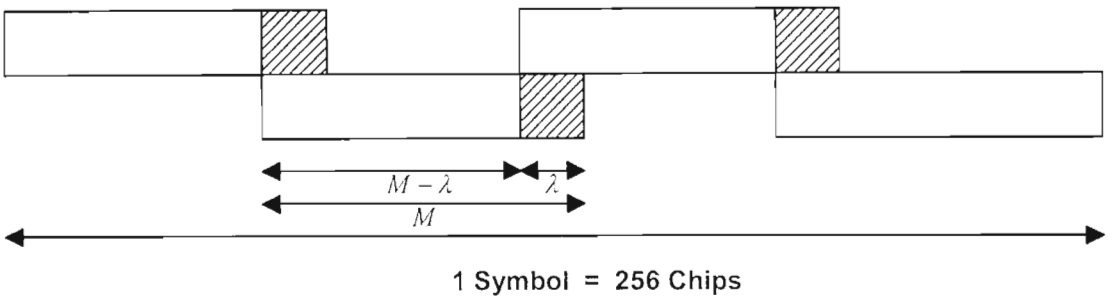

(b)

Figure 3-10: Symbol Exploitation of the Proposed Algorithm

This is possible because the correlations over the overlap region are performed twice and combined to give a decision variable. Once the correlations are performed using the first correlator, the receiver calculates the starting position for the next correlation. For this, the overlapping interval (in chips) has to be subtracted from M. The overlapping interval λ is calculated as (in chips)

$$\lambda = \left\lceil \frac{M * \left\lceil \frac{256}{M} \right\rceil - 256}{\left\lfloor \frac{256}{M} \right\rfloor} \right\rceil \tag{3.18}$$

where $\lceil \bullet \rceil$ denotes the closest upper integer value of the fraction and $\lfloor \bullet \rfloor$ denotes the closest lower integer value of the fraction. The numerator of (3.18) gives the total number of chips that spills over the allocated length of the correlator. This excess

number of chips is redistributed according to the number of partial correlations to be used which can be calculated using the denominator of (3.18).

For example, for a correlation length of 70 chips, there would be 24 chips spilling over the symbol duration. These chips would then be redistributed as an overlap by using four partial correlation intervals. Similarly, for a correlation length of 50 chips, there has to be six partial correlations for an overlap to take place. However, the receiver dynamically allocates the number of partial correlations per symbol once the correlation is selected.

3.7 Simulation Model

This section presents the system description of the model used in this dissertation to investigate the performance of the proposed algorithm.

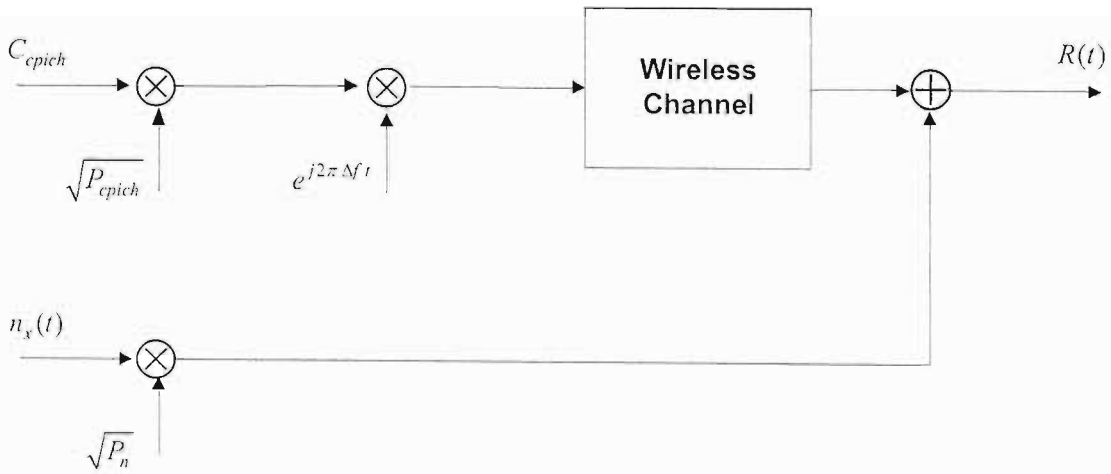

Figure 3-11: Model used to study Stage 3 performance

The Stage 3 of the cell searching process is selected to investigate the performance of the proposed algorithm. Figure 3-11 shows the model used to investigate the performance of Stage 3 of the cell search process. C_{cpich} represents the base station data that is scrambled with the scrambling code of the base station. P_{cpich} is the power of the transmitted base station data. $n_x(t)$ is the system noise and is modelled as an additive white Gaussian noise. P_n is the noise power. Δf represents the frequency

offset at the receiver. The signal-to-noise ratio (dB) is considered to be the power ratio between P_{cpich} and P_n. The expression $e^{j2\pi\Delta f t}$ is used to model the effect of frequency offset on the transmitted data. A flat Rayleigh fading channel is assumed. *R(t)* represents the received signal and is fed into a Stage 3 synchronising system. For a flat fading channel envelope $\alpha(t)$, the received signal *R(t)* can be written as

$$R(t) = \sqrt{P_{cpich}}\, C_{cpich}(t) e^{j2\pi\Delta f t}\, \alpha(t) + \sqrt{P_n}\, n_x(t) \tag{3.19}$$

It is assumed the slot timing, frame and scrambling code group are already known to the receiver. Moreover, discrete samples at intervals of the chip duration are used. The conventional way of detecting the scrambling code is presented in Section 3.3 is modified to accommodate the partial correlation interval M as

$$D(q,k) = \sum_{j=1}^{256/M} \left| \sum_{i=1}^{M} R\left(i + M(j-1) + T(q-1)\right) C^{(k)}\left(i + M(j-1) + T(q-1)\right) \right|^2 \tag{3.20}$$

The proposed algorithm builds on the conventional algorithm by incorporating the overlap interval length λ as

$$D(q,k) = \sum_{j=1}^{256/M} \left| \sum_{i=1}^{M} R\left(i + (M-\lambda)\right)(j-1) + T(q-1)\right) C^{(k)}\left(i + (M-\lambda)\right)(j-1) + T(q-1)\right) \Big|^2 \tag{3.21}$$

The rest of the procedure is the same as outlined in Section 3.3.3. The contribution of the new algorithm is to reconfigure the partial correlation structure of every received symbol with a view to investigating the possibility of using a wide variety of M depending upon the frequency offset.

3.8 Simulation Results

This section presents the simulation results. Performance evaluation is done through simulation. This section focuses on the Stage 3 of the cell search process. Hence the PSC and SSC codes are not included in the base station data. In order to represent the pre-defined common pilot channel, the base station data is generated using the all 1's sequence which is then scrambled by a cell specific scrambling code. The cell-specific scrambling code is generated using the Gold code generator described in Chapter 2.

The effects of frequency offset and wireless channel coefficients are then included to the base station data. This dissertation considers the frequency offset to be in the range 0 - 20 kHz. The filtered white Gaussian noise model described in Section 3.5 is used to derive the channel coefficients of a flat fading channel with a Doppler frequency of 9.26 Hz (corresponding to a receiving terminal velocity of 5 km/hr) and an FIR length of 127. The noise is modelled as additive white Gaussian. The received signal is then passed through the Stage 3 synchronisation algorithm described in Section 3.3 with further modification described in (3.21) to cater for partial correlation intervals. The probability of miss detection is used as a performance measure. It is defined as the probability of the algorithm to fail to detect the transmitted scrambling code from the received signal [17]. The assumption is the algorithm exactly knows where the start of the slot, start of frame and the scrambling code group of the transmitted signal. Monte Carlo simulations are used with 1000 iterations for each probability of miss detection.

Figure 3-12 shows the performance of Stage 3 for the conventional and the proposed algorithms. The frequency offset is 20 kHz. Different values of the partial correlation length M are considered. $M = 64$ gives an optimum performance with the conventional system. The miss detection probability for $M = 64$ agrees closely with the values shown in [16]. The performance degrades for higher values of M due to the high value of carrier frequency offset. An improvement is recorded when considering low signal to noise ratios. The proposed algorithm, however, performs better that the conventional one for values of M in the range 16 to 128. The performance degrades

for values of M between 128 and 256 due to the presence of large phase rotations in the received signal. It can be shown that these phase rotations do not get corrected when large values of partial correlation length are used. It can also be noted that it is not a good practice to use large values of M for carrier frequency offsets larger than 15 kHz. Optimum performance is achieved for values of M in the range 32 to 64. When M = 16, 32, 64, 128 and 256 chips, the proposed algorithm reduces to the conventional one. This is because the overlapping length λ is zero in (3.18) for the above values of M. However, there may be very minute deviations between the two due to the difference in the noise sequences required the simulation. The proposed algorithm is therefore a modified version of the algorithm presented in Section 3.3.

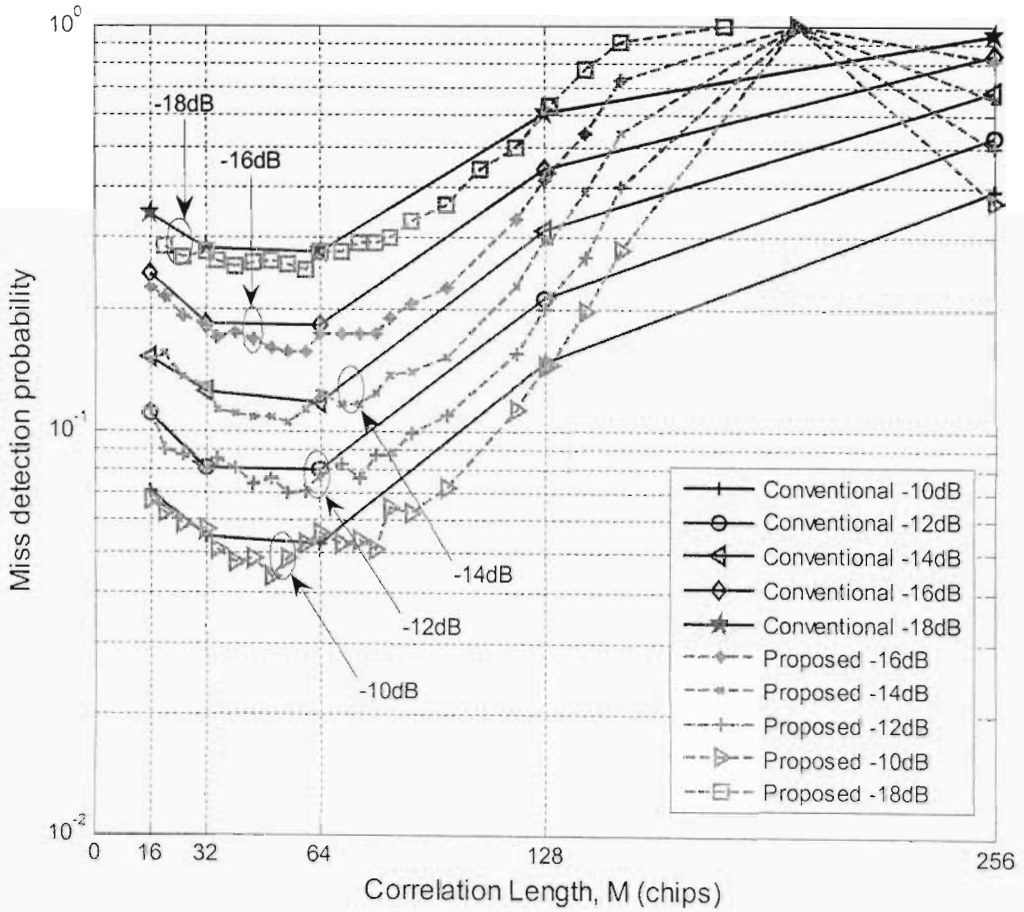

Figure 3-12: Performance of Stage 3 (Frequency Offset = 20 kHz.)

Figure 3-13, Figure 3-14 and Figure 3-15 show the performance for different frequency offset values. At lower frequency offsets, the higher correlation lengths tend to improve their performance. In Figure 3-13, worst performance is recorded for both the proposed and the conventional algorithms at correlation lengths of 128 and 256 chips. At these points, there is a complete phase rotation of the received signal due to the 15 kHz frequency offset. The proposed algorithm is shown to have a better performance for most values of M when compared to the conventional algorithm.

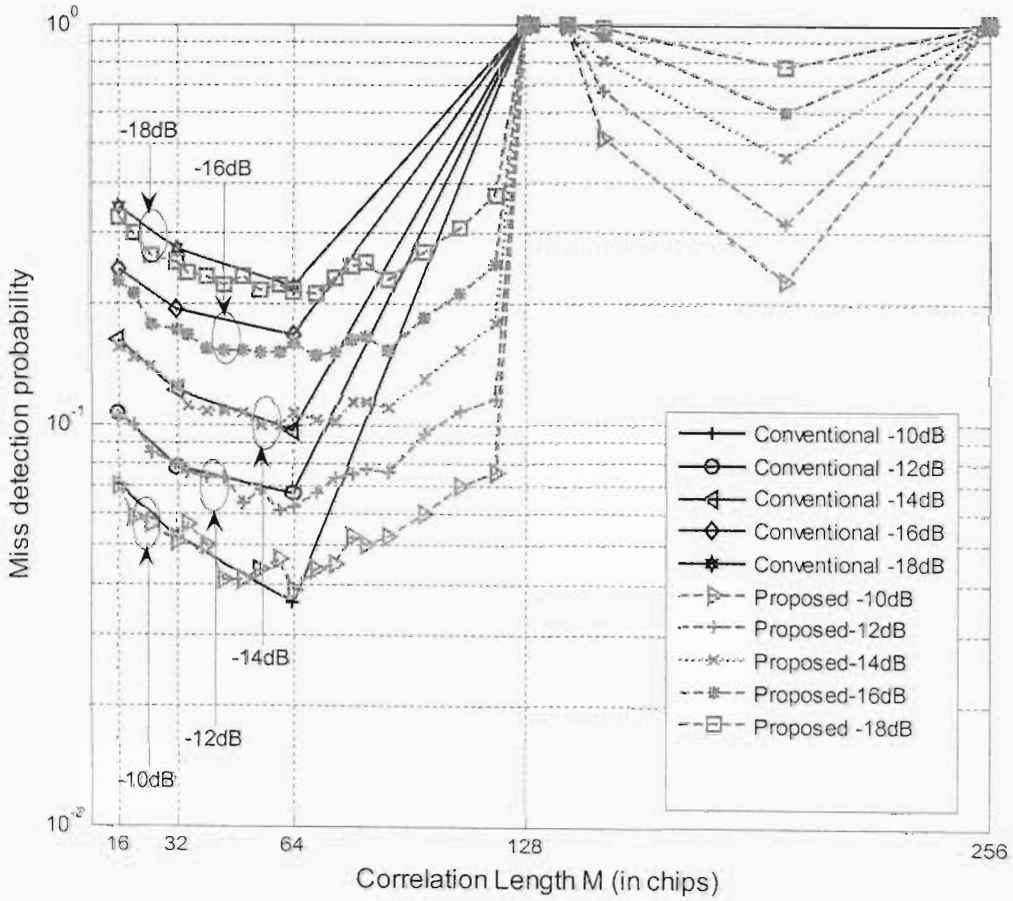

Figure 3-13: Performance of Stage 3. (Frequency Offset = 15 kHz.)

In Figure 3-14, the Stage 3 performance is shown when a 10 kHz carrier frequency offsets is considered. For all values of the correlation length considered, the proposed algorithm is seen to have an improved performance when compared to the conventional algorithm. Moreover, an improvement is shown as the signal to noise ratio decreases. Furthermore, when the carrier frequency offsets of 10 kHz is considered, it can be shown that the performance of both algorithms tend to improve when compared to the results shown in Figure 3-12 and Figure 3-13.

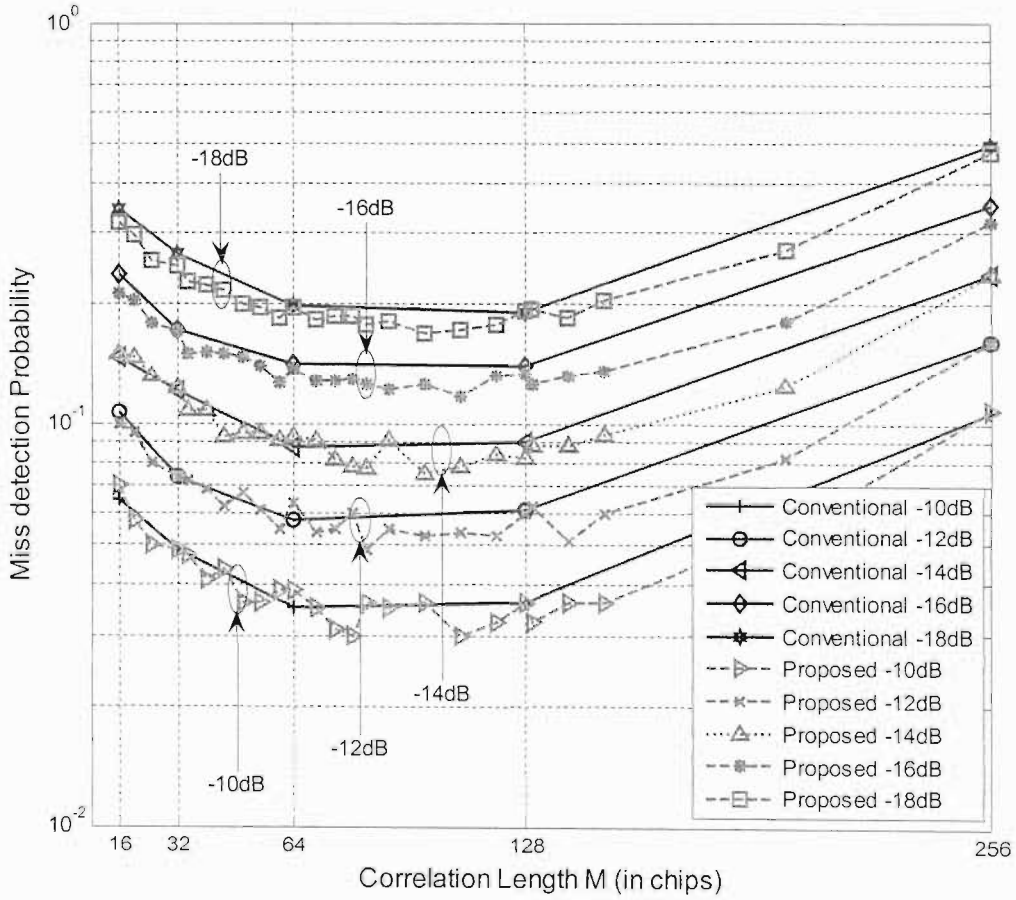

Figure 3-14: Performance of Stage 3. (Frequency Offset = 10 kHz.)

In Figure 3-15, the results of the proposed and conventional algorithms are shown for a carrier frequency offset of 5 kHz. It can be shown that the proposed algorithm performs better for most values of the partial correlation lengths. Moreover, it can be noticed that the performance tends to increase for large values of the partial correlation length. For example, when comparing the partial correlation lengths of 16 and 256 chips, the performance is better when using the correlation length of 256 chips than when using 16 chips. This can be attributed to the low carrier frequency offset. The results show that it is better to accumulate over 256 chips than 16 chips. This is due to the lower degree of signal rotations occurring at lower carrier frequency offsets.

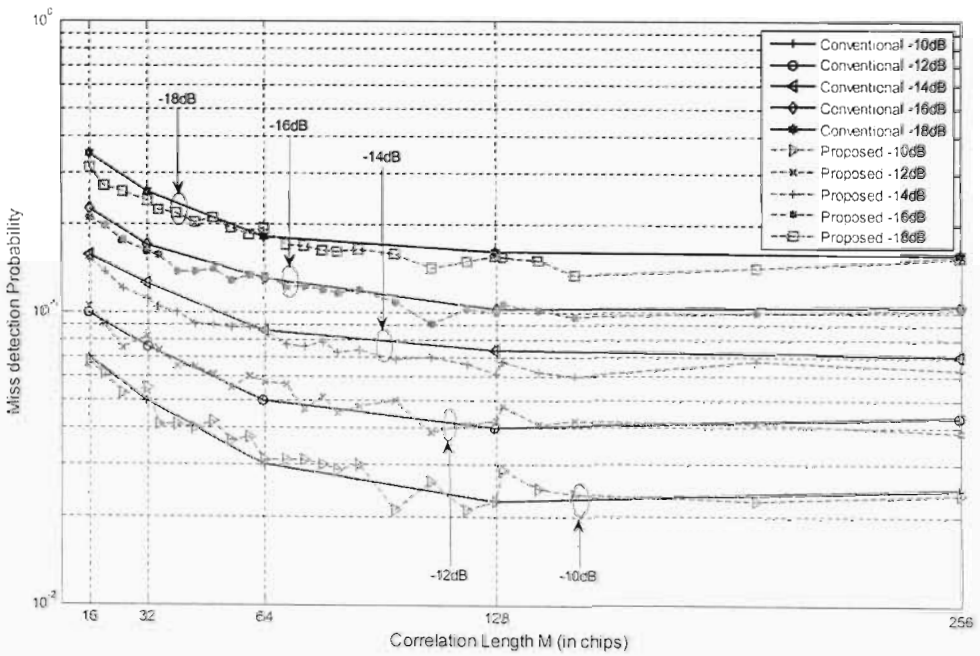

Figure 3-15: Performance of Stage 3. (Frequency Offset = 5 kHz.)

3.9 Summary

This chapter has presented an overview of the performance enhancing studies of cell searching systems. The three types of cell searching algorithms have been described in detail. Various studies from the literature that provided performance enhancement have been discussed. Some of these methods include the serial and parallel cell searching arrangements. Different combining schemes for the correlator outputs have been presented. These are the non-coherent, coherent and differentially coherent schemes. Mitigation techniques of the carrier frequency offset has been highlighted. The wireless channel has been modelled as a flat fading channel by filtering two white Gaussian noise variates. Finally, a method that exploits the symbol arrangement of the WCDMA frame was proposed and its performance was compared with the conventional algorithm by using the third stage of the cell searching process. It was found out that this method shows a better performance at high carrier frequency offsets when compared with the conventional algorithm for various values of the partial correlation lengths when simulated in a flat fading channel with a Doppler of 9.26 Hz. The proposed algorithm has an advantage over the conventional algorithm due to its flexibility to use an arbitrary length of correlation length. It has also been observed that as the carrier frequency offset decreases, the length of the partial correlation can be increased without compromising the performance.

CHAPTER 4

CARRIER FREQUENCY OFFSET ESTIMATION

4.1 Introduction

Chapters 2 and 3 have described cell search systems in WCDMA systems and described the challenges caused by the presence of a carrier frequency offset in the development of signal processing algorithms. Section 4.2 formulates the mathematical model for the estimation of the carrier frequency offset. Section 4.3 reviews the literature of a generalised carrier frequency offset estimation. Section 4.4 discusses carrier frequency offset estimation in a WCDMA environment and presents three types of frequency offset estimators found in the literature. In Section 4.5, a new algorithm that builds on the conventional WCDMA frequency offset estimator is proposed and Section 4.6 presents the simulation results for the proposed algorithm. An analysis model is developed in Section 4.7 to verify the validity of the proposed enhancement and its results are compared to the simulation values. Section 4.8 presents a new technique that improves further the performance of the conventional method and simulation results are provided to illustrate this effect. Finally, conclusions are drawn in Section 4.9.

4.2 The problem of carrier frequency offset estimation

Carrier frequency offset arises when the oscillator at the receiver oscillates at a different frequency to that of the transmitter [60]. This frequency error is seen as a frequency offset to the receiver. This section presents the generation of a carrier frequency offset and establishes the mathematical model used to formulate the problem of carrier frequency offset estimation.

In order to illustrate the generation of a carrier frequency offset, Figure 4-1 shows a model used in a digital communication system using a crystal oscillator at the transmitter and receiver.

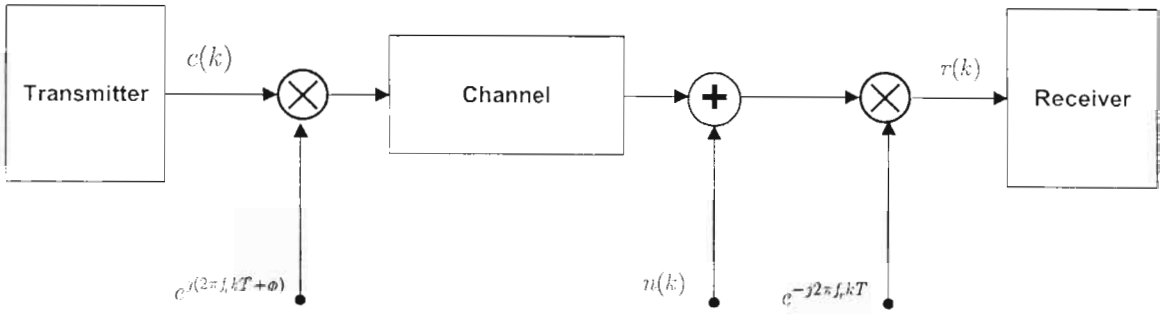

Figure 4-1: Frequency offset modelling

The data to be transmitted $c(k)$ is up-converted using a crystal controlled oscillator with frequency f_c. The modulated signal is then propagated through a radio channel with additive white Gaussian noise $n(k)$. At the receiver, the signal is down-converted using a crystal oscillator with frequency f_r and sampled at the chip period T to give $r(k)$.

Assuming a perfect channel, the received signal $r(k)$ can be expressed as

$$r(k) = \left(c(k) e^{j(2\pi f_c kT + \phi)} + n(k) \right) e^{-j2\pi f_r kT} \tag{4.1}$$

where ϕ represents the phase offset at the transmitter. (4.1) can be further manipulated to give

$$r(k) = c(k)e^{j(2\pi(f_c - f_r)kT + \phi)} + n(k)e^{-j2\pi f_r kT} \tag{4.2}$$

Multiplying both sides of (4.2) with the conjugate of $c(k)$ gives a parameter $y(k)$

$$y(k) = c^*(k)r(k) \tag{4.3}$$

Therefore,

$$y(k) = c^*(k)\left\{c(k)e^{j(2\pi(f_c - f_r)kT + \phi)} + n(k)e^{-j2\pi f_r kT}\right\} \tag{4.4}$$

Using the property of conjugates, $c^*(k).c(k) = 1$ and since the statistics of the second term in (4.4) is equivalent to the noise $n(k)$, (4.4) can be simplified further to

$$y(k) = e^{j(2\pi\Delta f kT + \phi)} + n(k) \tag{4.5}$$

where $\Delta f = f_c - f_r$ is the carrier frequency offset. The challenge posed to the designer is to find some estimate $\widehat{\Delta f}$ that compensates the frequency error introduced. Once a reliable estimate has been found, receiver structures (eg. the PLL) can be implemented to correct the frequency error. Therefore, the problem of carrier frequency offset estimation is finding algorithms that give a good estimate $\widehat{\Delta f}$.

4.3 Literature review on frequency offset estimators

The problem of carrier frequency offset recovery may be alleviated sometimes by imposing strict requirements on the frequency stability of the transmit and receive oscillators [61]. For instance GSM recommendations [62] demand that the un-compensated frequency offset at the demodulator output should not exceed a few

hundred Hz inclusive of Doppler shifts, thus calling for oscillator stabilities better than 0.1 ppm. In a similar way, the WCDMA standard [8] recommends the frequency offset at the receiver must not exceed 200 Hz (0.1 ppm). Therefore, using very stable frequency oscillators is not a feasible way to approach the problem as there is always a Doppler shift that can not be avoided. Hence, it is clear that specialised algorithms need to be investigated to estimate and reduce the carrier frequency offset to meet the specification.

The subject has been discussed extensively in the literature over the past three decades. Rife *et al.* in [63] presented a well developed introduction to frequency offset estimation. The authors investigated the frequency offset estimation problem in a channel with additive white Gaussian noise. They also derived the lower bound for any unbiased frequency offset estimator – the Cramer Rao Lower Bound (CRLB). Their algorithm made use of the Maximum-Likelihood (ML) technique to estimate the frequency offset. However, the ML method is a lengthy and tedious process. Hence, following the results of the investigations presented in [63], other researchers developed techniques that reduce the time and complexity of frequency offset estimation.

In [64], Tretter proposed the use of a first order least squares method to acquire a phase-increment based frequency offset. A few years later, [65] proposed an estimator for a single sinusoid in complex white Gaussian noise. The author showed this algorithm is more computationally efficient than the optimal ML estimator, while attaining equally good performance at high signal-to-noise ratios. In [64] and [66], a differential detector estimates are used to cancel data modulation from the received signal. This makes the average phase slope of the received sequences proportional to the frequency offset. The exploitation of the phase slope would thus give an estimate of the carrier offset.

Before continuing further, it is worth mentioning efforts directed at deriving bounds for frequency estimators. This is an important goal since it provides benchmarks for evaluating the performance of actual estimators. Several authors have addressed this problem from the sense of parameter estimation theory [64][68]. These give fundamental limits to the variance of any un-biased parameter estimator. Other

bounds are discussed in [69][70][71][72]. The CRB for clock and carrier phase recovery in linear modulations and continuous phase modulation is derived in [73][74] and [75], respectively. An analogous treatment of carrier frequency offset estimation is given in [76] where the authors calculated an approximate CRB for frequency estimators. However, the derivation of exact CRM is a complex task and for this reason the ones derived in [76] and alike are called Modified CRB (MCRB) and they are found to be usually used in the literature to compare the performance of proposed estimators [77][78].

Further improvement to the knowledge of carrier frequency offset estimation was reported when [61] proposed algorithms for fast frequency offset recovery based on the removal of data modulation and channel distortion from the received signal. The authors presented an application of their algorithm on satellite link based on a TDMA system and on a GSM based mobile communication system. They used the ML principles to derive their algorithm and when simulated in a channel with additive white Gaussian noise, its performance was reported to lie very close to the CRLB for unbiased estimators as already established in [76].

A subsequent work by Mengali *et al.*[79] discussed a data-aided frequency offset estimation technique in burst-mode PSK transmissions. The authors obtained an algorithm that exploits the autocorrelation of the sample correlations. Moreover, the authors compared the performance of this technique with those proposed by Fitz *et al.*, Luise *et al.* and Lovell *et al.* in [80], [61] and [81] respectively. Employing a design criteria explained in [79], it was reported that apart from the technique proposed by Lovell *et al.*, the others were found to lie very close to the CRLB when simulated in a channel with additive white Gaussian noise. It is worth mentioning at this point that the estimator by Mengali *et al.* showed no dependence on the design parameter while the others are reported to do so.

Due to the complexity encountered in deriving and analysing frequency offset estimators in frequency selective channels, most published work emphasised investigations on the additive white Gaussian noise channels [61][63][64][65][66] [76][79][80][81]. However some researchers have made efforts to investigate the problem of frequency offset estimation in frequency selective channels and can be

consulted in [78][82][83][84]. Estimation in flat fading channels is presented in [85][86]. Studies relating antennae diversity are studied in [87] [88]. To give an insight to the reader, a brief summary of the work in [83] and [78] is presented below.

In [83], the authors proposed a robust low complexity estimation technique for frequency acquisition in frequency selective channels. The motivation behind their proposal is that conventional estimators are no longer adequate when the delay spread is large. This effect presents a challenge to the designer as it is generally not possible to do frame synchronisation, channel estimation or data demodulation before the carrier frequencies are aligned. To attack this requirement, most algorithms rely on having a preamble at the beginning of the packet which is either a tone or an alternating pattern or ones and zeros. These preamble sequences are inadequate to estimate the offset in frequency selective channels, especially for packet switched systems that require frequency synchronisation on every packet. For robust operation in this case, the frequency must be acquired with a short preamble and yet remain robust to frequency selective fading. Conventional estimators are inadequate in deep fades when they use tone preambles. The same effect applies when using an alternating pattern of ones and zeros. Thus to counteract this problem, the authors in [83] used short preamble sequences made of pseudo noise sequences of 100 bits. They have showed a superior performance to the existing algorithm in a wireless Local Area Network (LAN) environment,

Another comprehensive treatment of frequency selective channels is presented in [78] where the authors studied frequency offset estimators in slowly fading multipath channels. They were inspired by the way a RAKE receiver improves the detection performance in multipath channels, and thus looked into techniques where frequency estimators can also exploit multipath diversity to improve estimation accuracy. Therefore, they derived frequency estimation algorithms exploiting multipath diversity and statistical characteristics of the channel to improve the accuracy performance. Their work has a good advantage in that it was shown to operate in a low SNR environment. The implementation of their algorithm is based on a course and fine search of the peaks of a periodogram.

The previous discussions were focused on the estimation of small carrier frequency offsets. It would sometimes be of interest to investigate estimation techniques when the carrier frequency offset is large. The fact that the relative movement between the transmitter and receiver induces various degrees of frequency variation at the receiver end makes it even more critical in a mobile communications channel. [89] and [90] give a good treatment of this topic. This problem is especially difficult to overcome in a high dynamic environment such as mobile low-earth-orbit (LEO) satellite communications [89]. The same authors showed that the Doppler shifts seen by an earth terminal of a 1.5 GHz signal transmitted from a LEO satellite travelling in a circular earth orbit of 350 km can be a prohibiting 35 kHz or changing at a rate of 800 Hz/s. Therefore, the same authors in [89] proposed algorithms for the very high Doppler shifts and its effects on the estimation of the frequency offset.

Although the discussions hitherto focused on frequency offset estimation in generalised digital communication systems, the next section emphasises estimation in a WCDMA system.

4.4 Carrier frequency offset estimation in WCDMA systems

The previous section highlighted the evolving landscape of algorithms used in the literature of carrier frequency offset estimation. Most authors limit their application to a generalised communication system. For this reason, the estimation problem in a WCDMA system has been given little attention in the literature. This section describes the techniques that are currently used to estimate the carrier frequency offset in a WCDMA system.

A WCDMA system has a unique frame structure. In order to investigate new estimation algorithms for these systems, or alternatively adopt suitable ones from the literature, it is important to proceed the investigation by reverting to the frame structure of a WCDMA system. This has been shown in Figure 2-6 in Chapter 2 and is used as a basis for this chapter. Rykaczewski *et al.* [77] states that the presence of a pilot channel in such systems could use data-aided algorithms as an attractive option.

This means that the receiver would have to know the scrambling code of the transmitter before initiating the de-spreading process. Figure 4-2 shows a generalised system model used for frequency offset estimation in WCDMA systems. In the algorithms presented in this chapter, it is assumed that the receiver has knowledge of the scrambling code which is obtained from the 'SEARCHER'.

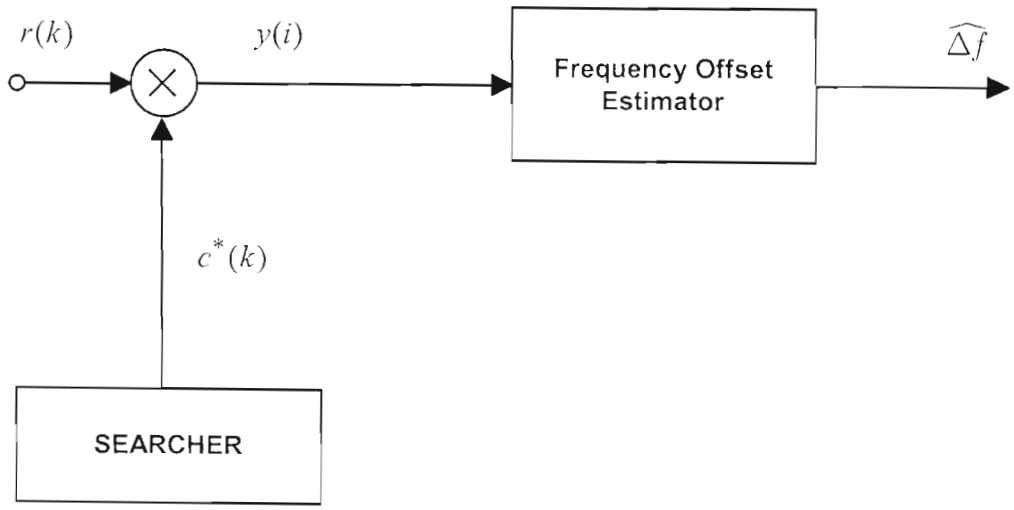

Figure 4-2: A generalised model for frequency offset estimation in WCDMA systems

The received signal can be written as,

$$r(t) = \sqrt{p_k}\, d(t)\, c(t)\, e^{j(2\pi \Delta f\, t + \phi)} + \sqrt{p_n}\, n_x(t) \tag{4.6}$$

where p_k represents the power of the complex scrambling code $c(t)$ used to spread the complex transmitted data signal $d(t)$ and $e^{j(2\pi \Delta f t + \phi)}$ is used to model the effect of the frequency offset Δf and phase ϕ. Additive White Gaussian Noise (AWGN) $n_x(t)$ is introduced with power p_n. The de-spread signal $y(i)$ is computed as,

$$y(i) = \sum_{k=0}^{S_F - 1} r(i \times S_F + k)\, c^*(i \times S_F + k) \qquad i = 0, 1, 2, \ldots, P-1 \tag{4.7}$$

where S_F is the de-spreading factor in chips and $P = \frac{N_f \times 38400}{S_F} - 1$ is the total number of de-spread sequences in one frame and N_f represents the number of frames considered for estimation. Each W-CDMA frame has a period of 10 ms and contains 38400 chips. Each frame is divided into 15 parts called 'slots'. A slot is made up of 2560 chips [8]. Using chip duration T_c, (4.7) can be re-written as

$$y(i) = Y_0 e^{j(2\pi \Delta f \times S_F \times i \times T_c + \phi)}, \qquad i = 1, 2, \ldots, P \tag{4.8}$$

where Y_0 is the magnitude of the complex de-spread signal with components I and Q with amplitude +V and -V. Hence, it can be seen that (4.8) resembles the general frequency offset equation represented in (4.5).

To illustrate the degradation effect of the frequency offset on the de-spread signal, the complex signal in (4.8) is simulated assuming the I and Q components of the de-spread signal to be all ones with an amplitude V of $\frac{1}{\sqrt{2}}$ or 0.707 to give a unity power. A de-spreading factor of 64 is assumed and the frequency offset is introduced. Figures 4-3(a) – (f) shows the effect of different frequency offset values on the de-spread signal. In Figure 4-3(a), there is no frequency offset included and the de-spread signal remains unchanged. The de-spread signal is shown to rotate with the frequency offset in Figures 4-3(b) - (f) caused by the exponential term in (4.8) which changes the amplitudes of the in-phase (I) and quadrature (Q) parts of the de-spread signal. This signal rotation is the main cause of communications failure and it needs to be corrected [17]. With an offset of 200 Hz shown in Figure 4-3(b), the amplitude of the in-phase de-spread signal changes during three WCDMA slot intervals (i.e. within 2 ms) from 0.7 to -0.7 which results in a 180^0 phase rotation. Even higher phase rotations occur with larger frequency offsets. Therefore, it is very crucial to estimate the frequency offset and correct these phase rotations to ensure reliable data recovery.

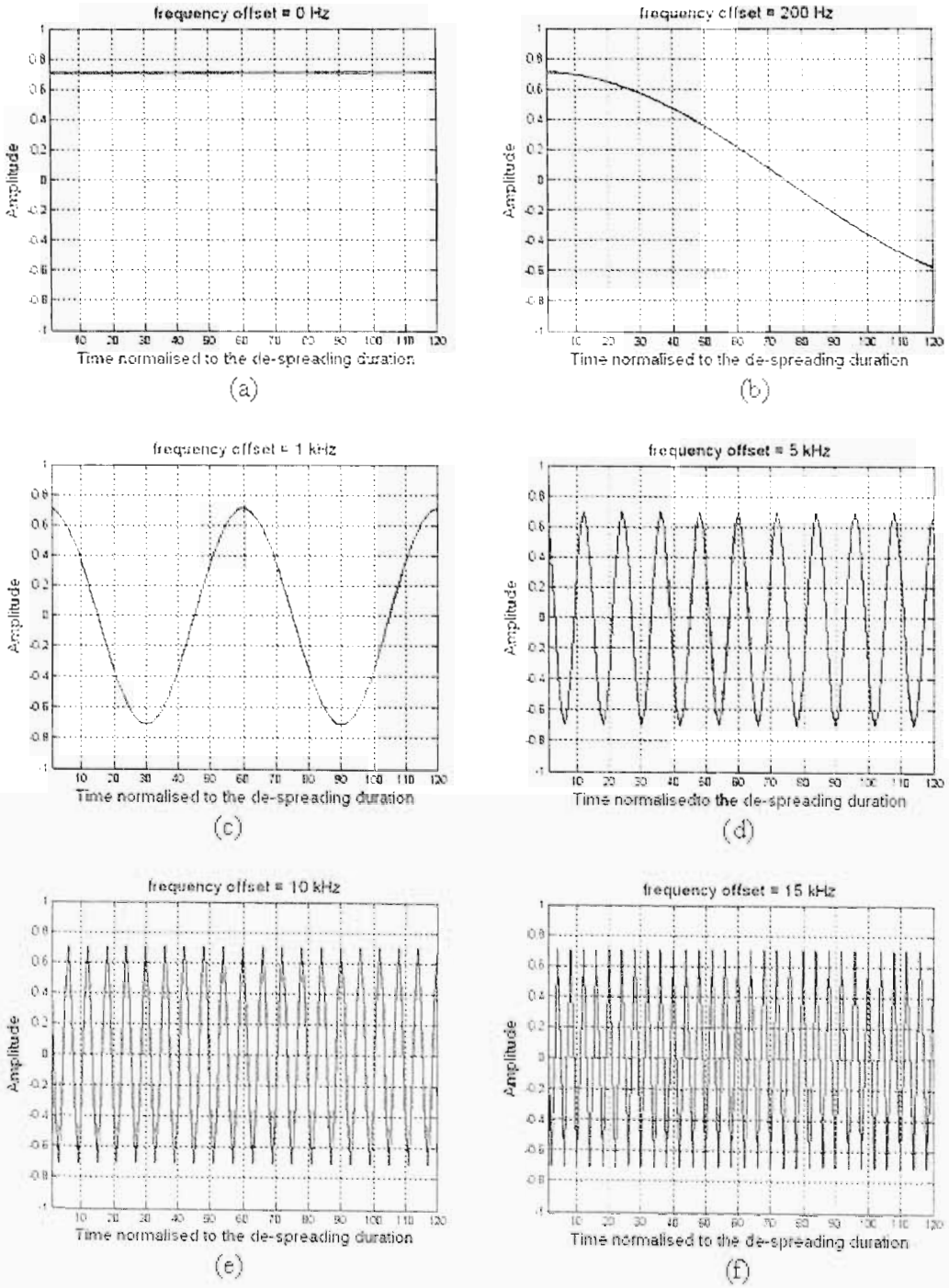

Figure 4-3: Variation of the de-spread signal (I or Q) for different frequency offset values. (De-spreading duration = $64T_c$)

The following sub-sections discuss the three types of estimation algorithms currently used in WCDMA systems. These are the phase increment based, the autocorrelation based and the FFT based algorithms. It is important to stress the fact that the first two estimation algorithms originated from [65] and [79], respectively while the FFT based algorithms are based on the work done in [17][77][91].

4.4.1 Phase Increment Based Estimators

Phase increment based estimators have been studied in [64][65][77][81]. In [77], the estimator proposed by [65] was applied to a WCDMA system. It is referred to here as a phase increment based estimator and is discussed below.

Consider the de-spread symbols in (4.8). The phase increment algorithm first computes the phase difference $z(i)$ between two consecutive de-spread values as

$$z(i) = \arg\{ y(i) \} - \arg\{ y(i-1) \}, \qquad i = 1, 2, ..., P \tag{4.9}$$

and calculates an estimate of the carrier frequency offset

$$\widehat{\Delta f} = \frac{1}{2\pi S_F T_c} \sum_{i=1}^{L-1} w(i)\, z(i) \tag{4.10}$$

where w_i is a smoothing function represented by

$$w(i) = \frac{6i(L-i)}{L(L^2-1)}, \qquad i = 1, 2, ..., L-1 \tag{4.11}$$

The parameter L defines the width of the smoothing function. This can be understood as a number of symbols considered for giving an estimate of the frequency offset.

4.4.2 Autocorrelation Based Estimators

Instead of exploiting the phase difference between successive de-spread sequences, autocorrelation based algorithms use the autocorrelation values of the de-spread sequences to give an estimate of the frequency offset. This technique of estimating the frequency offset has been studied in [61][79][80][84]. In this dissertation, the autocorrelation based estimation technique is discussed briefly. A more detailed discussion can be found in [79] and [84].

The autocorrelation based algorithm computes the sample correlations,

$$R(m) = \frac{1}{L-1}\sum_{i=m}^{L-1} y(i)\, y^{*}(i-m), \qquad m = 1, 2, ..., N \tag{4.12}$$

where L is the number of symbols considered for estimation and N is a design parameter not greater than $\frac{L}{2}$. It uses these sample correlations to estimate the frequency offset as

$$\widehat{\Delta f} = \frac{1}{2\pi S_F T_c}\sum_{m=1}^{N} w(m)[\arg\{R(m)\} - \arg\{R(m-1)\}] \tag{4.13}$$

with the smoothing function $w(i)$ defined as

$$w(i) = \frac{3\left[(L-i)(L-i+1) - N(L-N)\right]}{N\left(4N^2 - 6NL + 3L^2 - 1\right)} \tag{4.14}$$

It can be noticed that the complexity of the above technique is large, mainly due to the computational complexity of (4.12). It is of interest to provide a technique in which the complexity of the above estimator can be simplified at high signal-to-noise ratios [79]. This is achieved by modifying the sample correlations as [79]

$$\tilde{R}(m) = \frac{1}{L-1} \sum_{i=m}^{L-1} \exp\{j[\arg\{y(i)\} - \arg\{y(i-m)\}]\}, \qquad m = 1, 2, ..., N \qquad (4.15)$$

The authors in [79] state that (4.15) can be used instead of (4.12) at high signal-to-noise ratios, but they have not used the WCDMA system to compare their performance. In [77], Rykaczewski *et al.* used the above algorithm to estimate the frequency offset in a WCDMA system. However, it is not stated whether they have used (4.12) or (4.15) in presenting the performance of the autocorrelation based estimators in WCDMA systems.

4.4.3 Conventional FFT Based Estimators

The Fast Fourier Transform (FFT) has been widely used for applications that require frequency estimation from given sequences. In this dissertation, emphasis is given to the use of the FFT in estimating the frequency offset from the de-spread sequences as represented in (4.8). For this purpose, [17][91] studied FFT based techniques and proposed the use of quadratic interpolation of the FFT peaks to improve the estimation accuracy in WCDMA systems. On another front, 12 years before the above publications, researchers from the Stanford University's Department of Music were using the same technique for the analysis and synthesis of in-harmonic sounds based on a sinusoidal representation [92]. In this section, the basic technique of quadratic interpolation of the FFT peaks is presented along with its applicability to WCDMA systems.

However, it is important to mention briefly some of the important parameters related to the FFT.

Frequency resolution of an FFT

The frequency resolution of an FFT relates to the degree of accuracy of the FFT computation. In a WCDMA system, the frequency resolution depends on the chip rate, de-spreading factor and FFT length. To decrease implementation complexity, the length of the FFT is usually chosen to be a power of 2. The frequency resolution

$f_{resolution}$ is calculated as $f_{resolution} = \frac{1}{(S_F T_c) \times K}$, where K represents the length of the FFT, S_F is the de-spreading factor in chips and T_c is the chip duration.

Zero padding factor

Zero padding represents the appending of zeros to the end of the de-spread sequences and the zero padding factor is calculated as the ratio of the number of de-spread sequences per slot to the length of the FFT.

Figure 4-4 shows the FFT based WCDMA estimator exploiting quadratic interpolation. Similar to the last two groups of estimators discussed above, it first computes the de-spread sequences using the knowledge of the scrambling sequence used at the transmitter.

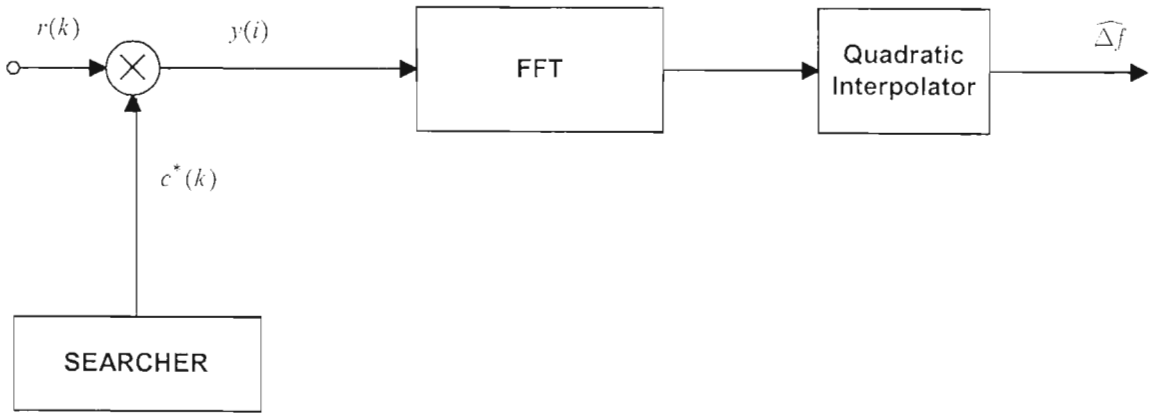

Figure 4-4: Schematics of an FFT-based frequency offset estimator

The FFT coefficients of (4.8) are then computed with a Rectangular window function with zero padding in order to use an FFT length of a power of 2. Quadratic interpolation is then applied to the peaks of the FFT. Figure 4-5 illustrates the technique of finding the peak of the spectrum from three adjacent spectral lines. Point B (f_k, h_k) is the point of maximum FFT energy detected by the receiver, whereas points A (f_{k-1}, h_{k-1}) and C (f_{k+1}, h_{k-1}) are the spectral lines adjacent to it. The true frequency f is located at Point D.

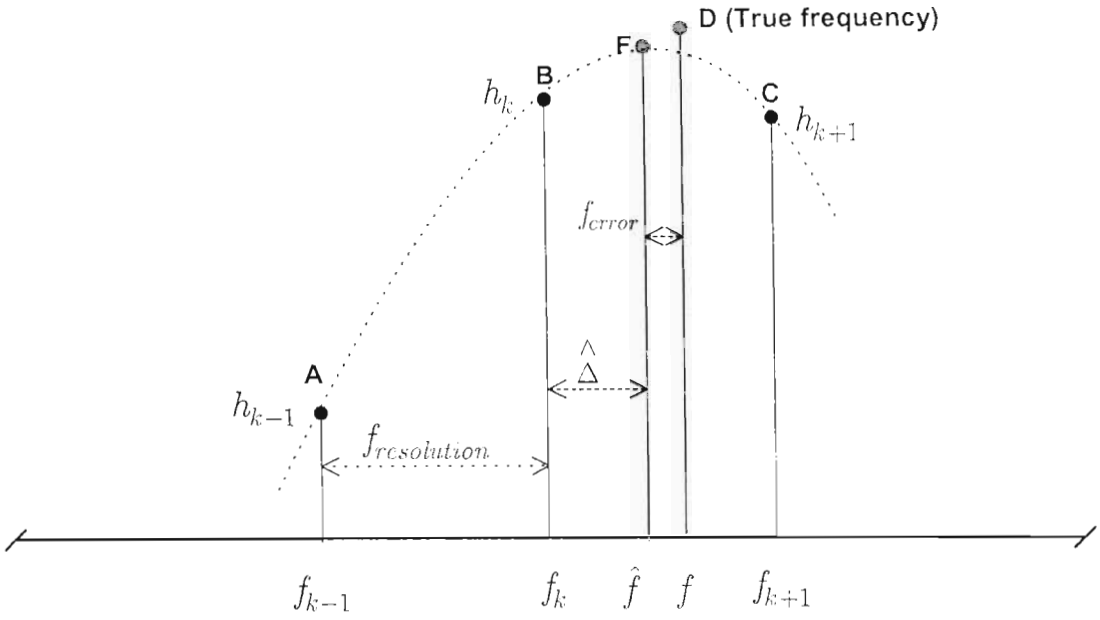

Figure 4-5: Representation of the peaks of an FFT sequence

A quadratic polynomial is then applied between the spectral peaks A, B and C to estimate the true peak which is located at point D. This operation gives point F and $\hat{\Delta}$ is the bias arising from interpolation. The estimated frequency $\hat{f}$ given in [17] can be rewritten as

$$\hat{f} = f_k + \hat{\Delta} \times f_{resolution} \tag{4.16}$$

where $\hat{\Delta} = \frac{1}{2}\left(\frac{h_{k-1} - h_{k+1}}{h_{k-1} - 2h_k + h_{k+1}}\right)$ and $f_{resolution}$ is the frequency resolution of the FFT.

The error in estimation is the difference in frequency between points F and D, and is computed as

$$f_{error} = f - \hat{f} \tag{4.17}$$

4.5 Proposed Estimator

In this section, a new technique that improves the estimated frequency offset of an FFT based estimator is proposed. This technique is based on the work done by [93] and its performance is extended to the WCDMA system. The motivation and simulation model of the proposed algorithm is presented below.

4.5.1 Motivation

Due to the operation of quadratic interpolation of the FFT peaks, the estimated frequency offset is biased [93][77]. A correction algorithm for estimating sinusoidal parameters of music signals is proposed in [93]. This algorithm is dependent on the specific window function used and the zero padding factor of the FFT. The bias in the estimated frequency offset $\hat{\Delta}$ in (4.16) is then corrected by [93] using

$$\check{\Delta} = \hat{\Delta} + \xi_{Z_p}\left(\hat{\Delta} - 0.5\right)\left(\hat{\Delta} + 0.5\right)\hat{\Delta} \tag{4.18}$$

where $\check{\Delta}$ is the new bias after correction depicted in Figure 4-6 at Point G and ξ_{Z_p} is a scaling factor that is dependent on the zero padding factor and the type of window function used [93] and is calculated by

$$\xi_{Z_p} = c_0 Z_p^{-2} + c_1 Z_p^{-4} \tag{4.19}$$

where c_0 and c_1 are window-specific filter coefficients and $Z_p = K/M$ is the zero padding factor where K is the FFT size and M the window length. The corrected frequency estimate $\check{f}$ is then given by

$$\check{f} = f_k + \check{\Delta} \times f_{resolution} \tag{4.20}$$

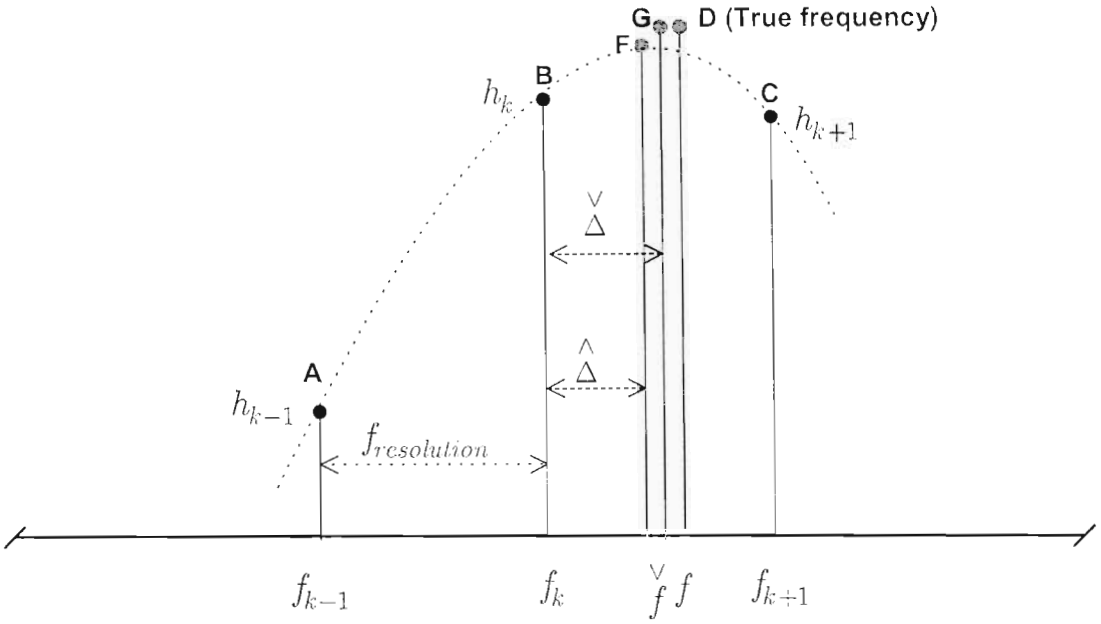

Figure 4-6: Representation of the peaks of an FFT sequence for the proposed algorithm

Although the authors in [93] exploited the performance of the estimation algorithm in music signals, they make no mention of its applicability to WCDMA systems. In this dissertation, it is modified to suit the structure of the WCDMA system and the simulation model used for the investigation is presented.

Table 4-1: Coefficients of the correction function [93]

Window function	c_0	c_1
Rectangular window	1.279369	1.756245
Hanning window	0.247560	0.084372
Hamming window	0.256498	0.075977
Blackman window	0.124188	0.013752

4.5.2 Simulation model

This section presents the simulation procedures. Table 4-2 shows the simulation parameters used in this investigation. The window functions used are Rectangular, Hanning, Hamming and Blackman windows. To apply the correction algorithm

(4.20), the scaling factor for the window functions considered was computed using knowledge of the filter coefficients presented in [93] given in Table 4-1.

Table 4-2: Simulation parameters

Number of frames	1
FFT size (K)	64 point
De-spread values per slot (M)	40
Zero padding factor (Z_p)	1.6
De-spreading factor (S_F)	64
De-spread values per frame (P)	600
Slot duration (t_1)	2/3 ms
FFT window duration (t_2)	(64/40) x (2/3) ms
Resolution of FFT ($1/t_2$)	937.5 Hz
SNR	20 dB
Number of iterations	2500

The received data was generated as follows. A Gold code generator [8] of length 18 was used to generate the scrambling code sequence needed to spread the data signal. Its length was then truncated to 38400 chips in order to satisfy the WCDMA frame length requirement of 10 ms. This data was then corrupted with a frequency offset at the start of the frame and AWGN added to give a signal-to-noise ratio of 20 dB. The phase ϕ was assumed to be uniformly distributed in the interval 0 to 2π. At the receiver, the same Gold code was used to de-spread the received signal. The following procedures were then performed to estimate the frequency offset.

Step 1. De-spread signal using a spreading factor of 64.

Step 2. Collect 40 samples per slot.

Step 3. Apply a window function.

Step 4. Compute the 64 point FFT of the above sequence with 24 zeros to fill up the FFT window.

Step 5. Perform steps 1 – 4 on each slot in the available frames and find the average spectral amplitude at each bin frequency.

Step 6. Perform quadratic interpolation on the averaged FFT sequence.

Step 7. Apply (4.16) to estimate the frequency offset.

Step 8. Apply (4.20) to correct the bias value obtained in step 7.

4.6 Simulation Results

In this section, the simulation results for the conventional FFT estimator and the proposed algorithm are presented. The mean frequency error is used as a measure of performance of the estimator. It is defined as the difference between the transmitted and estimated carrier frequencies. Figures 4-7 to 4-11 show the results obtained.

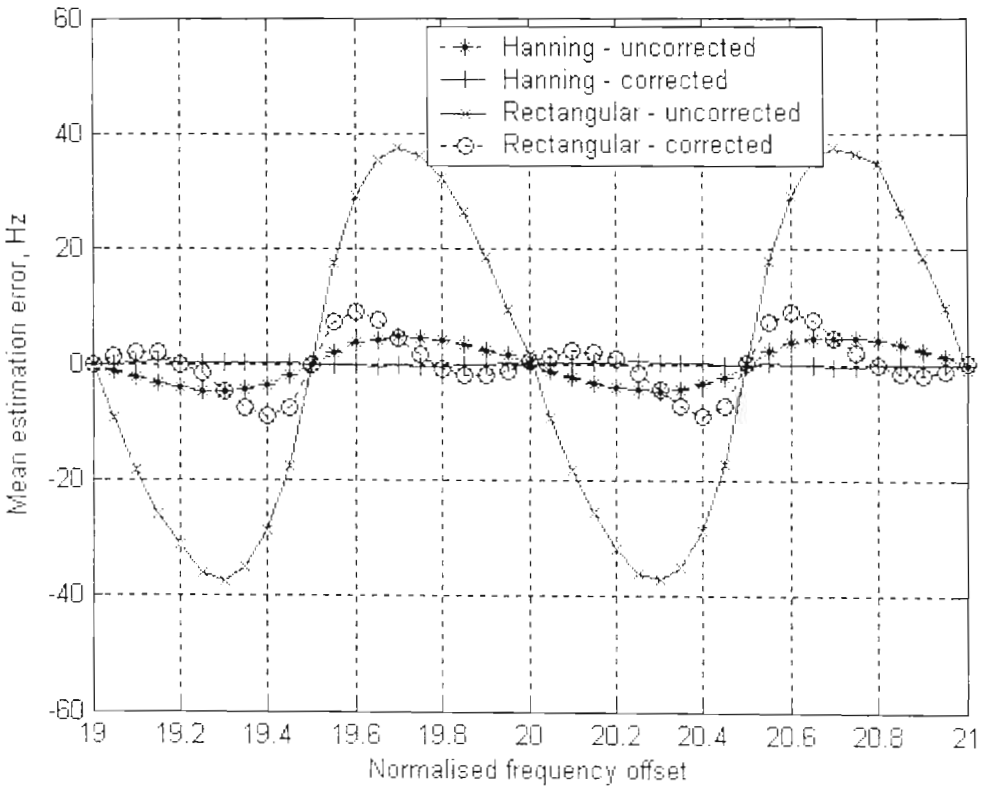

Figure 4-7: Mean estimation error with Rectangular and Hanning windows as function of frequency offset normalised to the frequency resolution of the FFT.

Figure 4-7 shows the frequency estimation performance using Rectangular and Hanning window functions. An accuracy of ± 38 Hz is obtained when a Rectangular window function is used. This is greatly improved to ± 4.66 Hz when a Hanning window is applied.

The Hanning window function is shown to have a better estimation performance than the Rectangular window. This is attributed to its low relative sideband leakage with a side-lobe falloff of -18 dB/octave and highest side-lobe level of -32 dB [94]. Moreover, the width of the central lobe of a Hanning function (3 dB bandwidth of 1.44 bins) also contributes to this improvement. The correction algorithm (4.20) is able to reduce the error in the Rectangular and Hanning function to within ± 9.06 Hz and ± 0.48 Hz respectively.

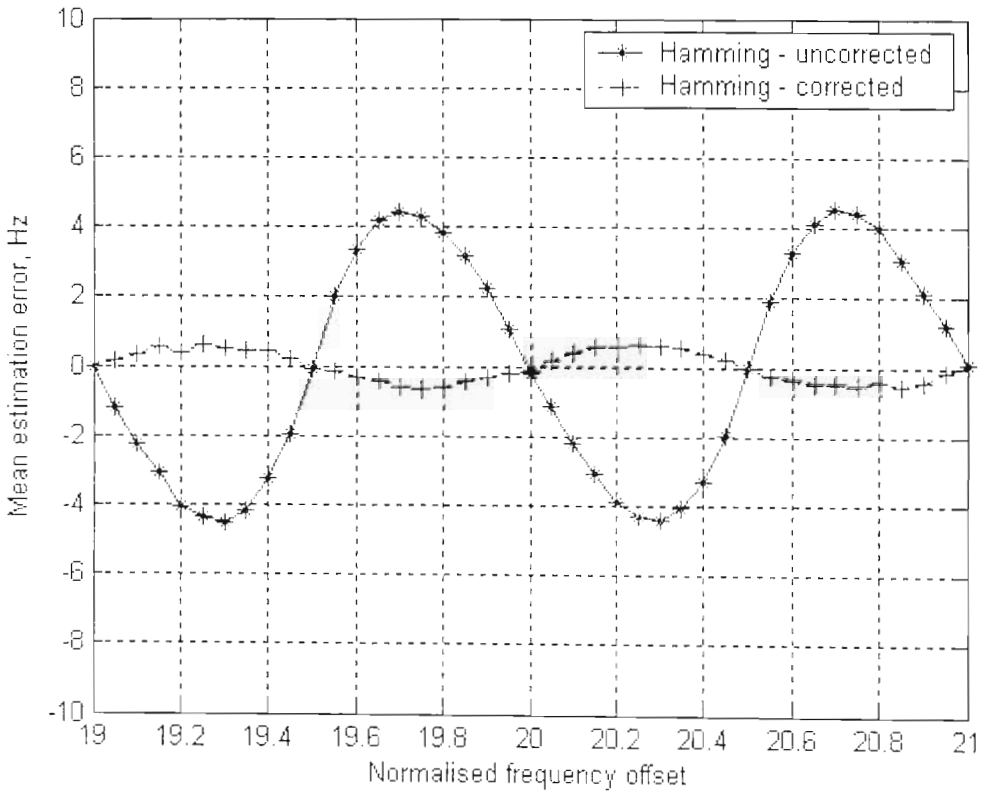

Figure 4-8: Mean estimation error with a Hamming window as a function of frequency offset normalised to the frequency resolution of the FFT.

Figure 4-8 shows the mean estimation error of a Hamming window function and when correction is not used, the algorithm in (4.16) estimates the frequency offset with an accuracy of ± 4.53 Hz. The correction algorithm (4.20) further reduces the error to within ± 0.64 Hz. This improved performance is caused by the higher side-lobe level of – 42 dB of a Hamming window in comparison with a Hanning window [94]. However, although the Hamming window shows a smaller leakage than the

Hanning window, it has a slow falloff rate of only -6 dB/octave and a 3 dB bandwidth of 1.30 bins [94].

The estimation performance of a Blackman window is shown in Figure 4-9. The Blackman window shows a better estimation performance than the three other windows. A maximum accuracy of ± 2.25 Hz is recorded when correction is not used. This brings an improvement factor of almost 17 compared to a Rectangular window function.

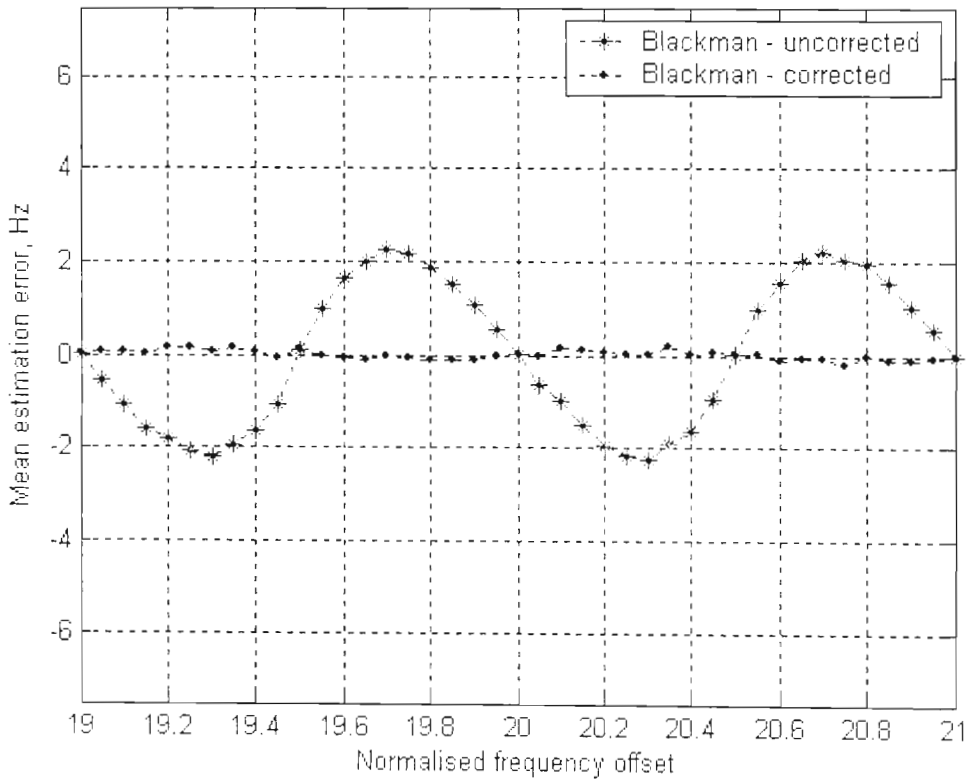

Figure 4-9: Mean estimation error of a Blackman window as a function of frequency offset normalised to the frequency resolution of the FFT.

Its efficiency can be attributed to its small sideband leakage with a side-lobe falloff of -18 dB/octave, highest side-lobe level of -58 dB and a slightly wider central lobe (3 dB bandwidth of 1.68 bins) [94]. When the bias correction algorithm is applied, the mean estimation error is found to be bounded to within ± 0.19 Hz, further increasing the performance by factor of almost 12. Thus the Blackman window performs better

than the other windows with an overall performance improvement of almost 200 compared to the conventional Rectangular window. Table 4-3 summarises the improvement factors achieved using uncorrected and corrected window functions with respect to the conventional Rectangular window in an AWGN channel with a signal-to-noise ratio of 20 dB.

Table 4-3: Frequency offset estimation improvement factors in an AWGN channel with a SNR of 20 dB.

Window	Uncorrected	Corrected
Rectangular	1	4
Hanning	8.2	79
Hamming	8.4	59
Blackman	17	200

The noise sensitivity of the conventional and the modified FFT based estimators is studied in an additive white Gaussian channel and a flat fading channel with a conventional Rectangular window and a Blackman window with correction. The results are shown in Figure 4-10 and Figure 4-11 respectively.

A frequency offset of 20 kHz ($20.33 f_{resolution}$) is assumed between the transmitted and the received data sequences which corresponds to uncorrected and corrected peak estimation errors of -2.25 Hz and +0.19 Hz respectively. See Figure 4-9. A filtered white Gaussian noise model [52] is used to model the flat fading channel with a Doppler frequency of 9.26 Hz. The root mean square error between the transmitted and estimated received frequencies as used in [94] is normalised to the chip frequency of a WCDMA system (3.84 MHz) and is used to measure the estimator performance. The signal-to-noise ratio is considered to be the ratio of the transmitted scrambling code power to the noise power.

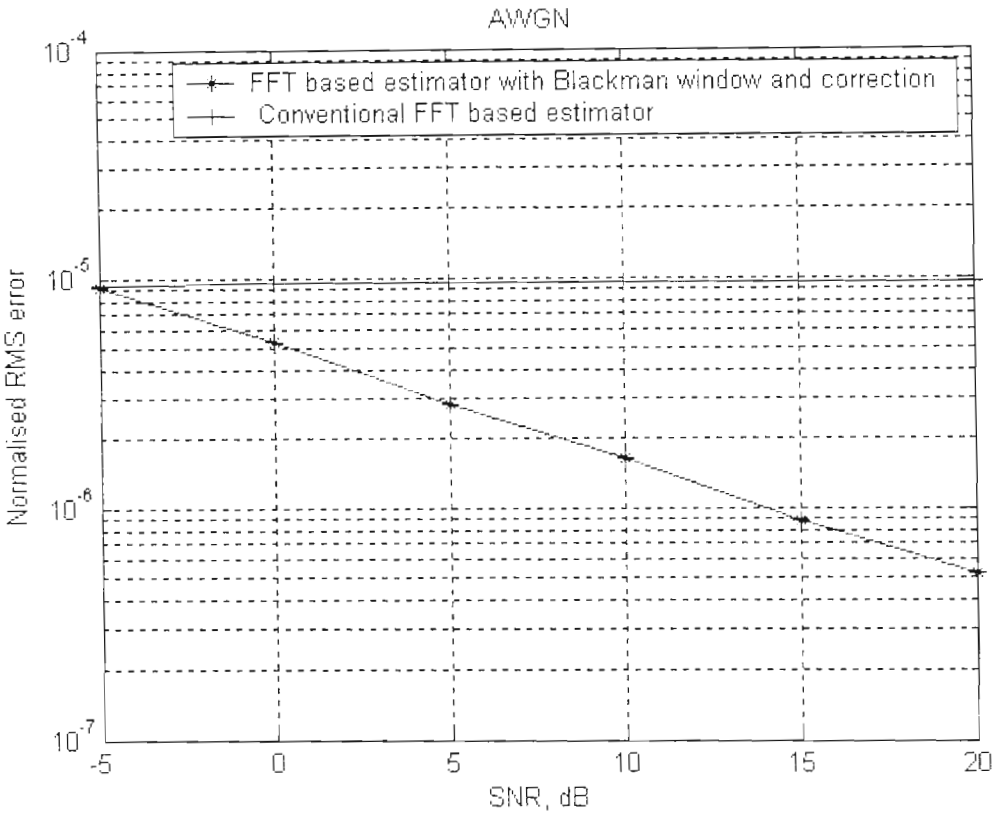

Figure 4-10: The RMS estimation error normalised to the WCDMA chip rate as a function of SNR in an AWGN channel. (Frequency offset = 20 kHz)

In Figure 4-10, the conventional algorithm with a Rectangular window in an AWGN channel shows a steady normalised rms estimation error floor of 10^{-5}. This corresponds to ± 38.4 Hz error as explained earlier in Figure 4-7. This is because the bias arising from quadratic interpolation of the FFT peaks is not changing considerably for the SNRs considered. However, a considerable improvement is shown when a Blackman window function with correction is used to modify the conventional algorithm. This modified algorithm performs better than the conventional one for higher signal-to-noise ratios. This is due to the additional correction to the bias of the quadratic interpolation and is observed to increase with a decrease in SNR.

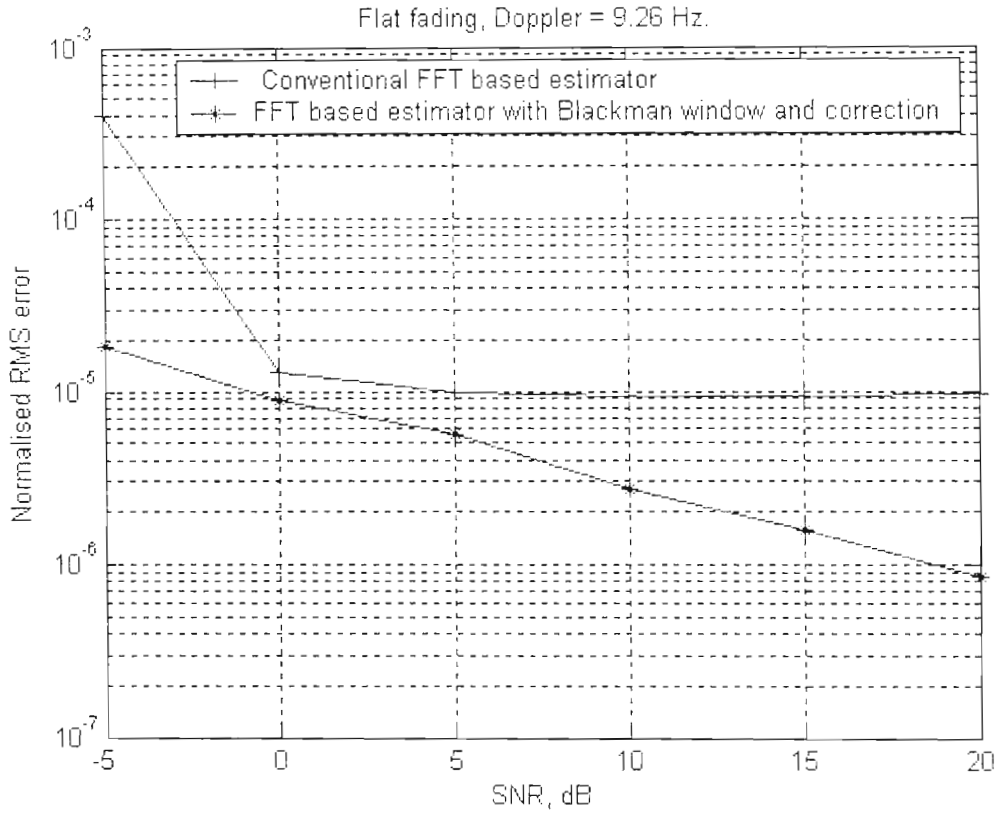

Figure 4-11: The RMS estimation error normalised to the WCDMA chip rate as a function of SNR in a flat fading channel (Frequency offset = 20 kHz)

In Figure 4-11, a case where a flat fading channel is considered, the conventional algorithm estimates the frequency offset to within ± 1.54 kHz or 10^{-5} at a signal-to-noise ratio of -5 dB. This is due to the difficulty of the algorithm to cope with the variations of the channel and clearly invalidates the estimation limit of 200 Hz set by the 3GPP standard. The modified algorithm, however, shows robustness to the channel fluctuations as shown in its estimation performance of about 76.8 Hz at the same SNR. The results show the robustness of the modified algorithm at low SNR.

4.7 Analysis

To determine the validity of the simulation results presented in the previous section, an analysis is presented in this section. Figure 4-12 shows the analytical model. The scrambling code is assumed to be known by the receiver and hence its effect is not included in this model. The sinusoidal signal shown at Point 1 models the received de-spread signal with a frequency offset at the receiver. The de-spread signal is assumed to be an all ones sequence. The phase ϕ is uniformly distributed in the interval 0 to 2π. At Point 2, $W(t)$ models the window function used. The waveform shown at Point 3 incorporates the effect of the FFT window size t_2 and the W-CDMA slot duration t_1. The zero padding length $t_2 - t_1$ is also shown. Fourier series coefficients (a_n, b_n) are computed for the signal at Point 4 to model the effect of the FFT operations. Finally, quadratic interpolation is performed on the largest peak of the coefficients $(\sqrt{a_n^2 + b_n^2})$ and its adjacent spectral lines. This gives the estimated frequency offset $\widehat{\Delta f}$. The derivation of the frequency offset for the Rectangular and Blackman window functions is shown in the next subsections.

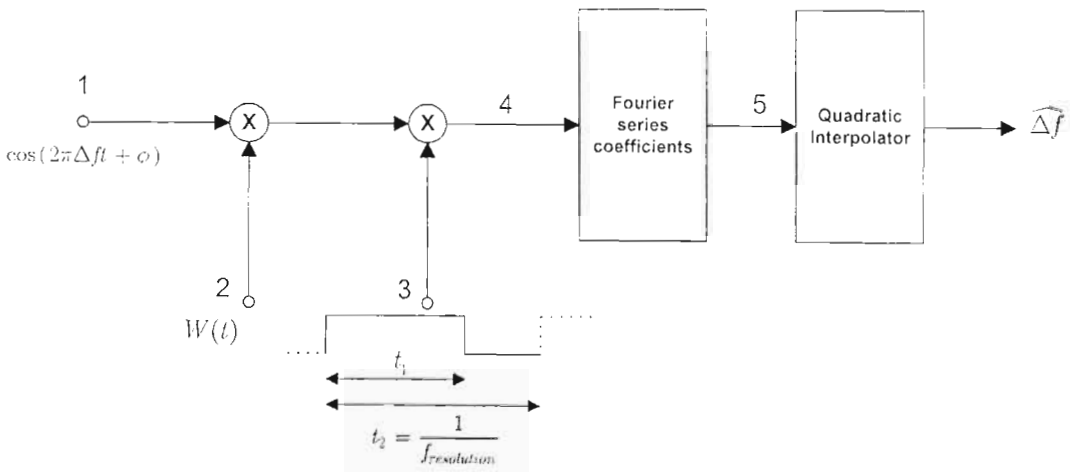

Figure 4-12: Analytical model

4.7.1 Rectangular Window

The Fourier series coefficients for a Rectangular window ($W(t)=1$) are derived as follows.

$$a_n = \frac{2}{t_2}\int_0^{t_1} W(t)\cos(\Delta wt+\phi)\cos(nw_0 t)\,dt$$
$$= f_{resolution}\left(\frac{\sin((\Delta\omega - n\omega_o)t_1+\phi)-\sin\phi}{(\Delta\omega - n\omega_o)} + \frac{\sin((\Delta\omega + n\omega_o)t_1+\phi)-\sin\phi}{(\Delta\omega + n\omega_o)}\right)$$

(4.21)

$$b_n = \frac{2}{t_2}\int_0^{t_1} W(t)\cos(\Delta wt+\phi)\sin(nw_0 t)\,dt$$
$$= f_{resolution}\left(\frac{\cos((\Delta\omega - n\omega_o)t_1+\phi)-\cos\phi}{(\Delta\omega - n\omega_o)} - \frac{\cos((\Delta\omega + n\omega_o)t_1+\phi)-\cos\phi}{(\Delta\omega + n\omega_o)}\right)$$

(4.22)

where $\Delta\omega = 2\pi\Delta f$ is the true frequency offset to be estimated, $w_0 = \frac{2\pi}{t_1}$ represents the slot frequency and n describes the harmonics integer. In the special case of the denominator in (4.21) and (4.22), if $(\Delta\omega - n\omega_o) = 0$, appropriate numerical approximations can be carried out.

The analysis result for a Rectangular window function is shown in Figure 4-13 and compared with the simulation values given in Figure 4-7. It is shown that the analytical values are closely fitted to the simulation results. It is important to note the estimation at the normalised frequency offsets of 19, 19.5, 20, 20.5 and 21 is made possible with an appropriate numerical approximation.

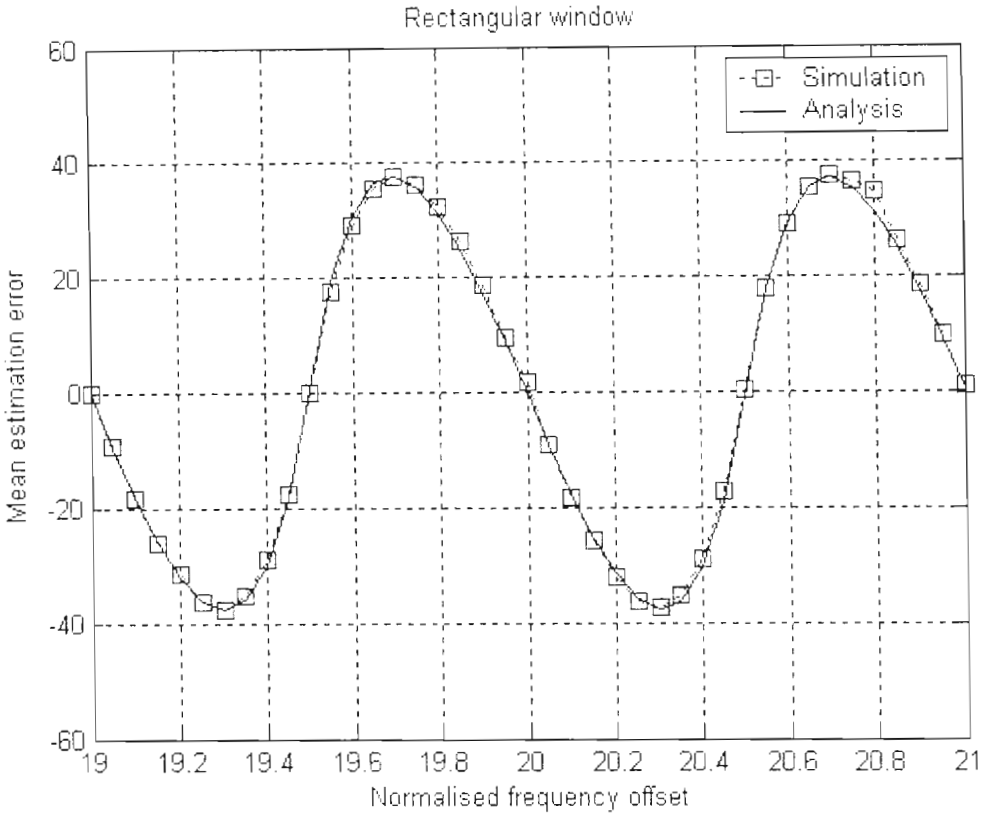

Figure 4-13: Simulation and analysis results for a Rectangular window function

4.7.2 Blackman Window

Similarly, an analytical approach was used on a Blackman window function and the equations are derived as follows. A Blackman window is represented by $W(t) = 0.42 - 0.5\cos(w_0 t) + 0.08\cos(2w_0 t)$ where $t \in [0, t_1]$, t_1 is shown in Figure 4-12. The Fourier series coefficients are derived below.

$$\begin{aligned} a_n &= \frac{2}{t_2}\int_0^{t_2} W(t)\cos(\Delta w t + \phi)\cos(nw_0 t)\,dt \\ &= \frac{2}{t_2}\left(0.21A - \frac{1}{8}(B_1 + B_2) + 0.02(C_1 + C_2)\right) \end{aligned} \tag{4.23}$$

$$
\begin{aligned}
b_n &= \frac{2}{t_2}\int_0^{t_2} W(t)\cos(\Delta w t + \phi)\sin(n w_0 t)\,dt \\
&= \frac{2}{t_2}\left(0.21X - \frac{1}{8}(Y_1 + Y_2) + 0.02(Z_1 + Z_2)\right)
\end{aligned} \tag{4.24}
$$

where

$$
\begin{aligned}
A &= \frac{\sin(\lambda_1 t_1 + \phi) - \sin\phi}{\lambda_1} + \frac{\sin(\lambda_2 t_1 + \phi) - \sin\phi}{\lambda_2} \\
B_1 &= \frac{\sin(\lambda_3 t_1 + \phi) - \sin\phi}{\lambda_3} + \frac{\sin(\lambda_4 t_1 + \phi) - \sin\phi}{\lambda_4} \\
B_2 &= \frac{\sin(\lambda_5 t_1 + \phi) - \sin\phi}{\lambda_5} + \frac{\sin(\lambda_6 t_1 + \phi) - \sin\phi}{\lambda_6} \\
C_1 &= \frac{\sin(\lambda_7 t_1 + \phi) - \sin\phi}{\lambda_7} + \frac{\sin(\lambda_8 t_1 + \phi) - \sin\phi}{\lambda_8} \\
C_2 &= \frac{\sin(\lambda_9 t_1 + \phi) - \sin\phi}{\lambda_9} + \frac{\sin(\lambda_{10} t_1 + \phi) - \sin\phi}{\lambda_{10}}
\end{aligned} \tag{4.25}
$$

$$
\begin{aligned}
X &= \frac{\cos(\lambda_2 t_1 + \phi) - \cos\phi}{\lambda_2} - \frac{\cos(\lambda_1 t_1 + \phi) - \cos\phi}{\lambda_1} \\
Y_1 &= \frac{\cos(\lambda_4 t_1 + \phi) - \cos\phi}{\lambda_4} - \frac{\cos(\lambda_3 t_1 + \phi) - \cos\phi}{\lambda_3} \\
Y_2 &= \frac{\cos(\lambda_6 t_1 + \phi) - \cos\phi}{\lambda_6} - \frac{\cos(\lambda_5 t_1 + \phi) - \cos\phi}{\lambda_5} \\
Z_1 &= \frac{\cos(\lambda_8 t_1 + \phi) - \cos\phi}{\lambda_8} - \frac{\cos(\lambda_7 t_1 + \phi) - \cos\phi}{\lambda_7} \\
Z_2 &= \frac{\cos(\lambda_{10} t_1 + \phi) - \cos\phi}{\lambda_{10}} - \frac{\cos(\lambda_9 t_1 + \phi) - \cos\phi}{\lambda_9}
\end{aligned} \tag{4.26}
$$

and

$$\begin{aligned}
\lambda_1 &= \Delta w + n w_0 & \lambda_6 &= \Delta w - (n+1) w_0 \\
\lambda_2 &= \Delta w - n w_0 & \lambda_7 &= \Delta w + (n-2) w_0 \\
\lambda_3 &= \Delta w + (n-1) w_0 & \lambda_8 &= \Delta w - (n-2) w_0 \\
\lambda_4 &= \Delta w - (n-1) w_0 & \lambda_9 &= \Delta w + (n+2) w_0 \\
\lambda_5 &= \Delta w + (n+1) w_0 & \lambda_{10} &= \Delta w - (n+2) w_0
\end{aligned} \tag{4.27}$$

Appropriate numerical approximations are carried out to calculate the Fourier coefficients when the values for λ_2, λ_4, λ_6, λ_8 and λ_{10} are zero. Figure 4-14 shows the analytical results of a Blackman window closely fitting to the simulation results presented in Figure 4-9. By presenting very closely fitting curves, the analytical results verify the simulation results for the Rectangular and Blackman window functions. This approach can be similarly extended to the Hanning and Hamming window functions.

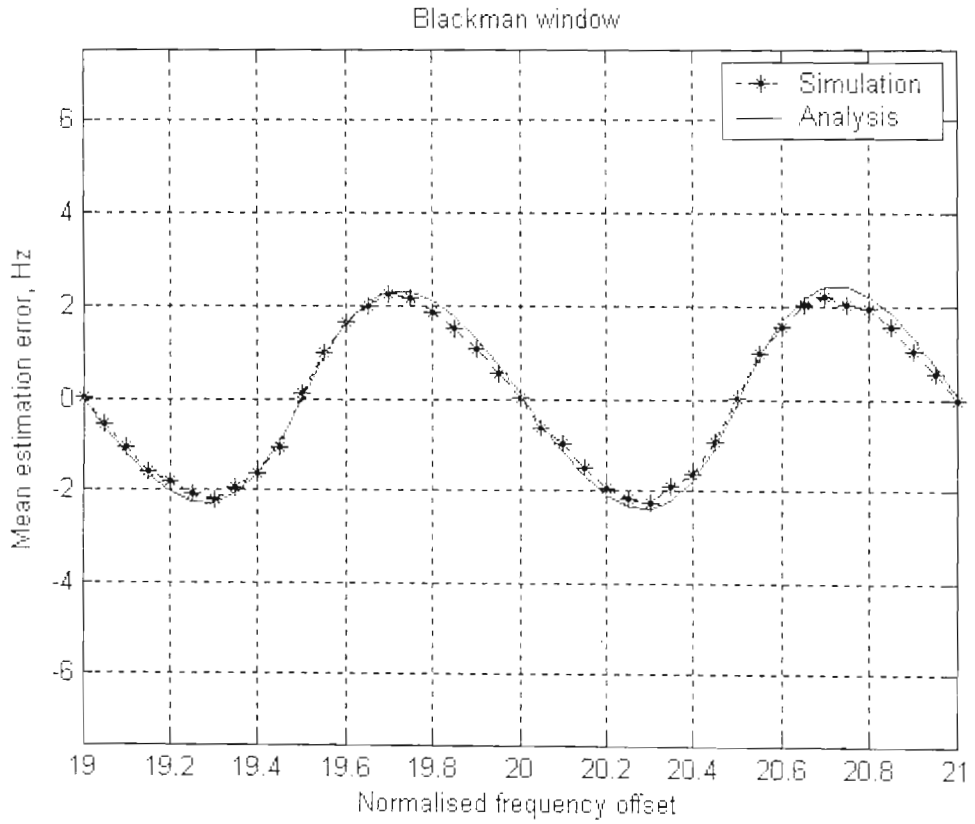

Figure 4-14: Simulation and analysis results for a Blackman window function

4.8 Further Enhancements to the FFT Based Estimator

In this section, a new technique that improves further the performance of the FFT based estimator is proposed. The motivation, system description and simulation results of the proposed algorithm are presented below.

4.8.1 Proposed Method

The FFT based estimators that were considered in the previous sections calculate the Fourier transform of the de-spread sequences in a non-overlapping manner. Figure 4-15(a) depicts this situation where window functions are applied to the de-spread sequences for the duration of every slot in a non-overlapping way. It is important to mention these windowed sequences were zero padded as explained in the previous section before the FFT was computed.

The proposed technique is inspired by the work done in [94] where the author reported the following observations about the non-overlapping technique of computing the Fourier Transform.

- If the window and the FFT are applied to non-overlapping partitions of the de-spread sequences, a significant part of the series is ignored due to the window exhibiting small values near the boundaries.

- If the transform is used to detect short duration tone-like signals, the non-overlapping method could miss the event if it occurred near the boundaries.

To avoid this loss of data, the transforms are usually applied to the overlapped partition sequences as shown in Figure 4-15(b). In this dissertation, the case where the duration of overlap is 50% of the de-spread sequences per slot is considered. The simulation model is mostly similar to the one outlined in Section 4.5.2 with the exception of Step 3. Instead of directly applying the window function on the de-spread sequences, the de-spread sequences are first aligned as shown in Figure 4-

15(b). In order to assess the degree of improvement to the conventional algorithm, the bias correction algorithm proposed in Section 4.5 is not used.

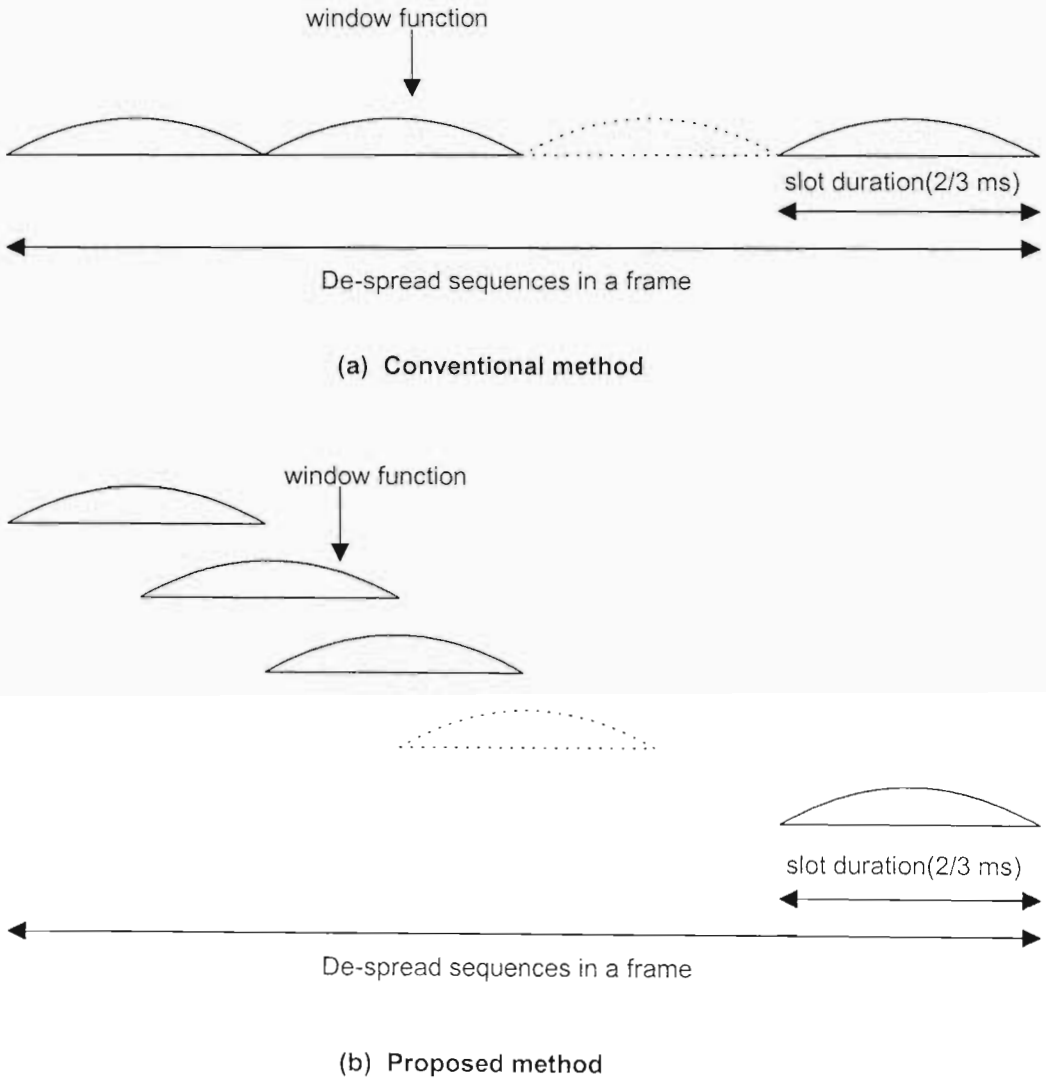

Figure 4-15: Arrangement of de-spread sequences in the conventional and proposed methods.

4.8.2 Simulation Results

The performance of the proposed method is performed through simulations. Rectangular and Hanning window functions are used to compare the performance of the conventional and proposed algorithms. The algorithm presented in Figure 4-4 is used as a conventional algorithm. A 20 kHz frequency offset is assumed to be present

in the received data. A flat fading channel with a Doppler shift of 9.26 Hz is considered. The fade duration is assumed to last one slot duration (2/3 ms). The error probability is taken as a measure of performance and is defined as the probability that the estimated frequency offset exceeds the true frequency by 200 Hz. Monte Carlo simulations with 1000 iterations were used for the simulations. The remaining simulation parameters are as described in Section 4.5 unless otherwise stated to the contrary.

Figure 4-16 shows the error probability of the proposed method in a flat fading channel. A frequency offset of 20 kHz is considered in the simulations. It is shown that the proposed method using the Rectangular and Hanning window functions performs better than the conventional FFT based algorithm in signal-to-noise ratios ranging from -40 dB up to -5 dB. For an error probability of 2×10^{-2}, an improvement close to 4 dB and 2 dB is recorded by the proposed method using Hanning and Rectangular windows, respectively, when compared to the conventional algorithm.

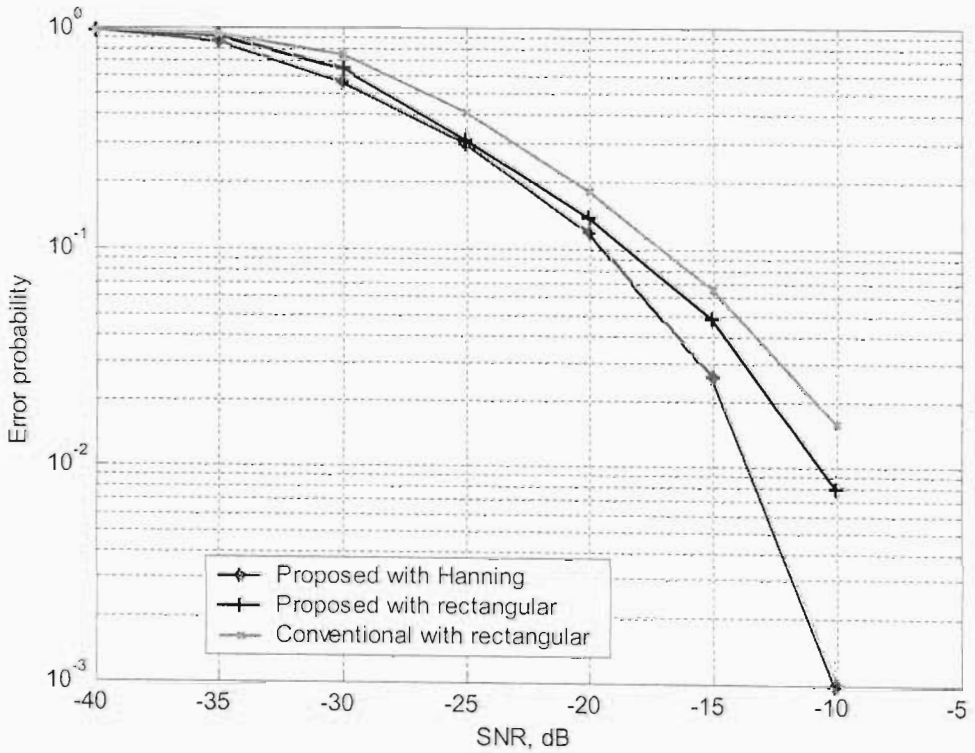

Figure 4-16: Error probability of the proposed method in a flat fading channel with a Doppler frequency of 9.26 Hz. (Frequency offset = 20 kHz)

The main reason for this improvement is the fact that the proposed algorithm exploits the data-omissions caused by the windowing process. The conventional algorithm fails to exploit this condition. Another reason for the increase in performance can be attributed to the extra computations introduced by the overlapping sequences. For example for one frame estimation duration, 15 FFT operations are performed by the conventional algorithm. This compares with 29 FFT operations for the proposed algorithm. This brings about a refined frequency offset estimate in the averaging process of the Fourier transforms. Although it can be argued that this method increases the computational complexity of a WCDMA terminal, the good performance gain obtained would give a reason to compromise.

4.9 Summary

This chapter has described the frequency offset estimation problem in a generalised communications environment. It has also provided literature review of frequency offset estimators in a WCDMA environment. The conventional quadratic interpolation of an FFT based frequency offset algorithm was presented and a correction algorithm proposed for parameter estimation of music signals is modified to estimate the frequency offset in a WCDMA system. The estimation performance was investigated by introducing the use of window functions which are followed by the correction algorithm. The window functions used are Rectangular, Hanning, Hamming and Blackman windows. The performance of the modified algorithm was compared with the conventional estimator in a channel with AWGN and a flat fading channel with AWGN. The results showed the proposed method outperforms the conventional algorithm in both channels. The results have highlighted the importance of using window functions with a correction algorithm in WCDMA terminals to minimise the carrier frequency offset estimation errors.

An analytical approach was also developed to verify the simulation results and it was found the analytical values closely fitting to the simulation values. Moreover, a new technique that exploits the arrangement of the FFT window was proposed and the results showed it performs better than the conventional algorithm.

CHAPTER 5

CONCLUSION AND FUTURE WORK

5.1 Conclusion

This dissertation has tackled two aspects of code acquisition in the WCDMA system. In the first part, the identification of the transmitted scrambling code by the receiving terminal, a process commonly called cell search, has been investigated. The second part of this dissertation has investigated the effect of carrier frequency offsets in the cell searching systems along with the mitigation techniques. In order to achieve this, a new technique has been proposed and its performance investigated.

In Chapter 1, the evolving landscape of wireless communication systems has been presented. Following this, a brief description of the spread spectrum wireless communications systems has been given. The need for synchronisation in a CDMA system has also been highlighted. Finally, the original contributions of this dissertation were described briefly along with the published work.

In Chapter 2, the fundamental principles of code acquisition in WCDMA systems have been presented. Before focusing on the study of the WCDMA system, the conceptual design of code acquisition in the CDMA2000 systems has been described briefly and its differences with the WCDMA system has been highlighted. A

background on code acquisition in the WCDMA system based on selected pioneering research efforts has been described. The development of the above studies into the three stage cell searching process which is adopted by the 3GPP Standard has been discussed. The construction of the synchronisation and scrambling codes used in the WCDMA system has been presented. The different types of downlink channels transmitted by the base station have been presented. Moreover, a model for the base station is presented and its data has been generated. Finally, the effects of carrier frequency offset on the transmitted base station data have been investigated. It has been observed that the carrier frequency offset can damage the transmitted base station data.

In Chapter 3, an overview of the research efforts that enhanced the performance of cell searching systems has been described along with a discussion of the three stage cell searching algorithm. A technique of modelling the wireless channel has been presented. A proposed technique that exploits the symbol structure of a WCDMA frame system has been presented. The performance of this proposed technique has been investigated for various chip correlation lengths and carrier frequency offsets. From the results obtained through simulations, it has been observed that as the carrier frequency offset increases, the miss detection probably of the transmitted scrambling code by the receiving terminal increases. It has also been observed that higher value of correlation length result is a greater loss of performance in the presence of large carrier frequency offsets. Moreover, the proposed algorithm has been observed to achieve a better performance when compared to the conventional algorithm for most values of correlation lengths.

In Chapter 4, an emphasis has been given on the effects and mitigation techniques of the carrier frequency offset in cell searching algorithms. A mathematical model for the estimation of carrier frequency offset has been presented. A review of the literature on the estimation of carrier frequency offset in a WCDMA system has been presented. A proposed algorithm that builds on the conventional FFT based estimator has been presented. From the results obtained through simulations and analysis, the proposed algorithm has been observed to give a significant improvement in performance when compared to the conventional algorithm in both additive Gaussian noise and flat fading channels. Furthermore, a second proposed algorithm that

exploits the overlapping interval of the FFT symbols has been presented and the simulation results have shown that it performs better than the conventional algorithms.

5.2 Future Work

The good predictions of the carrier frequency offset obtained in Chapter 4 of this dissertation have given the promise of digitally compensating the carrier frequency offset at the receiver. However, in order to correct the received signal, similar predications of the carrier phase has to be obtained in addition to the predictions of the carrier frequency offset. Future work could continue to develop efficient algorithms to solve this combined problem of estimation and correction of the carrier frequency offset and phase for WCDMA systems. This approach would use a crystal controlled free running oscillator as compared to the conventional receiver implementations which use feedback architectures to achieve the same effect.

Future work could also extend to investigate the suitability of the estimation and correction algorithms in other radio access technologies besides WCDMA. This is inspired by the fact that the 3GPP Standard has started work to evolve the current WCDMA system in order to meet the growing user and operator requirements [95]. Some of the most promising technologies that are being considered to provide an evolutionary path from the current WCDMA system [95] is the Orthogonal Frequency Division Multiplex (OFDM) and this have been reported to suffer from the effects of carrier frequency offset. Hence, it would be interesting to continue investigations in this regard.

APPENDIX

Allocation of Secondary Synchronisation Codes for S-SCH

Scrambling Code Group	slot number														
	#0	#1	#2	#3	#4	#5	#6	#7	#8	#9	#10	#11	#12	#13	#14
Group 0	1	1	2	8	9	10	15	8	10	16	2	7	15	7	16
Group 1	1	1	5	16	7	3	14	16	3	10	5	12	14	12	10
Group 2	1	2	1	15	5	5	12	16	6	11	2	16	11	15	12
Group 3	1	2	3	1	8	6	5	2	5	8	4	4	6	3	7
Group 4	1	2	16	6	6	11	15	5	12	1	15	12	16	11	2
Group 5	1	3	4	7	4	1	5	5	3	6	2	8	7	6	8
Group 6	1	4	11	3	4	10	9	2	11	2	10	12	12	9	3
Group 7	1	5	6	6	14	9	10	2	13	9	2	5	14	1	13
Group 8	1	6	10	10	4	11	7	13	16	11	13	6	4	1	16
Group 9	1	6	13	2	14	2	6	5	5	13	10	9	1	14	10
Group 10	1	7	8	5	7	2	4	3	8	3	2	6	6	4	5
Group 11	1	7	10	9	16	7	9	15	1	8	16	8	15	2	2
Group 12	1	8	12	9	9	4	13	16	5	1	13	5	12	4	8
Group 13	1	8	14	10	14	1	15	15	8	5	11	4	10	5	4
Group 14	1	9	2	15	15	16	10	7	8	1	10	8	2	16	9
Group 15	1	9	15	6	16	2	13	14	10	11	7	4	5	12	3
Group 16	1	10	9	11	15	7	6	4	16	5	2	12	13	3	14
Group 17	1	11	14	4	13	2	9	10	12	16	8	5	3	15	6
Group 18	1	12	12	13	14	7	2	8	14	2	1	13	11	8	11
Group 19	1	12	15	5	4	14	3	16	7	8	6	2	10	11	13
Group 20	1	15	4	3	7	6	10	13	12	5	14	16	8	2	11
Group 21	1	16	3	12	11	9	13	5	8	2	14	7	4	10	15
Group 22	2	2	5	10	16	11	3	10	11	8	5	13	3	13	8
Group 23	2	2	12	3	15	5	8	3	5	14	12	9	8	9	14
Group 24	2	3	6	16	12	16	3	13	13	6	7	9	2	12	7
Group 25	2	3	8	2	9	15	14	3	14	9	5	5	15	8	12
Group 26	2	4	7	9	5	4	9	11	2	14	5	14	11	16	16
Group 27	2	4	13	12	12	7	15	10	5	2	15	5	13	7	4
Group 28	2	5	9	9	3	12	8	14	15	12	14	5	3	2	15
Group 29	2	5	11	7	2	11	9	4	16	7	16	9	14	14	4
Group 30	2	6	2	13	3	3	12	9	7	16	6	9	16	13	12
Group 31	2	6	9	7	7	16	13	3	12	2	13	12	9	16	6
Group 32	2	7	12	15	2	12	4	10	13	15	13	4	5	5	10
Group 33	2	7	14	16	5	9	2	9	16	11	11	5	7	4	14
Group 34	2	8	5	12	5	2	14	14	8	15	3	9	12	15	9
Group 35	2	9	13	4	2	13	8	11	6	4	6	8	15	15	11
Group 36	2	10	3	2	13	16	8	10	8	13	11	11	16	3	5
Group 37	2	11	15	3	11	6	14	10	15	10	6	7	7	14	3
Group 38	2	16	4	5	16	14	7	11	4	11	14	9	9	7	5
Group 39	3	3	4	6	11	12	13	6	12	14	4	5	13	5	14
Group 40	3	3	6	5	16	9	15	5	9	10	6	4	15	4	10
Group 41	3	4	5	14	4	6	12	13	5	13	6	11	11	12	14

Scrambling Code Group	slot number														
	#0	#1	#2	#3	#4	#5	#6	#7	#8	#9	#10	#11	#12	#13	#14
Group 42	3	4	9	16	10	4	16	15	3	5	10	5	15	6	6
Group 43	3	4	16	10	5	10	4	9	9	16	15	6	3	5	15
Group 44	3	5	12	11	14	5	11	13	3	6	14	6	13	4	4
Group 45	3	6	4	10	6	5	9	15	4	15	5	16	16	9	10
Group 46	3	7	8	8	16	11	12	4	15	11	4	7	16	3	15
Group 47	3	7	16	11	4	15	3	15	11	12	12	4	7	8	16
Group 48	3	8	7	15	4	8	15	12	3	16	4	16	12	11	11
Group 49	3	8	15	4	16	4	8	7	7	15	12	11	3	16	12
Group 50	3	10	10	15	16	5	4	6	16	4	3	15	9	6	9
Group 51	3	13	11	5	4	12	4	11	6	6	5	3	14	13	12
Group 52	3	14	7	9	14	10	13	8	7	8	10	4	4	13	9
Group 53	5	5	8	14	16	13	6	14	13	7	8	15	6	15	7
Group 54	5	6	11	7	10	8	5	8	7	12	12	10	6	9	11
Group 55	5	6	13	8	13	5	7	7	6	16	14	15	8	16	15
Group 56	5	7	9	10	7	11	6	12	9	12	11	8	8	6	10
Group 57	5	9	6	8	10	9	8	12	5	11	10	11	12	7	7
Group 58	5	10	10	12	8	11	9	7	8	9	5	12	6	7	6
Group 59	5	10	12	6	5	12	8	9	7	6	7	8	11	11	9
Group 60	5	13	15	15	14	8	6	7	16	8	7	13	14	5	16
Group 61	9	10	13	10	11	15	15	9	16	12	14	13	16	14	11
Group 62	9	11	12	15	12	9	13	13	11	14	10	16	15	14	16
Group 63	9	12	10	15	13	14	9	14	15	11	11	13	12	16	10

REFERENCES

[1] G. Marconi, British Patent No. 12039, June 1896.

[2] J. Belrose, "Fessenden and the early history of radio science," *Radio Scientist and Bulletin,* Vol. 5, No. 3, URSI, pp 94-110, 1994.

[3] S. Christopher, Electronic Media: A Guide to Trends in Broadcasting and Newer Technologies, 1920-1983, Praeger, 1984.

[4] J. Korhonen, Introduction to 3G Mobile Communications, Artech House mobile communications series: 2nd Edition, 2003.

[5] GSM World: The Website of GSM Association, http://www.gsmworld.com, last accessed Dec. 2006.

[6] R. Scholtz, The Evolution of Spread Spectrum Multiple Access Communications, in *Code Division Multiple Access Communications,* S. Glisic and P. Leppanen (eds.) Kluwer Academic Publishers, 1995.

[7] S. Stanley Chia and W. Lee, "A synchronized radio system without stable clock sources," *IEEE Personal Communications*, pp. 45-50, Apr. 2001.

[8] 3GPP TSG-RAN, "Spreading and Modulation (FDD)," TS 25.213, v5.0.0 (2002-2003).

[9] A. Polydoros and C. Weber, "A unified approach to serial search spread spectrum code acquisition, Part I: General theory," *IEEE Trans. Commun*. Vol. COM-32, No. 5, pp. 542-549, May 1984.

[10] F. Adachi, M. Sawahashi, T. Dohi and K. Ohno, "Coherent DS-CDMA: Promissing multiple access for wireless multimedia communications," *IEEE Int. Symposium on Spread Spectrum Techniques and Applications,* Vol. 1, pp. 351-358, Sept. 1996.

[11] K. Higuchi, M. Sawahashi and F. Adachi, "Fast cell search algorithms in DS-CDMA mobile radio using long spreading codes," *in Proc. IEEE Vehicular Technology Conf.*, Phoenix, AZ, pp. 1430-1434, May 1997.

[12] J. Nystrom, K. Jamal, Y. Wang and R. Esmailzadeh, "Comparison of cell search methods for asynchronous wideband CDMA cellular system," *in Proc. IEEE Int. Conf. on Universal Personal Commun.*, Vol. 2, pp. 783-787, Oct. 1998.

[13] S. Sriram and S. Hosur, "An analysis of the 3-stage cell search process in W-CDMA," *in Proc. IEEE Vehicular Technology Conf.*, Vol. 6, pp. 2672-2679, Sept. 2000.

[14] S. Sriram and H. Hosur, "Cyclically permutable codes for rapid acquisition in DS-CDMA systems with asynchronous base stations," *IEEE Journal on Selected Areas in Commun.*, Vol. 19, No. 1, pp. 83-94, Jan. 2001.

[15] S. Xia and F. Fu, "Non-parametric cyclic equivalence classes of cyclic codes and algebraic constructions of cyclically permutable codes," *in Proc. 12th Int. symposium on Applied Algebra, Algebraic algorithms and Error correcting codes,* pp. 341-352, Jun. 1997.

[16] Y. Wang and T. Ottosson, "Cell search algorithms and optimization in W-CDMA," *in Proc. IEEE Vehicular Technology Conf.*, Vol. 1, pp. 81-86, May 2000.

[17] Y. Wang and T. Ottosson, "Cell search in W-CDMA," *IEEE Journal on Selected Areas in Commun.*, Vol. 18, No. 8, pp. 1470-1482, Aug. 2000.

[18] 3GPP TSG-RAN, "FDD: Physical layer procedures," TS 25.214, v5.0.0 (2002-2003).

[19] J. Nystrom, R. Esmailzadeh, K. Jamal and Y. Wang, "Comparison of cell search methods for asynchronous wideband CDMA cellular system," *IEICE Trans. Fundamentals*, Vol. E82-A, No. 10, pp. 2115-2120, Oct. 1999.

[20] Siemens, "A new hierarchical correlation sequence with good correlation properties in the presence of a frequency error," 3GPP TSG RAN W1 Tdoc 99/146.

[21] Texas Instruments, "Reduced complexity primary and secondary synchronisation codes with good autocorrelation properties for the WCDMA systems," 3GPP TSG RAN W1 Tdoc 99/373.

[22] Texas Instrumnets, "Further results on Golay codes based PSC and SSC," 3GPP RAN W1 Tdoc 99/422.

[23] M. Golay, "Complementary series," *IRE Trans. Inform. Theory*, Vol. IT-7, pp. 82-87, Apr. 1961.

[24] Siemens and Texas Instruments, "Generalised hierarchical Golay sequence for PSC with low complexity correlation using pruned Golay correlators," TSG Ran W1 Tdoc 99/554.

[25] A. Graham, Kronecker Products and Matrix Calculus with Applications, Halsted Press, John Wiley and Sons, 1981.

[26] A. Nielson and S. Korpela, "WCDMA initial cell search," *in Proc. IEEE Vehicular Technology Conf.*, Vol. 1, pp. 377-383, Sept. 2000.

[27] W. Hai, C. Zhqiang and M. Sundelin, "The impact of cell search on system performance in WCDMA," *in Proc. IEEE Vehicular Technology Conf.*, Vol. 2, pp. 1425-1429, May 2000.

[28] C. Liu, "Adaptive synchronisation and cell search algorithm for WCDMA systems," *in Proc. IEEE Int. Conf. on Commun. Systems,* Vol. 2, pp. 678-682, Nov. 2002.

[29] Z. Chunhui, M. Lin, X. Xibin, Z. Ming and Y. Yan, "Transfer power allocation of WCDMA synchronization channel and common pilot channel," *in Proc. IEEE Int. Conf. on Commun. Tech.*, Vol. 1, pp. 946-949, Aug. 2000.

[30] M. Song, "Performance Comparison of stepwise serial and parallel cell search in WCDMA," *IEICE Trans. Commun.*, Vol E88-B, No. 6, pp. 2539-2547, June 2005.

[31] W. Sheen and J. Ho, "Cell search for 3GPP W-CDMA/FDD with chip clock shift and non-ideal sampling," *in Proc. IEEE Vehicular Technology Conf.,* Vol. 4, pp. 2369-2373, Oct 2001.

[32] S. Hwang, B. Kang and J. Kim, "Performance analysis of initial cell search using time tracker for W-CDMA," *in Proc. IEEE Global Commun. Conf., Globecom,* Vol. 5, pp. 3055-3059, Nov. 2001.

[33] M. Kiessling and S. Mujtaba, "Performance enhancements to the UMTS (W-CDMA) initial cell search system," *in Proc. IEEE Int. Conf. Commun.*, Vol. 1, pp. 590-594, Apr. 2002.

[34] Kang Lee and J. Yong Chun, "An initial cell search scheme robust to frequency error in W-CDMA system," *IEEE Int. PIMRC*, Vol. 2, pp. 1400-1404, Sept. 2000.

[35] T. Chulajata, H. Kwon and K. Min, "Coherent slot detection under frequency offset for W-CDMA," *in Proc. IEEE Vehicular Technology Conf.,* Vol. 3, pp. 1719-1723, May 2001.

[36] J. Moon and Y Hwan Lee, "Cell search robust to initial frequency offset in WCDMA systems," *in Proc. IEEE PIMRC,* Vol. 5, pp. 2039-2043, Sept. 2002.

[37] N. Kai, H. Qun Feng, W. Wei-ling, "Improvements on acquisition of secondary synchronisation channel in W-CDMA," *in Proc. IEEE Int. Conf. Info-tech. and Info-net.*, Vol. 2, pp. 632-641, Nov. 2001.

[38] Kai Niu, S. Wang, Qun-Feng He and Wei-Ling Wu, "A novel matched filter for primary synchronisation channel in W-CDMA," *in Proc. IEEE Vehicular Technology Conf.,* Vol. 4, pp. 2052-2055, May 2002.

[39] N. Darbel, Y. Rasse, O. Batsidas-Garcia, G. Faux, B. Jubelin and M. Carrie, "Reconfigurable low power cell search engine for UMTS-FDD mobile terminals," *IEEE Workshop Signal Processing Systems*, pp. 171-176, Oct. 2002.

[40] S. Bae, Sung Yun and Jae Sung Lim, "Fast cell search algorithm using polarization code modulation for WCDMA systems," *in Proc. IEEE Vehicular Technology Conf.*, Vol. 2, pp. 709-712, May 2002.

[41] Dong Kim and Yu Ro Lee, "Fast cell search using I/Q multiplexed code in asynchronous DS/CDMA cellular systems," *in Proc. IEEE Int. Spread Spectrum Techniques and Applications,* Vol. 3, pp. 832-836, Sept. 1998.

[42] Dong Kim and Yu Ro Lee, "I/Q multiplexed code assignment for fast cell search under hierarchical cell structure," *in Proc. IEEE Int. Conf. Universal Personal Communications*, Vol. 1, pp. 389-393, Oct. 1998.

[43] Han Sup Lee, Hyun Pyo, Dong In Kim, "Cell search scheme using I/Q multiplexed code assignment in asynchronous W-CDMA system," *in Proc. IEEE Vehicular Technology Conf.,* Vol. 2, pp. 1560-1564, May 1999.

[44] J. Ahn, S. Hwang, E. Hong, J. Koo, and K. Whang, "New cell search algorithm for inter cell asynchrnous mode DS-CDMA mobile radio system," *in Proc. IEEE Vehicular Technology Conf.,* Vol. 2, pp. 1336-1340, May 1998.

[45] Jung Hyun Choi, Nak-Myeong Kim and So-Yeong Park, "A fast cell search algorithm using code block CPM in asynchronous W-CDMA system," *in Proc. IEEE Vehicular Technology Conf.,* Vol. 1, pp. 280-285, Sept. 2000.

[46] Andre Zoch and Gerhard Fettweis, "Cell search performance analysis for W-CDMA," *in Proc. IEEE Int. Conf. Commun.*, Vol. 2, pp. 940-944, May 2002.

[47] M. Song and V. Bhargava, "Performance analysis of cell search in W-CDMA systems over Rayleigh fading channels," *IEEE Trans. Vehicular Technology,* Vol. 51, No. 4, pp. 749-759, July 2002.

[48] S. Kourtis, "investigation of the mobile terminal optimum operating point in UMTS-FDD initial cell search procedure," *IEEE Int. Symposium PIMRC,* Vol. 1, pp. 348-352, Sept. 2000.

[49] Y. Jeong, O. Shin and K. Lee, "Fast slot synchronisation for intercell asynchronous DS/CDMA systems," *IEEE Trans. Wireless Commun.*, Vol. 1, No. 2, pp. 353-360, Apr. 2002.

[50] A. Viterbi, CDMA: Principles of Spread Spectrum Communications, Addison-Wesley, 1995.

[51] R. Clarke, "A statistical theory of mobile radio reception," *Bell Syst. Tech., J.* 47, pp. 957-1000, 1968.

[52] D. Young and N. Beaulieu, "A quantitative evaluation of generation methods for correlated Rayleigh random variates," *in Proc. Global Telecom. Conf., Globecom*, Sydney, Vol. 6, pp. 3332-3337, Nov. 1998.

[53] J. Smith, "A computer generated multipath fading simulation for mobile radio," *IEEE Trans. Commun.*, Vol. COM-22, pp. 1607-1617, Oct. 1974.

[54] C. Loo and N. Secord, "Computer models for fading channels with applications to digital transmission," *IEEE Trans. Vehicular Technology,* Vol. VT-44, No. 4, pp. 700-707, Nov. 1991.

[55] P. Mclane, "Two stage Doppler phasor corrected TCM/DMPSK for shadowed satellite channels," *IEEE Trans. Commun.*, Vol. 41, No. 8, pp. 1137-1141, Aug. 1993.

[56] D. Verdin and T. Tozer, "Generating a fading process for the simulation of land mobile radio communications," *Electronic Letters*, Vol. 29, No. 23, pp. 2011-2012, Nov. 1993.

[57] W. Jakes, Microwave Mobile Communications, Wiley, New York, 1974.

[58] M. Abranowitz and I. Stegun, Handbook of Mathematical Functions with Fromulas, graphs and Mathematical Tables, Dover publications, 9th Edition, New York, 1972.

[59] S. Rezenom and A. Broadhurst, "Stage 3 Performance of W-CDMA Cell Search for Various Chip Correlation Lengths", *in Proc. South African Telecommunication, Networks and Applications Conference (SATNAC),* Drakensberg, South Africa, Sept. 2005.

[60] Y. J. Guo, Advances in Mobile Radio Access Networks, Artech House Mobile Communication Series, 2004.

[61] M. Luise and R. Reggiannini, "Carrier frequency recovery in all digital modems for burst mode transmissions," *IEEE Trans. Commun.*, Vol. 43, No 2/3/4, pp. 1169-1178, Feb./Mar./Apr. 1995.

[62] GSM Recommendation 11.10, Part II.3, V.1.07.00, March 1990.

[63] D.C. Rife and R.R. Boorstyn, "Single-tone parameter estimation from discrete time observations," *IEEE Trans. Inform. Theory*, Vol. IT-20, pp. 591-598, Sept. 1974.

[64] S.A. Tretter, "Estimating the frequency of a noisy sinusoid by linear regression," *IEEE Trans. Inf. Theory*, Vol. 31, No. 12, pp. 832-835, Nov. 1985.

[65] S.M. Kay, "A fast and accurate single frequency estimator," *IEEE Trans. Acoust., Speech and Signal Processing,* Vol. 37, pp. 1987-1990, Dec. 1989.

[66] S. Bellini, C. Molinari and G. Tartara, "Digital frequency estimation in burst mode QPSK transmission," *IEEE Trans. Commun.*, Vol. 38, pp. 959-961, July 1990.

[67] H.L. van Trees, Detection, Estimation and Modulation theory, New York, Wiley 1968.

[68] H.W. Soreson, Parameter Estimation, New York, Marcel Dekker, 1980.

[69] L.P.Seidman, "Performance limitations and error calculation for parameter estimation," *Proc. IEEE*, Vol. 58, pp. 644-652, May 1970.

[70] J. Ziv and M. Zakai, "Some lower bounds on signal parameter estimation," *IEEE Inf. Theory*, Vol. IT-15, pp. 386-391, May 1969.

[71] S. Bellini and G. Tartara, "Bounds on error in signal parameter estimation," *IEEE Trans. Commun.*, Vol. COM-22, pp. 340-342, March 1974.

[72] S.C. White and N.C. Beaulieu, "On the application of the Cramer Rao and detection theory bounds to mean square error of symbols timing recovery," *IEEE Trans. Commun.*, Vol. COM-40, pp. 1635-1643, Oct. 1992.

[73] M. Moeneclaey, "A simple lower bound on the linearised performance of practical symbol synchronisers." *IEEE Trans. Commun.*, Vol. COM-31, pp. 1029-1032, Sept. 1983.

[74] M. Moeneclaey, "A fundamental lower bound to the performance of practical joint carrier and bit synchronisers," *IEEE Trans. Commun.*, Vol. COM-32, pp. 1007-1012, Sept. 1984.

[75] M. Moeneclaey and I. Bruyland, "The joint carrier and symbol synchronizability of continuous phase modulated waveforms," *Conf. Rec. ICC'86*, Vol. 2, paper 31.5, pp. 987-991, Jun. 1986.

[76] A.N.D' Andrea, U. Mengalli and R. Reggiannini, "The modified Cramer Rao Lower Bound and its applications to synchronisation problems," *IEEE Trans. Commun.*, Vol. 42, No. 2/3/4, pp. 1391-1398, Feb./Mar./Apr. 1994.

[77] P. Rykaczewski, D. Pienkowski, R. Circa and B. Steinke, "Signal path optimisation in software-defined radio systems," *IEEE Trans. Microwave Theory and Techniques*, Vol. 53, No. 3, pp. 1056-1064, 2005.

[78] V. Baronkin, Y. Zakharov and T. Tozer, "Frequency estimation in slowly fading multipath channels," *IEEE Trans. Commun.*, Vol. 50, No. 11, pp. 1848-1859, Nov. 2002.

[79] U. Mengali and M. Morelli, "Data-aided frequency estimation for burst digital transmission," *IEEE Trans. Commun.*, Vol. 45, No. 1, pp. 23-25, Jan. 1997.

[80] M.P. Fitz, "Planar filtered techniques for burst mode carrier synchronisation," in *Proc. IEEE Globecom*, Phoenix, AZ, pp. 365-369, Dec. 1991.

[81] B.C Lovell and R.C Williamson, "The statistical performance of some instantaneous frequency estimators," *IEEE Trans. Acoust., Speech and Signal Processing*, Vol. 40, No. 7, pp. 1708-1723, Jul. 1992.

[82] Hebbley and P. Taylor, "The effect of diversity on a burst mode carrier frequency estimator in the frequency selective multipath channel," *IEEE Trans. Commun.*, Vol. 46, No. 4, pp. 553-560, Apr. 1998.

[83] V. Aggarwal, and C. Chien, "A robust low complexity technique for frequency acquisition over frequency selective channels," *in Proc. IEEE Int. Conf. Commun.*, ICC, Vol. 2, pp.1262–1266, June 1999.

[84] M. Morelli and U. Mengalli, "Carrier frequency estimation for transmissions over selective channels," *IEEE Trans. Commun.*, Vol. 48, No. 9, pp. 1580-1589, Sept. 2000.

[85] W.Y. Kuo and M.P. Fitz, "Frequency offset compensation of a pilot-assisted modulation in flat fading channels," *IEEE Trans. Commun.*, Vol. 45, No. 11, pp. 1412-1416, Nov. 1997.

[86] M. Morelli, U. Mengali and G.M Vitetta, "Further results in carrier frequency estimation for transmissions over flat fading channels," *IEEE Commun. Letters*, Vol. 2, No. 12, pp. 327-330, Dec. 1998.

[87] E.R. Jeong, S.K. Jo and Y.H. Lee, "Least squares frequency estimation in frequency selective channels and its applications to transmissions with antennae diversity," *IEEE Journal on Select. Areas Commun.*, Vol. 19, No. 12, pp. 2369-2380, Dec. 2001.

[88] Y. D. Kim, J. K. Lim, C. H. Suh, E. R. Jeong and Y. H. Lee, "Carrier frequency estimation for transmissions with antennae diversity," *in Proc. IEEE Vehicular Technology Conf.*, Vol. 3, pp. 1569-1563, May 2002.

[89] Y.T. Su, and R.C. Wu, "Frequency acquisition and tracking in high dynamic environments," *IEEE Trans. Vehicular Technology*, Vol. 49, No. 6, pp. 2419-2429, Nov. 2000.

[90] T. Vaidis and A. Polydoros, "Effects of large frequency offset in digital receivers and related algorithms," *in Proc. Global Telecom. Conf., Globecom '01,* Vol. 2, pp. 1349 – 1355, Nov. 2001.

[91] Y.P.E Wang and T. Ottosson, "Initial frequency acquisition in W-CDMA," *in Proc. IEEE Vehicular Technology Conf.*, Amsterdam, pp. 1013-1017. Sept. 1999.

[92] J.O. Smith and X. Serra, "A program for the analysis/synthesis of inharmonic sounds based on a sinusoidal representation," *in Proc. ICMC*, pp. 290-297, 1987.

[93] M. Abe and J. Smith, "CQIFFT: Correcting bias in a sinusoidal parameter estimator based on quadratic interpolation of FFT magnitude peaks", *Technical Report, STAN-M-117*, Dept. of Music, Stanford University, Oct. 2004.

[94] J. Harris, "On the use of windows for harmonic analysis with the discrete Fourier transform," *Proc. IEEE*, Vol. 66, pp. 51-83, 1978.

[95] H. Ekstrom, A. Furuskar, J. Karlsson, M, Meyer, S. Parkval, J. Torsner, and M. Wahlsqvist, "Technical Solutions for the 3G long term evolution," *IEEE Communications Magazine*, Vol. 44, No. 3, pp. 38-45, Mar. 2006.